GEOCHEMICAL STUDY OF HYDROCARBON-PRONE SEDIMENTS OF LOWER JURASSIC AGE IN THE SLYNE BASIN, OFFSHORE IRELAND

by

Charles Andrew Maurice Carlisle

Submitted in partial fulfilment of the requirements
for the degree of Master of Science

at

Dalhousie University
Halifax, Nova Scotia
March 2017

TABLE OF CONTENTS

LIST OF TABLES

LIST OF FIGURES

ABSTRACT

The Slyne Basin, a narrow Mesozoic basin located offshore Ireland, has been the subject of significant exploration with several proven commercial hydrocarbon discoveries. While the Corrib gas field within the Slyne Basin is sourced from Carboniferous Coal Measures, Lower Jurassic intervals represent a separately viable hydrocarbon source rock system of regional significance in the Irish offshore. In marine environments, and particularly in epeiric sea settings, the processes leading to deposition of these hydrocarbon source rocks are governed by complex interplay of local (different carbonate producers, transgressive–regressive cycles) and/or global (worldwide preservation of organic matter, variation of continental weathering, input of volcanogenic light CO_2) mechanisms.

Stable carbon isotope chemostratigraphy, RockEval pyrolysis and X-ray fluorescence (elemental geochemistry) have been applied to geochemically characterize samples from Lower Jurassic source rocks in two wells (18/25-1 and 27/13-1, Slyne Basin). To determine $\delta^{13}C$ and $\delta^{18}O$, the selected samples were analysed by Continuous Flow–Isotope-Ratio Mass Spectrometry (for carbonates) and Elemental Analysis- Isotope-ratio Mass Spectrometry (for total organic carbon, TOC). Results from well 18/25-1, present a negative $\delta^{13}C$ trend from 2610 m to 2664 m, while $\delta^{13}C$ values from organic matter present less variation: a negative trend is observed from 2610 m to 2688 m followed by a generally positive trend from 2694 m to 2824 m - the negative excursion of the carbon isotope signature is thought to correspond, in part, to the Toarcian Oceanic Anoxic Event. The slight post-T-OAE negative carbon isotope excursion (CIE) recovery to more positive values and the continuation of a relatively high organic content is coeval with a regional organic matter preservation interval observed in several Northern-European locations. Total Organic Carbon content and Rock-Eval data show that Pliensbachian-aged source rock intervals are gas/oil prone (Type II/III) and Toarcian-Aalenian aged sediments are oil-prone (Type II).

These new datasets and their interpretation add to the understanding of the palaeoenvironmental dynamics during the Early–Middle Jurassic in the Northern European domain and may offer new insights for hydrocarbon exploration offshore Ireland.

LIST OF ABBREVIATIONS USED

$\delta^{13}C$	Delta-Carbon-13
BCF	Billion Cubic Feet
CF-IRMS	Continuous Flow Isotope Ratio Mass Spectrometry
CIE	Carbon Isotope Excursion
DCCAE	Department of Communications, Climate Action, and Environment
EA-IRMS	Elemental Analyser Isotope Ratio Mass Spectrometry
FID	Flame Ionisation Detector
HC	Hydrocarbons
HI	Hydrogen Index
ISPSG	Irish Shelf Petroleum Studies Group
LIP	Large Igneous Province
Ma	Megaanus - million years ago
MDBKB	Metres Depth Below Kelly Bushing
MDBRT	Meters Depth Below Rotary Table
MMBO	Million Barrels of Oil
NOC `	Normalised Oil Content
OAE	Oceanic Anoxic Event
OI	Oxygen Index
OMPI	Organic Matter Preservation Interval
PAD	Petroleum Affairs Division
PI	Production Index
PIP	Petroleum Infrastructure Programme
PPM	Parts Per Million
TCF	Trillion Cubic Feet
TD	Total Depth
T-OAE	Toarcian Oceanic Anoxic Event
TOC	Total Organic Carbon
TVDSS	Total Vertical Depth Subsea
UTM	Universal Transverse Mercator
V-PDB	Vienna Peedee Belemnite
WT. %	Weight percent
XRF	X-ray Fluorescence

ACKNOWLEDGEMENTS

I would like to thank Professor Grant D. Wach and Doctor Ricardo L. Silva of the Basin and Reservoir Laboratory at Dalhousie University for their guidance and mentorship. Thank you also to Professor Bernard Boudreau and Mr Neil Watson, members of my supervisory committee.

Within the Department of Earth Sciences, I acknowledge the efforts of Philip Sedore, Maya Soukup, Jonathan Thibodeau, Kallen Rutledge, Trudy Lewis, Chloe Younger, Ann Bannon, Norma Keeping and Darlene Van De Rijt for assistance throughout the project.

I kindly acknowledge the Source Rock and Geochemistry of the Central Atlantic Margins consortium (Dalhousie University, Basin and Reservoir Lab, Professor Grant Wach, Principal Investigator) and the Sable Operating grant for Petroleum Geoscience. I acknowledge the Petroleum Infrastructure Programme - Expanded Offshore Studies Group and the Nedimović Family Scholarship for additional funding which helped support me.

This project is funded by the Irish Shelf Petroleum Studies Group (ISPSG) of the Irish Petroleum Infrastructure Programme (PIP) Group 4. The ISPSG comprises: Atlantic Petroleum (Ireland) Ltd, Cairn Energy Plc, Chrysaor E&P Ireland Ltd, Chevron North Sea Limited, ENI Ireland BV, Europa Oil & Gas (Holdings) Plc, ExxonMobil E&P Ireland (Offshore) Ltd., Kosmos Energy LLC, Maersk Oil North Sea UK Ltd, Petroleum Affairs Division of the Department of Communications, Climate Action and Environment, Providence Resources Plc, Repsol Exploración SA, San Leon Energy Plc, Serica Energy Plc, Shell E&P Ireland Ltd, Sosina Exploration Ltd, Statoil (UK) Ltd, Tullow Oil Plc and Woodside Energy (Ireland) Pty Ltd.

CHAPTER 1: INTRODUCTION

Sedimentation during the Lower Jurassic (201.3±0.2 Ma –174.1±1 Ma (Cohen *et al.* 2013) in the Northern Atlantic basins coincided with a series of major environmental perturbations and dramatic changes in populations of marine organisms. The culmination of these planetary-scale changes during the Toarcian Stage is known as the Toarcian Oceanic Anoxic Event (T-OAE, e.g. Jenkyns and Clayton, 1986; Jenkyns, 1988, 2010, Hesselbo *et al.*, 2000a; Bailey *et al.*, 2003; Suan *et al.*, 2010; van de Schootbrugge *et al.*, 2013). The T-OAE is coeval with a major perturbation of the global carbon cycle, linked with a massive influx of ^{12}C into atmospheric and oceanic reservoirs, recorded in the geochemical record as a pronounced negative Carbon Isotope Excursion (CIE) in carbonates, fossil wood and kerogens (e.g. Hesselbo *et al.*, 2000a; 2007). The T-OAE is of interest as periods of oceanic anoxia, along with high sedimentation rates are responsible for preservation of high levels of Total Organic Carbon (TOC), the primary ingredient in the production of hydrocarbons. Whether anoxia or sedimentation plays a bigger role in preservation of organic matter (as TOC) is a major cause for debate to this day (for a concise summary, see Pedersen and Calvert, 1990). While basin-floor anoxia will prevent degradation of organic matter by inhibiting aerobic digestion, high levels of primary production will preserve settled organic matter through inability of grazers to maintain or increase consumption rates (Pedersen and Calvert, 1990).

$\delta^{13}C$ (the ratio of ^{13}C:^{12}C of sediment relative to that of a known standard), preserves a record of the signal in the water column derived from terrestrial material, primary production by aquatic organisms, microbial biomass, and diagenesis, among other mechanisms (see, for example, Tyson, 1995; Emerson and Hedges, 2008; Hoefs, 2015;

Suan *et al*., 2015). In turn, $\delta^{13}C$ records fluxes in the carbon isotope mix, such as massive inputs of carbon from biased sources. The carbon isotopic composition of organic matter depends mainly on the ^{13}C content of the carbon source, which will remain in equilibrium with seawater and the atmosphere. However, temperature, availability of CO_2, and nutrient availability have been shown to exert some control on the $\delta^{13}C$ of phytoplankton, a major source of carbon (Emerson and Hedges, 2008). Transformation of organic matter during its transit in the water column seems to not impact significantly the $\delta^{13}C$ of organic carbon in sediments, however, the contribution of the reworked material makes organic carbon in newly deposited sediments isotopically lighter (within 1–2‰) than its biological source (see Galimov, 2006).

Other observations of paleoclimatic conditions during Lower Jurassic sedimentation include warming of ~6 °C over 200,000 years, major volcanism, including the emplacement of the Karoo-Ferrar Large Igneous Province (Dera *et al.*, 2010; Duncan, 1997; Suan *et al.,* 2008a, 2008b, 2010, 2011; Bond and Wignall, 2014), and a possible link to astronomical forcing consistent with the Milankovitch "precession" cycle (Kemp, 2005 and 2011).

Marine sediments of Lower Jurassic age were deposited in a geological interval prone to organic matter preservation (*sensu* Silva *et al*., 2011) and are thus a significant source rock target in petroleum exploration in many areas around the world (e.g. Fleet *et al.*, 1987; Baudin, 1990; Scotchman, 2001; Riediger, 2002; Röhl and Schmid-Röhl, 2005; Duarte *et al.,* 2012; Sachse *et al.*, 2012; Silva *et al.*, 2011; 2015; Silva and Duarte 2015, and references therein). This is especially true of Ireland's offshore basins where Lower Jurassic organic-rich sediments has been the primary target of exploration drilling (Elf

Aquitaine, 1982.) and a proven source rock for Ireland's first oil discoveries, the Helvick and Dunmore wells (SLR, 2013; Doré, 2002; Caston, 1995) and a major component in charging Ireland's first gas field, Kinsale Head (SLR 2013).

The Slyne Basin, the subject of this study, is a narrow, half-graben basin offshore Ireland related to the opening of the Atlantic (Figure 1, Scotchman, 2016; Naylor and Shannon, 1982). It has been the subject of significant exploration (16 exploration, appraisal, sidetrack, and production wells since 1981: PAD 2016) with one commercial dry gas field at Corrib and one prospective oil discovery at Bandon. While the Corrib gas field (1 TCF recoverable) is sourced in Westphalian (Carboniferous) Coal Measures (Dancer *et al.*, 2005), the Bandon discovery (12 MMBO proven in-place) is sourced in the Portree Shale of Toarcian age (182.7 Ma – 174.1 Ma) (Serica Energy, 2014).

While source rock occurrences were encountered during exploration drilling in the Slyne Basin and assessed using chemostratigraphy, biostratigraphy and lithostratigraphy, they have seldom been geochemically compared with similarly aged black shale hydrocarbon source rocks outside the Northern European domain (see, for example, Scotchman *et al.*, 2016). To date, no studies have found evidence of the carbon isotopic excursions and carbon cycle perturbations associated with the T-OAE offshore Ireland.

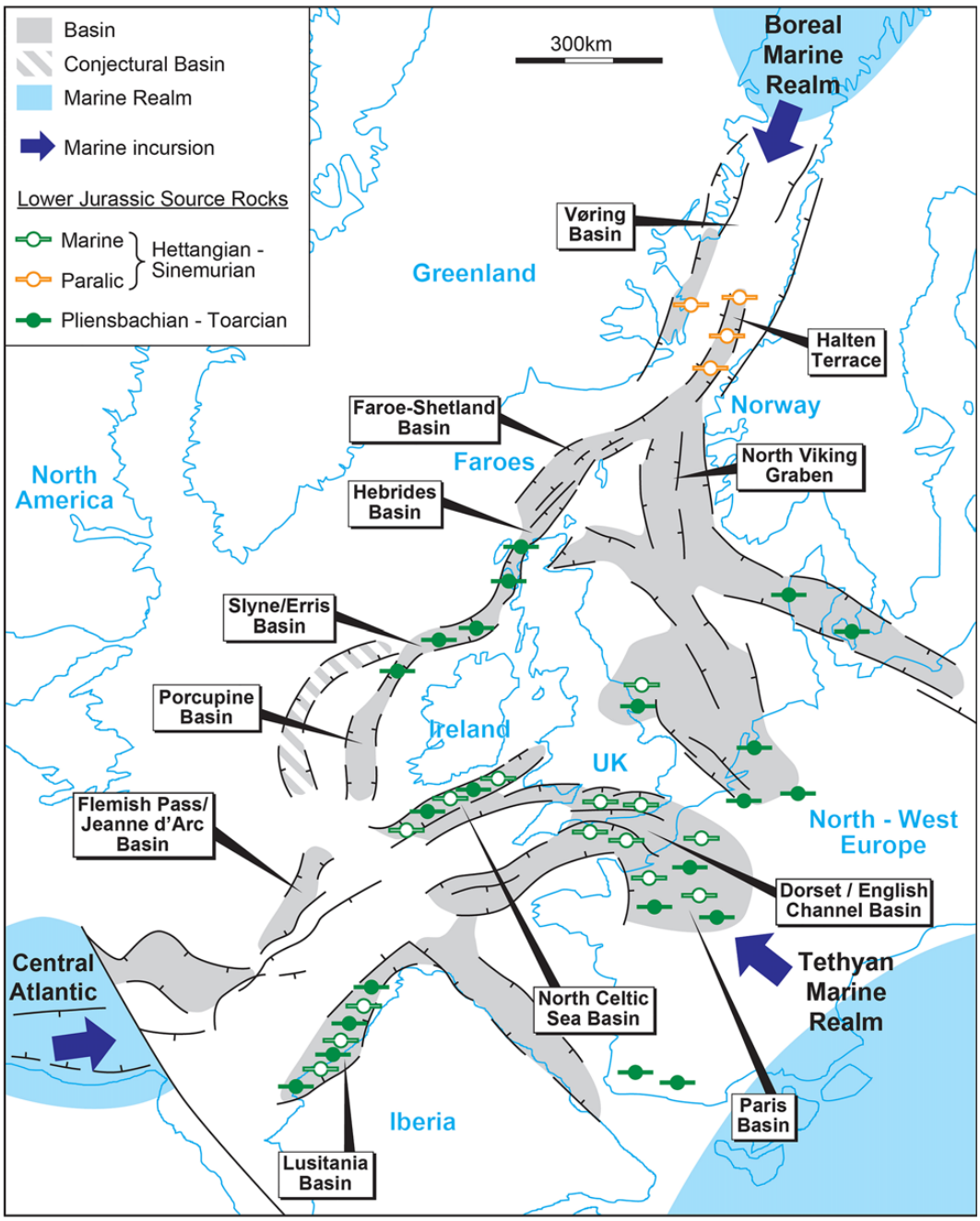

Figure 1: Reconstruction of Lower Jurassic basin configuration in the North and Central Atlantic and identified occurrences of hydrocarbon source rock (From Scotchman, 2016).

1.1 SOURCE ROCK: PRIMARY ELEMENT OF THE PETROLEUM SYSTEM

The core elements of a petroleum system include a) source rock, b) reservoir rock, c) seal rock and d) overburden rock (Magoon and Beaumont, 1999). Put simply, source rock consists of sediment containing enough organic material of suitable composition for hydrocarbon generation with sufficient thermal maturity; reservoir consists of porous rock (most often sandstone or carbonate, but can also be the source rock itself) capable of storing hydrocarbons expelled during hydrocarbon generation; and seal rock prevents hydrocarbons from exiting the reservoir rock (most often shale or halite). Finally, overburden blankets these strata, providing pressure and thermal insulation (e.g. Tissot and Welte, 1984; Magoon and Beaumont, 1999).

In petroleum geology, the term source rock is applied to a rock unit containing sufficient organic material of suitable chemical composition to generate and expel hydrocarbons via biogenic or thermogenic processes (Miles, 1994) and this is applied irrespective of whether its organic matter is mature or immature (Belaid *et al.*, 2010; Potter *et al.*, 1993; Suárez-Ruiz *et al.*, 2012 and Tissot and Welte, 1984). Source rock can originate in various sedimentary environments such as deep marine, lacustrine and deltaic depositional environments (e.g. Suárez-Ruiz *et al.*, 2012).

To characterize a source rock, it is necessary to interpret its origin and geological history and investigate its geochemical properties to determine the potential products that can be or were generated (e.g. Suárez-Ruiz *et al.*, 2012). For a petroleum geologist, the organic matter in rocks is usually divided into kerogen (high molecular weight and insoluble in organic solvents) and bitumen (low molecular weight and soluble in organic solvents) (Belaid *et al.*, 2010; Potter *et al.*, 1993; Suárez-Ruiz *et al.*, 2012 and Tissot and Welte,

1984) (See Figure 2). The final stage of hydrocarbon production from kerogen occurs in areas which have undergone regional metamorphism, resulting in graphite, a stable arrangement of carbon atoms (Tissot and Welte, 1984) (Figure 2).

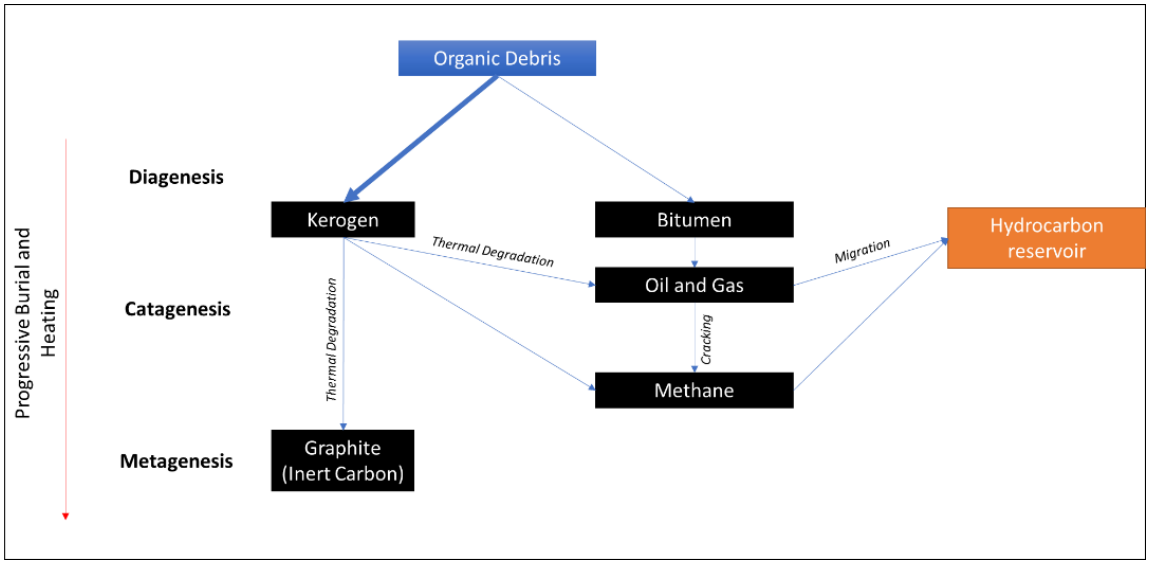

Figure 2: Schematic representation of fractionation of organic matter into kerogen and bitumen. Modified from Tissot and Welte, 1984.

The chemical composition of kerogen is divided into four categories: Type I, with highest H/C and O/C ratios, to Type IV with the lowest ratios (Tissot and Welte, 1984, Van Krevelen, 1993; Espitalié *et al.* 1977, 1985). More commonly used is the pseudo-Van Krevelen diagram, where Rock-Eval pyrolysis oxygen index (OI = mg HC/g TOC) is plotted against hydrogen index (HI = mg HC/g TOC). These ratios approximate the H/C and O/C elemental ratios. Van Krevelen (1993) noted a relationship between kerogen type (a reflection of its hydrogen content, from Type I kerogen, the richest in hydrogen, to Type IV, the poorest in hydrogen) and the depositional environment. Type I kerogen is usually associated with lacustrine settings with algal plant dominance or an area with a significant reworking of plant material to preserve only lipid-rich detritus. Type II kerogen is indicative of an open marine (or sometimes lacustrine) setting with plankton preserved in

sediment. Type III kerogen is usually associated with terrestrial "woody" plant matter, deposited in an environment proximal to a shoreline, while Type IV kerogen retains the visual appearance of other kerogens, but has already been oxidised or carbonised – depleting it of the potential to produce hydrocarbons. Due to the decreasing organic element content, kerogen types can also be used to predict the type of hydrocarbon fluids expected from maturation: Type I mainly produces oil, Type II generates mixed gas and oil, while Type III mainly produces gas. Marginal Type III/IV have been noted to produce exceptionally dry gas, while Type IV is non-productive (Suarez-Ruiz *et al.*, 2012).

The main criteria used in characterizing a given interval as a source rock include a) the quantity of organic matter in the sediment (due to depositional environment and degree of preservation); b) the type of organic matter capable of producing hydrocarbons (depositional environment and sediment source) and c) and the thermal maturity of organic matter (burial and inversion history). Law (1999) divides source rocks into four major categories:

1. **Potential source rocks** containing organic matter in sufficient quantity to generate and expel hydrocarbons if subjected to an increase in thermal maturation;
2. **Effective source rocks** which currently generate and expel hydrocarbons;
3. **Relic effective rocks** previously effective source rock with further potential to produce hydrocarbons. Relics have ceased generating and expelling hydrocarbons due to a thermal cooling event (such as inversion) before exhaustion of kerogen;
4. **Spent source rock** has produced all hydrocarbons available from a kerogen and will not produce more under increasing thermal maturity.

1.2 IMPORTANCE OF STUDY

Historically, conventional hydrocarbon exploration has targeted structural traps that may accumulate commercial quantities of oil and gas. As exploration becomes more expensive, it is important to better understand all elements of potential petroleum systems, including the source rock component.

1.3 STATEMENT OF PROBLEM: LOWER JURASSIC ORGANIC-RICH INTERVALS IN THE SLYNE BASIN

A record of the palaeoenvironmental conditions and presence of oceanic anoxia (waters depleted of oxygen, where free hydrogen sulphide exists; Pedersen and Calvert, 1990) or excessive primary production allowing for preservation of TOC have not been previously identified in sediments from Upper Triassic–Lower Jurassic times. In other coeval sediments, this has been characterized using stable isotopic analysis (Silva, 2015).

Lower Jurassic shales are proven hydrocarbon source rocks in the Celtic Sea (Murphy 1995). However, they are not well understood or recognized in the Irish Atlantic setting, where source rock may be a significant risk in exploration. This thesis will investigate the Lower Jurassic interval offshore Atlantic Ireland, to examine its source rock potential, spatial distribution, and geochemical similarities to other Jurassic shales on the Atlantic margin. This study will help discern the viability of this interval as key component of the petroleum system for exploration in the region. The thesis will also compare the paleoenvironment relative to the Early to Middle Jurassic in the Northern European domain.

1.4 HYPOTHESIS

Supported by existing work on planetary-scale events and changes in the Earth System during the Lower Jurassic, I hypothesise that:

1) the organic-rich intervals of Toarcian age in Ireland's offshore are coeval with the T-OAE and associated CIE;

2) the $\delta^{13}C$ (see section 3.5.3) record from this basin also records newly observed CIEs in Sinemurian and Pliensbachian-aged strata, known source rock intervals in the Slyne Basin;

3) Lower Jurassic sediments from offshore Ireland can be used to infer climatological and environmental conditions during deposition and thus are a valuable contribution to the study of this interval at a regional and global scale.

1.5 OBJECTIVES

The objectives of this thesis are to:

1) characterize the source-rock potential of the Broadford Beds Formation, Scalpa Sandstone Formation, Pabba Shale Formation, and Portree Shale Formation equivalent units and;

2) contribute to the understanding of palaeoenvironmental dynamics during the Lower Jurassic and the extent and causes of the non-cyclical events that ultimately led to the T-OAE.

CHAPTER 2: GEOLOGICAL BACKGROUND

2.1 EXPLORATION HISTORY

Hydrocarbon exploration offshore Ireland commenced in the wake of North Sea successes, with the first well drilled offshore Ireland in 1970 (Murphy, 1995). Toarcian rocks were first intersected in 1976 during exploration drilling south of Ireland in the North Celtic Sea Basin Well 57/6-1, with geochemical investigation of this and subsequent wells (such as one of the subject wells, 27/13-1) finding high total organic carbon (TOC) content (≤7 %), identifying it as a potential hydrocarbon source rock (Elf Aquitaine 1982).

Shannon *et al.* (2001) divided the exploration history of the Irish offshore basins into five major phases, starting with the first well drilled in 1970 by Marathon Petroleum Ireland Limited:

1. 1970 – 1973: targeting shallow inversion structures in the Celtic Sea,
2. 1973 – 1983: licensing rounds and added incentives are driven by the "Oil Crisis,"
3. 1983 – 1993: reduced activity due to local economic recession and low rate of success,
4. 1993 – 1999: low levels of seismic exploration and drilling,
5. 1999 – Present: high levels of 2D and 3D seismic exploration with low numbers of new wells drilled.

Historically, the number of wells drilled generally numbered fewer than 10 per year. An increase in activity in 1978 was a result of large discoveries in the North Sea and commencement of natural gas production at Kinsale Head, offshore southern Ireland. Since the beginning of hydrocarbon exploration offshore Ireland, there have been multiple

commercialised discoveries (data from Petroleum Affairs Division online data repository), including:

- Kinsale Head (1.8 TCF)
- Ballycotton (60 BCF)
- Southwest Kinsale (30 BCF)
- Seven Heads (304 BCF)
- Corrib (1 TCF)

In the past, geophysical exploration focused on traps and reservoirs; as such, source rocks remain unmapped. In general, source rocks have not been the target of offshore exploration in Ireland: drilling is typically abandoned once the reservoir has been penetrated. Therefore, cuttings samples from the lower Jurassic are few, and core is non-existent. In inferred source rock intervals, any resultant cuttings have been subject to extensive industry analysis, and therefore quantities available to researchers now are limited.

In previous industry analyses (e.g. Scotchman, 2001 and references therein), Lower Jurassic rocks have contained high TOC (1-6%) mudstones in well 27/13-1, and sandier intervals in 18/25-1 (Petroleum Affairs Division, 2006). Samples have been taken from these two wells for this study (see Figure 3 with well locations).

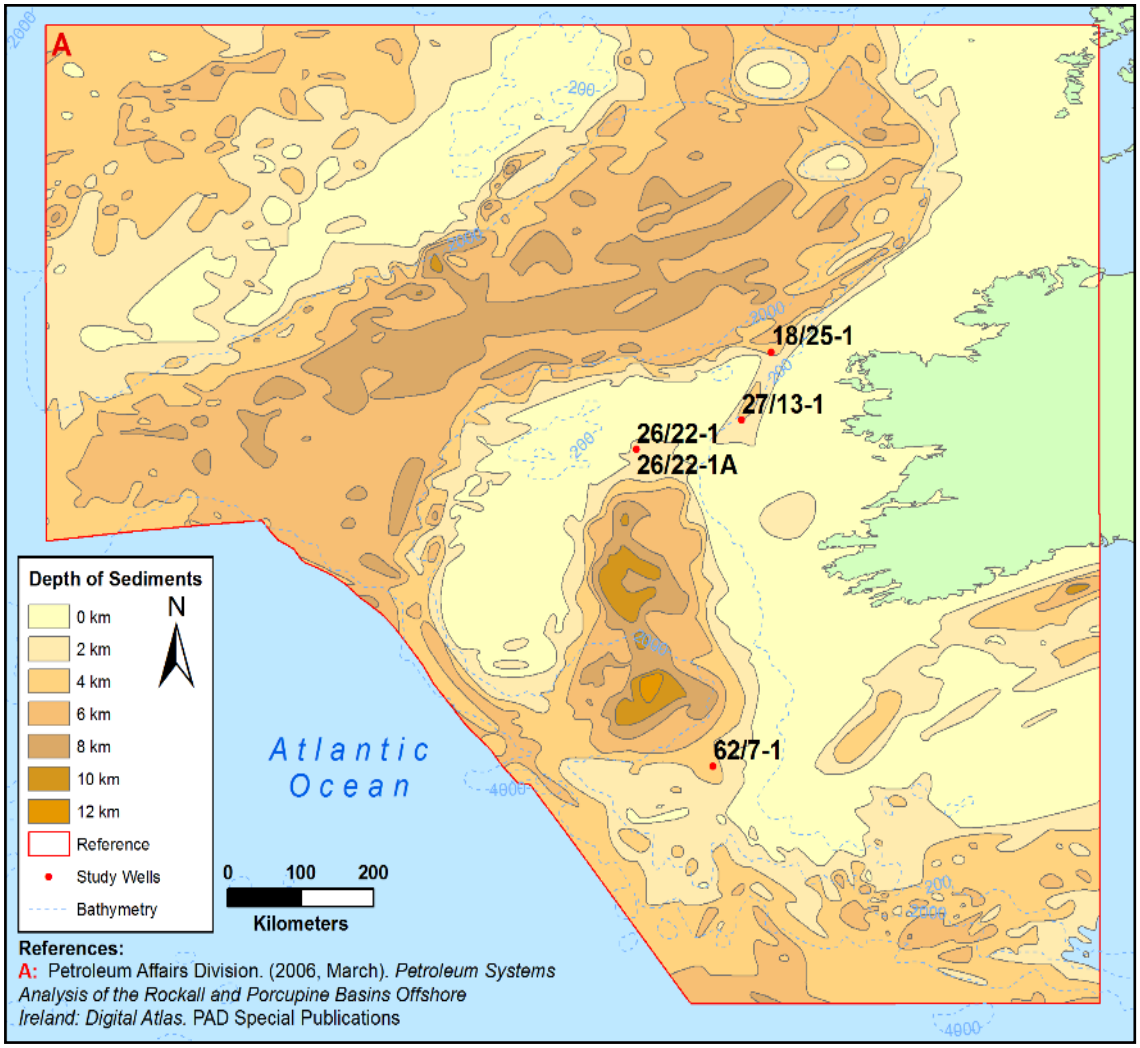

Figure 3: Irish Offshore Wells Sampled in this project and their position within significant depocentres. Green refers to continental landmass. Samples from well 18/25-1 and 27/13-1 were used in this study.

In the mid-1990s, the Petroleum Infrastructure Programme was founded to facilitate research partnerships between industry and academia, resulting in renewed enthusiasm for exploration. In a 2015 licensing round for offshore acreage, Ireland received the most applications (43, with 28 awarded) for licensing options in the history of its offshore exploration.

2.2 GEOGRAPHICAL SITUATION

To the west of Ireland, the Atlantic Margins encompass multiple sedimentary basins, including the subject of this study, the Slyne Basin, bounded to the South by the Slyne Ridge and to the North by the Erris Basin. The Slyne Basin lies within 100km of the Irish landmass, in less than 200 m water depth (Shannon, 2001) (Figure 4).

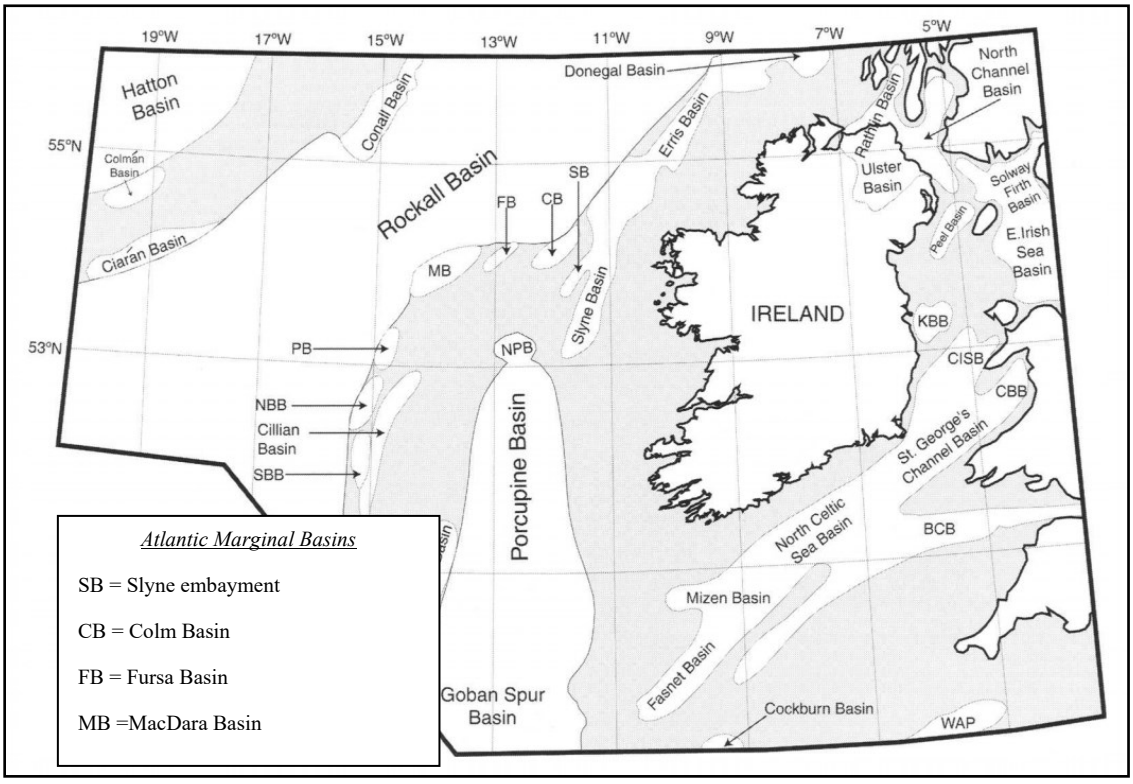

Figure 4: Location map of main sedimentary basins offshore Ireland. (adapted from Shannon et al., 2001; Naylor et al., 1999).

2.3 OFFSHORE GEOLOGY

Offshore geology reflects the formation of north-west European continental margins after intracratonic extension during the Mesozoic Era, with the formation of a half-graben (Figure 5; Shannon et al., 2001; Naylor et al., 1999; Spencer and MacTiernan, 2001). Pre-

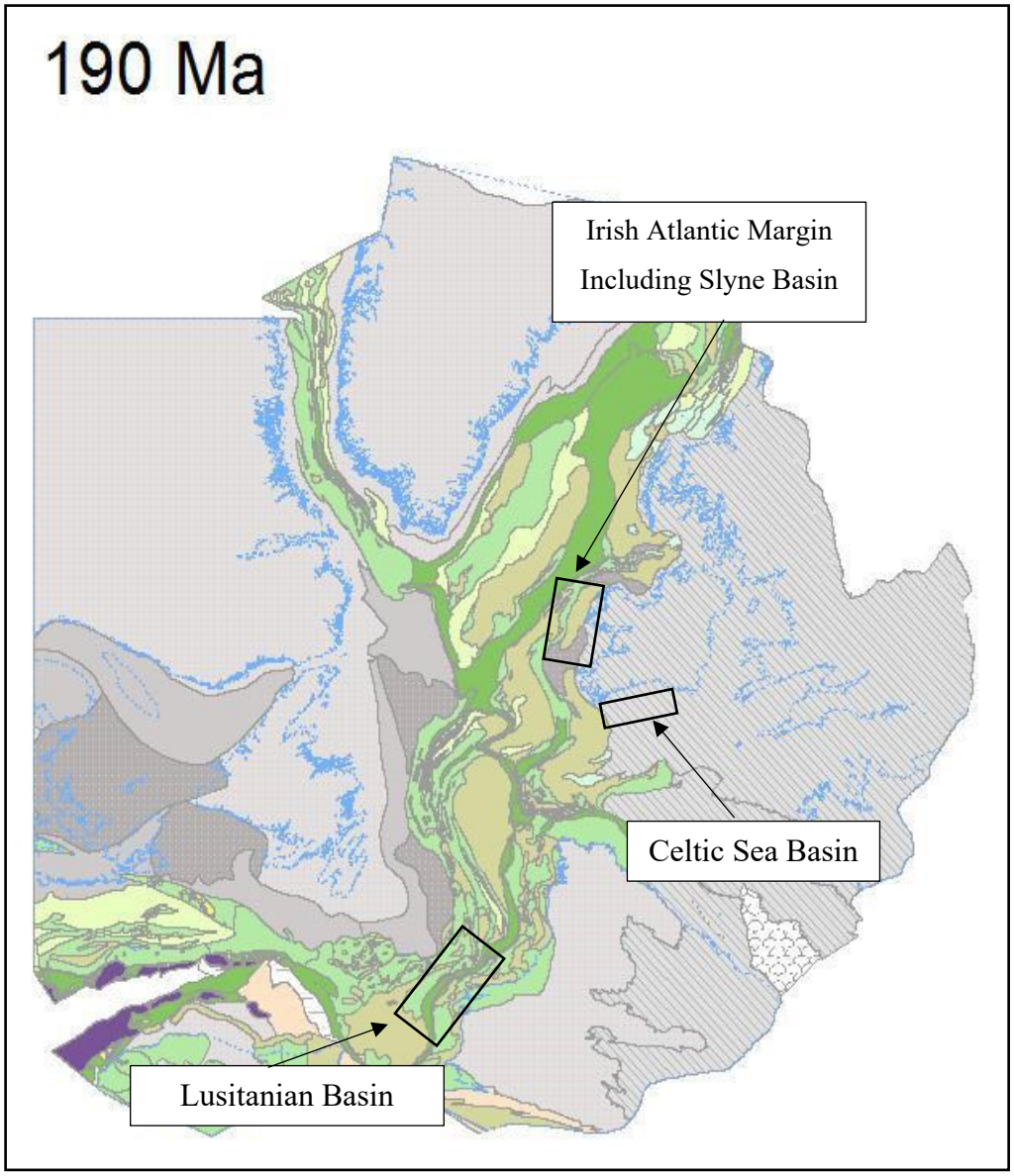

Figure 5: Post-rift tectonic setting of the central Atlantic during the Lower Jurassic (GeoArctic 2014). Basin accommodation space developed through continued rifting and subsidence from increased loading. Tertiary inversion of the basin halted the supply of sediment (Shannon, 2001.)

rift basement rock (i.e. that which lies below sedimentary cover) beneath the Slyne Basin is of Late Palaeozoic and Precambrian age (Spencer and MacTiernan, 2001). A plate reconstruction of the northern portion of the Atlantic Ocean between present-day Europe and Canada in the Lower Jurassic is presented in Figure 5 (GeoArctic 2014). This led to

the opening of the Atlantic Ocean during the Late Mesozoic – Early Cenozoic (Figure 6, Silva *et al.*, 2011, modified from Bassoulet, 1993, and Shannon *et al.,* 2005).

Three main phases of rifting occurred, during the Permo-Triassic (pre-Atlantic opening), the Mid-Late Jurassic and the Early-Mid Cretaceous. Rifting in the Slyne Basin appears to be along pre-Caledonian structural trends in an NE-SW orientation (Dancer, 1999; Shannon, 1991). Subsequently, the continental crust, which had experienced extension and thermal sag, provided accommodation space for proximal/inner neritic (max. ~200 m depth) shelf deposition of abundant terrestrial (including lacustrine/continental) sediment and marine organic matter from the Jurassic until the Tertiary – allowing for up to 7 km of sedimentation over 100 Ma until inversion (Murphy 1995).

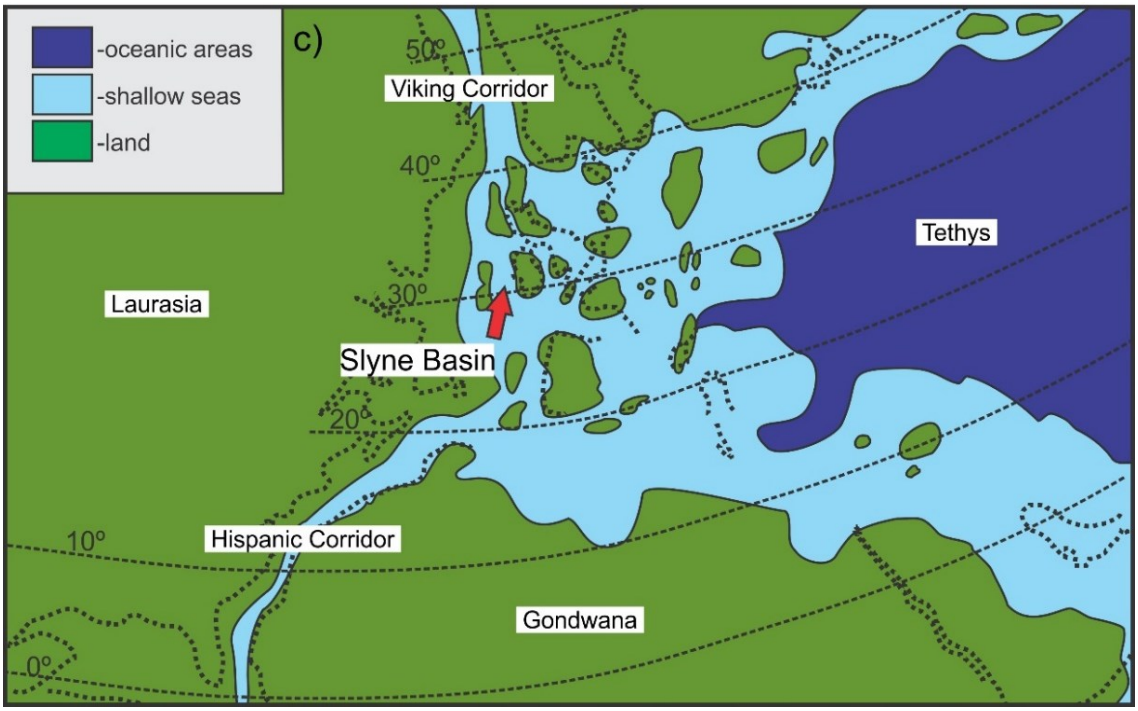

Figure 6: Palaeogeography of the Western Tethys and location of the Slyne Basin during the late Lower Jurassic (modified and simplified from Bassoulet et al., 1993, in Silva et al., 2011). The dashed line indicates present day shoreline.

The Slyne Basin has been the subject of significant exploration with proven commercial hydrocarbon discoveries. Originally, the primary target of exploration was Jurassic sandstone intervals. However, this interval has not yielded a commercial discovery. The secondary target, Permian sandstones containing dry gas sourced from Carboniferous Coal Measures, was named the Corrib gas field and commenced production in 2016.

2.4 TECTONIC HISTORY AND SEDIMENTARY INFILL OF THE SLYNE BASIN

The Slyne Basin was formed during the Permo-Triassic breakup of Pangea and rifting of Laurasia. Further south, the Porcupine Basin experienced two more significant phases of rifting in the Late Jurassic and Early Aptian, after which the basin failed to rift and remained as an NE-SW trending depocentre for continental siliciclastics to this day (Sinclair, 1995). Sinclair (1995) also describes the subsequent rift-induced subsidence and fault-block rotation during the mid-Aptian to Late Albian as forming a transgressive-regressive cycle, evident in sedimentary stacking cycles. This period was followed by intra-cratonic extension of the Continental European Margin, immediately preceding the Cenozoic period of Atlantic widening.

During the Lower Jurassic, especially in the Toarcian, this resulted in near-offshore mud-prone shelf deposition of abundant terrestrial and marine organic matter (e.g. Scotchman, 2001).

2.4.1 Lower Jurassic Sedimentary Formations in Slyne Basin

The following formations in the Slyne Basin have been studied for this project (Figure 7):

i) The Triassic Mercia Mudstone Formation marks the bottom of the Lower Jurassic section;

ii) Broadford Beds Formation Equivalent [Hettangian (-? Rhaetian)–Sinemurian] - clastic, carbonate and evaporitic sediments;

iii) Pabba Shale Formation Equivalent (Late Sinemurian) – carbonaceous pyritic claystone with TOC reaching up to 6.5 wt. %;

iv) Scalpa Sandstone Formation Equivalent (Early Pliensbachian) – predominantly sandstone/sandy limestones, to claystones, with calcareous siltstones;

v) Portree Shale Formation Equivalent (Toarcian) – thick sequence of carbonaceous claystones, with TOC reaching up to 7.8% wt.% (Scotchman, 2001).

vi) The informal "Middle Jurassic A and B" (Great Estuarine Group Equivalent) lie unconformably atop the Lower Jurassic.

Note that some completion reports use the now-defunct term "Middle Jurassic B" to include Aalenian to Bathonian sediments – this is now referred to as the Great Estuarine Group Equivalent (PAD*, pers. Comm.*; Trueblood and Morton, 1991; Dancer *et al.*, 1999; 2005 and references therein). Also, well reports on 18/25-1 discussing the Lower Jurassic section include references to the Pabba and Portree Shales (2630 m – 2734 m) and the Broadford Beds (2734 m – 3351 m). The terms "Broadford Beds" and "Pabba Shale" are informal terms for the entire Lower Jurassic section.

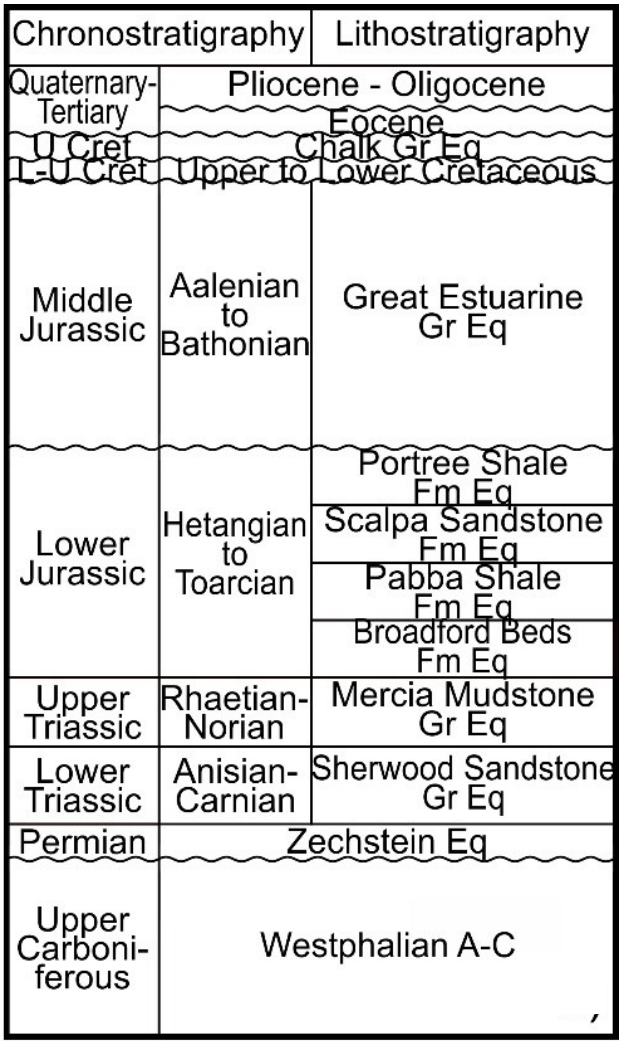

Figure 7: Chronostratigraphy and lithostratigraphy of the Slyne Trough, including the Basin, offshore Ireland. Modified from Dancer et al., 1999. Note that the Great Estuarine Group includes the Middle Jurassic B informal formation described in final well reports of 18/25-1.

2.4.1.1 Stratigraphy of studied wells

2.4.1.1.1 18/25-1, Slyne Basin

Enterprise Oil plc appraisal well 18/25-1 was spudded on 1st May 1999 (surface UTM coordinates E 366859.3 m; N 6021201.6 m). It reached the Lower Triassic Sherwood Sandstone Group equivalent at a total depth of 3770 m, intercepting approximately 700 m of Lower Jurassic sediments (Enterprise Oil, 2000) (Table 1).

A summary of this well is presented here; a detailed geological description can be found in well IRE 18/25-1 Geological Completion Report (Enterprise Oil, 2000) and a detailed biostratigraphic revision for the Slyne Basin was conducted by Millennia Limited (Millennia, 2004).

The Broadford Beds Formation Equivalent (Hettangian–Upper Pliensbachian; Millennia 2004) consists of interbedded claystone, sandstone, limestone, anhydrite and rare dolomite (Enterprise Oil, 2000). The claystone (occasionally grading to siltstone) is predominantly greyish black and massive. The sandstone is mostly light grey to brownish grey, translucent, very fine to fine, subangular, poorly to well sorted, contains loose quartz, and is occasionally well cemented, very hard, non-calcareous to slightly dolomitic (Enterprise Oil, 2000). Between 2766–2797 m, the sandstones are brownish-grey to brownish-black, with traces of organic matter and occasionally disseminated pyrite. The limestone is predominantly brownish grey, medium dark grey to olive grey, wackestone to packstone, is very hard, angular, and presents conchoidal fracture. Some organic matter and disseminated pyrite are also observed (Enterprise Oil, 2000).

The interval between 2706–2733.5 m MDBRT (Lower Jurassic Undifferentiated) is not assigned to a formal lithostratigraphic unit. It consists of thick light grey–greenish, fine-grained, slightly calcareous with quartz cement, sandstone beds interbedded with claystones (Enterprise Oil, 2000; Millennia, 2004). Although lithologically similar to the Scalpa Sandstone Formation Equivalent (Spinatum Zone, Upper Pliensbachian; Millennia, 2004), micropalaeontology and log analysis did not allow the definitive assignment of this unit to the aforementioned formation. The Pabba Shale Formation Equivalent (Davoei–

Margaritatus zones, Lower–Upper Pliensbachian; Millennia, 2004) is interpreted to be absent in this well.

The Portree Shale Formation Equivalent (Lower–?Middle Toarcian) consists of interbedded claystones (dark greenish grey to olive black, silty, slightly calcareous, slightly carbonaceous, and with rare pyrite nodules) and limestones (light brown and microcrystalline). From 2702 m, thick beds of fine-grained, light grey to greenish grey, slightly calcareous, quartz cemented sandstones are interbedded with the claystone (Enterprise Oil, 2000). A Lower–?Middle Toarcian age is assumed for this interval. This assumption is based on palynofacies (occurrence of abundant Amorphous Organic Matter) and limited macrofaunal evidence (abundant occurrence of prasinophyceaen algae and *Corollina* spp.; Millennia, 2004). At a basinal scale, this palynological assemblage is characteristic of the Portree Shale Formation Equivalent. A possible major stratigraphic break is interpreted between the Lower Pliensbachian and Lower Toarcian (Enterprise Oil, 2000; Millennia, 2004).

The Middle Jurassic (Great Estuarine Group Equivalent) comprises dark grey to greyish brown homogeneous claystones, with occasional traces of shell debris and rare nodular pyrite. The base of this unit is dated from the Aalenian (Enterprise Oil, 2000; Millennia, 2004).

2.4.1.1.2 Well 27/13-1, Slyne Basin

Well 27/13-1, located 90 km offshore Ireland, was the first well drilled in the Slyne Trough by then-operator Elf Aquitaine. Situated in 191 m of water at 53° 33’ 26.7” N, 11° 24’ 37.0” W, the well reached TD at 2,725 mDBKB (2,701 TVDSS) on 31st December 1981, targeting Upper Triassic sandstones (Elf Aquitaine, 1982).

In well 27/13-1, the depositional environment was interpreted to be deltaic to sabkha in the oldest sediments (Rhaetian - Hettangian), marginal marine in the Sinemurian, inner neritic from the Pliensbachian to the Early Bajocian. It then regressed briefly in the Bajocian to a marginal marine to inner neritic setting, followed by a trend from lacustrine to deltaic in the Bathonian to Bajocian and finally continental fluviatile in the Bathonian – Bajocian (Elf Aquitaine, 1982).

Unlike the previous well (18/25-1), well 27/13-1 was described using a different nomenclature, namely Dogger (615 m – 1975 m) and Lias (2035 m – 2611 m) for the interval of interest. Millennia (2004) re-assessed the well and assigned the following formation characteristics:

The Broadford Beds Formation (Hettangian–Lower Pliensbachian, Table 2) consists of alternating claystone, siltstone, and limestone, with some sand layers. It is interbedded with limestones that are locally argillaceous and oolitic with varying thicknesses (often thicker with increasing age). Sinemurian sections are intermittently well-defined biostratigraphically, with indications of a shallow marine deposition. However, the occasional poor recovery of microfauna also point to a fluctuating environment within said shallow environment (Millennia, 2004).

The Pabba Shale, of solely Pliensbachian age, comprises 127 m of well 27/13-1. It is a thick dark grey claystone with locally sandy intervals and occasional stringers of limestone and lignitic debris and micropyrite. It is well constrained biostratigraphically in well 27/13-1 and indicates an inner neritic to distal marine depositional setting (Millennia, 2004).

The Scalpa Sandstone features a cycle of claystone, siltstone and sandstone and coarsens upward within a 119 m section of well 27/13-1. It displays light grey, sandy siltstones and silty claystones, grading into silty micro micaceous claystones with local limestone stringers. The biostratigraphy encountered displays evidence of normal marine shelf conditions during deposition (Millennia, 2004).

The Portree Shale features brown organic-rich claystones, representing 84 m of section drilled in well 27/13-1. It is organic-rich and is biostratigraphically well-constrained with abundant amorphous organic matter (Millennia, 2004)

As the Late Toarcian is biostratigraphically absent between the Lower Toarcian and the Middle Jurassic B (Great Estuarine Group Equivalent) and a major unconformity is inferred. Beneath the Lower Jurassic section, the Penarth Group forms a conformable contact (Millennia, 2004; Ainsworth, 1990).

Table 1: Age and lithostratigraphy of the well 18/25-1, Slyne Basin, offshore Ireland (Enterprise Oil, 2000)

Age	Formation	Depth (m) (MDBRT)
Aalenian		2532–2622
stratigraphic break		
Lower Toarcian		2650–2706
	Top of Lower Jurassic Undifferentiated	2706.0
	stratigraphic break	
Lower Pliensbachian		2724.0
	Top of Broadford Beds Formation Eq.	2733.5
Lower Pliensbachian		2776.0
	stratigraphic break	
Upper Sinemurian		2779–2836
	stratigraphic break	
Lower Sinemurian-Hettangian		2857–3340

MDBRT - Measured Depth Below Rotary Table; Eq. - equivalent

Table 2: Age and lithostratigraphy of well 27/13-1, Slyne Basin Offshore Ireland (Elf Aquitaine, 1982)

Age	Formation	Depth (m) (MDBKB)
Bajocian - Bathonian		759.9-1873
	Dogger	
Bajocian		1875/85 – 2003
	|	
Early Bajocian – Toarcian		2019/23-2170
	Lias	
Pliensbachian		2178/85-2357
	|	
Sinemurian		2365-2591
	|	
Hettangian – Rhaetian		2615/18.5-2713
	|	
Rhaetian		2715-2725

2.5 SOURCE ROCKS IN THE LOWER JURASSIC RECORD OFFSHORE WEST IRELAND

The Upper Jurassic–Cretaceous Kimmeridge Clay Formation equivalent were originally thought to be the only viable hydrocarbon source rocks in Ireland's offshore, following exploration results in the North Sea (Scotchman, 2001). However, the recognition of Lower Jurassic source rocks as having contributed to hydrocarbons accumulations resulted in new approaches to offshore exploration in the region.

Hydrocarbon source rock development in the Jurassic was largely related to the early development of a marine setting, with the onset of transgressive-regressive depositional cycles (Scotchman, 2001). Cope (1997) relates these to both tectonic (extensional) and eustatic events. During the transgressive portion of these cycles, the main source rocks of the Irish offshore were laid down concurrently in the early Sinemurian, Sinemurian – Pliensbachian and Toarcian timeframes and in relatively deepwater settings. Reasons for enhanced preservation of TOC are thought to be a combination of high levels of primary production and anoxic prevention of decomposition in the water column (van Buchem, 1995; Pedersen and Calvert, 1990; van de Schootbrugge, 2013; Scotchman, 2001).

2.5.1 Geochemistry

Early geochemical analyses, for example by Scotchman (1995, 2001), investigated the nature of Irish hydrocarbon source rocks and how they could be compared to discoveries in other locations, such as the North Sea. He concluded that oil-source geochemical studies on produced oils and previously drilled Lower and Middle Jurassic mudrocks from the Atlantic margins display some similarities with Lower Jurassic-sourced oil production at

sites such as Wytch Farm and Kimmeridge Bay in the United Kingdom. Sediments of this age are found as predominantly shaly facies with good source potential in other basins where wells have penetrated great thicknesses of Toarcian sediments in the Irish Sea, Celtic Sea, and off northern coasts (Scotchman, 2016 and references therein). In Rockall and Porcupine Basins (Figure 4), Lower Jurassic strata are known to be present only in a few places where wells have penetrated deep enough. Although these strata are assumed to be laterally continuous and thicken in the synclines of the basin, drilling has not been able to prove this consistently (Scotchman, 2016 and references therein).

2.5.1.1 $\delta^{13}C$ Record

In the Slyne Basin, only one stable carbon isotope analysis was available for well 27/13-1 in Jones (1992). Results of the analyses of saturated hydrocarbon fractions from below 2095 m were rarely reported, but indicate a variation in $\delta^{13}C$ between -27 and -30 ‰. These data show organic matter input consisting of marine and terrestrial matter (Jones, 1992).

Multiple carbon cycle perturbations have been recorded in the $\delta^{13}C$ record across the Mesozoic time scale, including Toarcian (Hesselbo, *et al.* 2000, Kemp, *et al.* 2005), Albian-Cenomanian (Gale, *et al.* 1996) and Cenomanian/Turonian (Arthur, *et al.* 1988) ages and across the Permian-Triassic boundary. Large negative excursions (~6 ‰) in Iran and South China across the Permian-Triassic boundary are interpreted to indicate widespread changes to the carbon cycle (Shen, *et al.* 2013). Increased volcanic activity in Siberia and South China and subsequent release of carbon (from sill intrusion into organic-rich strata or evaporation of methane hydrates) is inferred to be the initial cause of these perturbations (Shen, *et al.* 2012). Berner (2003) refers to carbon cycle modelling that has

indicated volcanism as being non-viable for the whole $\delta^{13}C$ n-CIE (negative carbon isotope excursion), and that positive feedback measures are required (e.g., Clathrate release). Also, analysis of relevant samples from their study area indicated an n-CIE lasting >3 Ma, which may have required more than a local input of clathrate. When considering the Toarcian age, emplacement of the Karoo-Ferrar continental basalts (a Large Igneous Province - LIP) is the major volcanic event at 182 Ma (Duncan, 1997).

When comparing negative-CIEs in relation to organic matter origin, Toarcian sediments exhibited negative CIEs of 7 ‰ in typical marine organic matter and 6 ‰ in marine carbonates (Caswell, 2009). In "The Biomarker Guide (Peters, *et al.*, 2005)," it is surmised that source rock extracts (e.g., bitumen) are depleted by 0.5-1.5 ‰ compared with kerogen (or kerogen is enriched, compared to extracts). Peters, *et al.* (2005) also show $\delta^{13}C$ to be a valuable oil-source correlation tool, especially regarding identification of diagenetic fluid pass-through.

Hesselbo, *et al.* (2000, 2007) and McElwain, *et al.* (2005) indicate a negative CIE is also present in fossil wood – a finding which may indicate the presence of isotopically light CO_2 in both ocean and atmosphere during the period. This would indicate that the carbon-cycle perturbation was widespread, at least in the regions studied. The Early Toarcian also may bear evidence of increased chemical weathering of a continental landmass, i.e. accelerated hydrological cycles (Cohen, *et al.*, 2004).

However, Barbu (2014) concluded that because a high TOC value was recorded after a positive carbon isotope excursion in the Cretaceous record of the Carpathians, a relationship between TOC and a CIE is not always seen. They also issued caveats regarding diagenetic effect upon the interpretation of carbon and oxygen stable isotope records –

notably that meteoric water flowing through a rock body may overprint the carbon record and leave an isotopically lighter signature. $\delta^{18}O$ has not been previously investigated in these wells.

2.5.2 Palaeoenvironmental constraints by age

Table 3: Lower Jurassic stages and their corresponding ages (Cohen, et al. 2013).

Series	Stage	Age (Ma)
Lower Jurassic	Toarcian	182.7 ±0.7 Ma – 174.1 ±1.0 Ma
	Pliensbachian	190.8 ±1.0 Ma – 182.7 ±0.7 Ma
	Sinemurian	199.2 ±0.3 Ma – 190.8 ±1.0 Ma
	Hettangian	201.3 ±0.2 Ma – 199.3 ±0.3 Ma

2.5.2.1 Hettangian

Hettangian to Rhaetian ages sediments in the Slyne Basin were interpreted to be deposited in deltaic to sabkha depositional environments, with localised marginal marine conditions, specifically "brackish to fresh waters, marginal marine to lacustrine conditions" (Elf Aquitaine, 1982).

2.5.2.2 Upper Sinemurian (199.3 ±0.3 Ma – 190.8 ±1.0 Ma)

Upper Sinemurian depositional sequences further south of the study area, within the Celtic Sea, were interpreted to have been deposited in a marginal marine and inner shelf to marginal marine setting (Elf Aquitaine, 1982) with up to six transgression cycles evident (Kessler and Sachs, 1995).

2.5.2.3 Uppermost Sinemurian–lowermost Pliensbachian

An important source rock interval of the 27/13-1 well (Trueblood, 1992; Trueblood and Morton, 1991), in the sedimentary succession interpreted as inner shelf marine, topped by a restricted marine sequence in the Toarcian (Elf Aquitaine, 1982).

2.5.2.4 Pliensbachian Organic Matter Preservation Events

While OAEs are responsible for global scale organic matter preservation, Silva *et al.* (2011) suggest the term Organic Matter Preservation Interval (OMPI) for occurrences on a smaller scale. While two positive carbon isotope excursions had previously been identified in Lower Jurassic shales from the Lusitanian Basin (Jenkyns, 2002), a high-resolution analysis by Silva *et al.* (2011) resulted in the identification of a third. These three positive CIEs are all biostratigraphically age-constrained to around 187 Ma, prior to and possibly influencing the development of the T-OAE. These OMPIs are expressly identified by their $\delta^{13}C$ signature.

2.5.2.5 Toarcian Oceanic Anoxic Event

The T-OAE itself exhibits a global increase in marine organic carbon deposition in the form of black shales preserved by oxygen-depleted marine waters alongside a significant mass extinction event (Jenkyns and Clayton, 1986; Jenkyns, 1988).

Global climatic events during the Pliensbachian and Toarcian (190 – 174 Ma) resulted in the deposition of organic-rich shales bearing geochemical characteristics indicative of periods of oxygen-depleted conditions during the development of a young Atlantic Seaway (e.g. Silva and Duarte 2015 and references therein). In marine environments, the rate of accumulation and preservation of organic detritus governs the development of an organic carbon-rich shale – oceanic anoxia is, therefore, an important component in the development of some hydrocarbon source rocks by way of hindering carbon biodegradation and recycling (Figure 9).

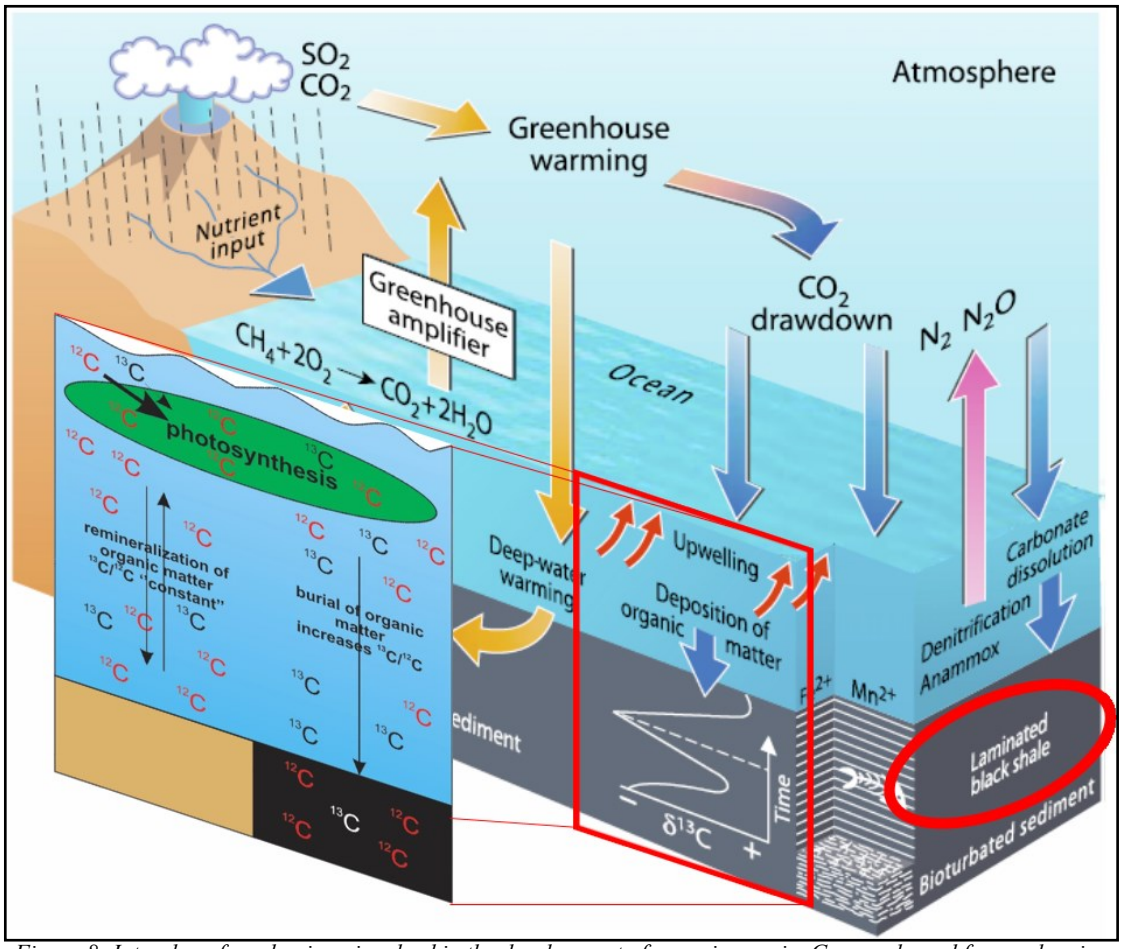

Figure 8: Interplay of mechanisms involved in the development of oceanic anoxia. Gases released from volcanic activity trigger atmospheric warming, with vented CO_2 causing acidification and warming of ocean waters. Further CO_2 is released from dissolved carbonates and now-destabilized gas hydrate deposits. Accelerated hydrological cycles increase the sediment supply, and enhanced primary productivity results in high sedimentation of organic matter and preferential uptake and preservation of ^{12}C. Aerobic biodegradation of organic matter results in oceanic anoxia, cessation of aerobic processes and high TOC preservation in black shale sediments (adapted from Jenkyns 2010).

The development of oceanic dysoxia (waters having a very low oxygen content; Tyson and Pearson, 1991) and anoxia is thought to have been brought about by a complex interplay of global mechanisms (variation of continental weathering, input of isotopically light CO_2 from volcanoes and/or dissociation of methane gas hydrates) and local conditions (enhanced nutrient supply allowing for increased primary productivity) (e.g. Silva *et al.*, 2015). Of the latter, high primary productivity depleted bottom waters of oxygen through oxidation of organic matter and non-mixing of bottom waters to replenish oxygen, resulting in TOC preservation (sometimes up to 20 wt.%, e.g., on the Yorkshire Coast; Gale, 2012). Of special interest to this project are Toarcian organic-rich shales which have been identified as potential hydrocarbon source rocks (Shannon *et al.*, 2007) in Ireland's Slyne and Celtic Sea Basins (Murphy 1995).

Studies of the T-OAE have resulted in many different interpretations of its origins (see Hesselbo *et al.*, 2007), with some suggesting that the effects of the T-OAE can be linked temporally to astronomical forcing parameters, specifically, 36 ka and 21 ka precession and obliquity Milankovitch cycles (Kemp *et al.* 2011). They quantified the duration of the negative carbon isotope excursion (indicating sequestration of lighter ^{12}C) to have been 1.9 Ma. This argument implies a 36 ka and 21 ka cyclicity (related to obliquity and precession, respectively) for the $\delta^{13}C$ (e.g. Kemp *et al.* 2005), TOC, $CaCO_3$, and S record on England's Yorkshire coast. Others suggest the onset of the T-OAE is due to the release of massive quantities of methane, reducing oceanic O_2 and allowing for preservation of TOC-rich black shales (Hesselbo *et al.* 2007). What is especially useful is the global expression of such CIEs, which has been recorded in the Posidonia shale of Northern Europe (Kuspert, 1982), the Cleveland Basin of present-day Great Britain (Cohen *et al.* 2007), Greece

(Kafousia *et. al.* 2014) Argentina (Al-Suwaidi, 2010), Canada (Caruthers *et al.* 2011) and Japan (Wignall, *et. al.* 2010, Gröcke *et al.* 2011). In Yorkshire, UK, outcrops of Toarcian-aged sediments allow for very high-resolution geochemical analyses which indicate that the overall negative CIE included several higher order cycles, lending support to the theory of episodic ^{12}C enrichment during volcanism or methane hydrate release – i.e. inputs of isotopically light carbon were pulsed, rather than steady (Jenkyns, 2010; Kemp, 2011). Where Toarcian-aged rocks can be seen on land (e.g. Lusitanian Basin, Portugal), high-resolution geochemical analyses (i.e. high density of samples of an outcrop) are possible: these include $\delta^{13}C$ and $\delta^{18}O$ bulk elemental analysis (Hesselbo *et al.*, 2007). Although Scotchman (2001) summarized similarities between the Slyne Basin and other hydrocarbon source rocks through geochemical analysis of their produced oils, it may be possible to use characteristics such as Rock-Eval pyrolysis, stable isotope analysis, bulk geochemistry and total organic carbon values from source rocks themselves to compare basins across the Irish Atlantic Shelf (di Primio *et al.*, 2008).

While their causes remain the subject of debate, OAEs are by no means rare in the geological record –prior to the T-OAE, they have been identified in the Late Valanginian ("Weissert Event"), Late Hauterivian ("Faraoni Event"), Early Aptian ("La Selli Event"), Early Albian ("Paquier Event"), Late Albian ("Breistroffer Event"), Cenomanian-Turonian ("Bonarelli Event"), Coniacian-Santonian ("OAE 3") and most recently at the Palaeocene-Eocene Thermal Maximum (Jenkyns, 2010, and references therein; Mattioli *et al.*, 2014; Baudin *et al.,* 1999, 2005, 2014; Schlanger and Jenkyns, 1976; Arthur *et al.,* 1990; Follmi *et al.,* 2012; Bréhéret, 1995)

CHAPTER 3: MATERIALS AND METHODS

3.1 SAMPLING

During original drilling of these wells, samples were collected on board the drilling rigs at intervals requested by the operator (e.g. intervals of 3 m or 6 m were designated for sample collection during drilling of well 18/25-1, while samples were collected at 2.5 m or 5 m intervals in well 27/13-1.). These samples were originally collected during drilling as wet, unwashed well cuttings (broken rock collected with drilling muds). Each collected sample was bagged and returned in duplicate to the operator and the national regulator, the Petroleum Affairs Division (PAD) in Dublin, Ireland.

Prior to sampling for this study, geological reports from offshore exploration were requested from the PAD in Dublin, including geological completion reports, micropalaeontological charts, palynological charts, maturity reports, sedimentological core logs, wireline and stratigraphical summary logs. Sampling targeted dark, shaley intervals of Lower Jurassic age. At the PAD sample storage facility in Sandyford, Ireland, twenty-three bulk samples and four core samples were collected from wells 18/25-1 and 27/13-1 by Dr Ricardo Silva and Charles Carlisle. Five more samples were collected at the storage facility from well 27/13-1 in 2015. Samples were collected as bulk samples directly from sample bags. Samples were also collected from wells 26/22-1(A) and 62/7-1, however these proved unsuitable to include in this study.

Table 4: Depth of samples collected from wells 18/25-1 and 27/13-1.

Well Number	Sample Type	Depth of Sample (m)
18_25-1	Cuttings (Wet, Unwashed	2610-2616
18_25-1	Cuttings	2622-2628
18_25-1	Cuttings	2634-2640
18_25-1	Cuttings	2646-2652
18_25-1	Cuttings	2658-2664
18_25-1	Cuttings	2670-2676
18_25-1	Cuttings	2682-2688
18_25-1	Cuttings	2694-2700
18_25-1	Cuttings	2706-2712
18_25-1	Cuttings	2718-2724
18_25-1	Cuttings	2730-2736
18_25-1	Cuttings	2742-2748
18_25-1	Cuttings	2785-2788
18_25-1	Cuttings	2791-2794
18_25-1	Cuttings	2797-2800
18_25-1	Cuttings	2809-2812
18_25-1	Cuttings	2821-2824
27_13-1	Cuttings	2095
27_13-1	Cuttings	2127
27_13-1	Cuttings	2157
27_13-1	Cuttings	2217
27_13-1	Cuttings	2333
27_13-1	Cuttings	2345
27_13-1	Core	2494.1
27_13-1	Core	2494.7
27_13-1	Core	2496.65
27_13-1	Core	2497.2
27_13-1	Cuttings	2585
27_13-1	Cuttings	2587
27_13-1	Cuttings	2665
27_13-1	Cuttings	2677
27_13-1	Cuttings	2685

3.1.1 Well 18/25-1

Cuttings from this well were collected at the drill site at 3-6 m intervals by separation from returned fluids with a screening system. Samples were then stored in four sets of both bulk unwashed and washed and dried specimens (then sent to Project partners and the PAD). Per the Geological Completion Report, the Lower Jurassic (1418m – 3523 m) section of well 18/25-1 was drilled using "BW Ecomul" synthetic muds. Ecomul is based on Poly Alpha Olefin (PAO), Linear Alpha Olefin, and Paraffin. At some point, suspected but not confirmed to be before drilling of well 18/25-1, Ecomul ceased to incorporate PAO – as such, samples required rinsing of remnant drilling fluids (Enterprise Energy Ltd, 2014). Note that due to the crushing of samples during drilling, it was not possible to screen bulk samples for cavings from other sections of the well (i.e. a section other than that reported).

Seventeen samples from unwashed wet drill cuttings (Table 4), corresponding to limestones and organic-rich marls and mudstones, were collected and shipped to the Basin and Reservoir Lab, Dalhousie University where they were rinsed with warm water to remove as much drill fluids as possible. Samples were viewed under a microscope and picked for visible contaminants (e.g. paint chips, lignite) to the best of my ability. The samples were then dried in an oven at 30°C. From each sample, about 10 g was crushed, packaged in sample tubes, and sent to GeoMark Laboratories for TOC determination, Rock-Eval Pyrolysis and IsoAnalytical Laboratories for $\delta^{13}C$ and $\delta^{18}O$ determination in bulk carbonates (carbonates) and carbonate-free (kerogen) isolates. The remainder of the sample was kept for XRF analysis in-house. The returns from the laboratories were also catalogued and preserved for return to the PAD on project completion.

3.1.2 Well 27/13-1

According to drilling reports, cuttings from this well were labelled as being from a specific depth within the well (rather than a range, as in 18/25-1, above – this is due to differing operating procedures between operators). Wet, unwashed samples were collected at 2.5 m intervals from drill fluid returns and separated into collections for the project partners and PAD. The core was cut for stratigraphic analysis at the depth sampled in this project (Elf Aquitaine, 1982). Drilling muds used are unknown. As with the previous well, it was not possible to screen bulk samples for cavings (samples returned from shallower well sections than the actual depth of the bit at the time of recording).

Eleven cuttings samples were taken in two separate visits to the core facility and prepared in a similar manner to those from well 18/25-1 above (rinsing, removing obvious contaminants, drying, crushing and dispatch). Also, four core samples were taken which were either dispatched whole or crushed. The remainder of the sample was kept for XRF analysis in-house. The returns from laboratories were catalogued and preserved for return to the PAD on project completion.

3.2 TOTAL ORGANIC CARBON (TOC)

3.2.1 Method

GeoMark Research Ltd. (USA) carried out TOC analysis using LECO C230 apparatus. Samples were rinsed, cleaned of obvious contaminants, crushed and dispatched to GeoMark where they were first decarbonated using hydrochloric acid for a minimum of two hours, then water rinsed and flushed in a filtration kit to remove acid traces. The sample was then weighed and dried in an LECO crucible at 110°C for at least 4 hours. This high

temperature volatilizes free hydrocarbons such as those introduced from drilling muds and those already expelled from source rock. An induction furnace within the LECO C230 apparatus then combusted samples, duplicates and standards at ~1200 °C in an oxygen-rich (99.5%) atmosphere. A catalyst converted CO to CO_2 in resultant gases, and CO_2 was then measured by an infrared cell and converted to TOC wt.%, based on the dry sample weight. GeoMark carry out in-house quality control, including analysis of "standards … as unknowns every 10 samples [in order] to check the variation and calibration of the analysis. Random and selected reruns are done to verify the data. The acceptable standard deviation for TOC is 3% variation from established value (GeoMark Procedures Report, 2016, pers. comm.).

3.2.2 Data presentation and analysis

Results from LECO TOC analysis are given as a weight percentage (wt. %) for each sample alongside other analyses in the results spreadsheet from GeoMark, indicating Project ID, well name, depth of sample and experimental notations. When plotted against depth, TOC shows the varying level of organic enrichment ("richness") of a well section and can be split per the following criteria from Tyson (1995):

- 0-1 wt.% = poor,
- 1-2 wt.% = fair,
- 2-4 wt.% = good
- 4+ wt.% = excellent

TOC is also used alongside pyrolysis results to calculate many of the parameters outlined in Section 3.3.2 below).

3.3 ROCK-EVAL PYROLYSIS

3.3.1 Method

In Rock-Eval, a sample is measured for the petroleum producing potential and the type and maturation state of the organic matter contained within. In the case of a mature source rock without a migration pathway, Rock-Eval will also indicate the quantities of free hydrocarbon present (Lafargue *et al.* 2003). RockEval is the registered trademark of the French Institute of Petroleum (Institut Français du Pétrole - IFP), the designer of the original pyrolizer.

Rock-Eval pyrolysis analysis was carried out by GeoMark Research Ltd (USA), as was LECO TOC (Section 3.2 above). Rock-Eval-2, based on the process designed by Espitalié *et al.* (1977), combines pyrolysis ("the decomposition of organic matter by heating in the absence of oxygen") with the prior results of TOC analysis (Section 3.2) to evaluate the propensity of a given sample to generate hydrocarbons and its thermal maturity.

For Rock-Eval pyrolysis determinations, ~100 mg of crushed sample was heated in a pyrolysis oven with an inert atmosphere of helium to 550 ºC, per the analytical procedures outlined by Espitalié *et al.* (1977, 1985) and Peters (1986). Standard samples with established concentrations were analysed as unknowns every ten samples to check precision and accuracy of the laboratory measurement process. In addition to TOC values, direct measurements obtained by this procedure include S_1 (mg HC/g rock), S_2 (mg HC/g rock), S_3 (mg CO_2/g rock), and T_{MAX} (ºC) (e.g. Tissot and Welte, 1984).

To carry out this analytical process, the pyrolysis oven is first flushed with an inert atmosphere (helium) then heated to and kept at 300 °C for five minutes as free

hydrocarbons are volatilized. These are measured as the S_1 peak (detected by Flame Ionization Detector - FID), and the temperature is increased to 550 °C at a steady rate of 25 °C/min. The released hydrocarbons are measured as the S_2 peak. The temperature at which S_2 peaks is registered as T_{MAX} (°C) and depends on the nature and maturity of the kerogen. Cracking of kerogens releases CO_2 between 300 and 390 °C. This trapped CO_2 is detected on a Thermal Conductivity Detector between these temperatures as the S_3 peak. Others parameters (derived measurements) such as Hydrogen Index (HI = S_2/TOCx100), Oxygen Index (OI = S_3/TOCx100), Production Index (PI = $S_1/(S_1 + S_2)$), and Normalised oil content (NOC = S_1/TOC) were calculated (e.g. Espitalié *et al.*, 1977, 1985; Peters, 1986).

To address analytical uncertainty, GeoMark adhere to the following in-house process: "Instrument calibration is achieved using a rock standard. Its values were determined from a calibration curve to pure hydrocarbons of varying concentrations. This standard is analyzed every 10 samples as an unknown to check the instrument calibration. If the analysis of the standard ran as an unknown does not meet specifications, those preceding data are rejected, the instrument recalibrated, and the samples analyzed again. However, normal variations in the standard are used to adjust any variation in the calibration response. The standard deviation is considered acceptable under the following guidelines: T_{MAX}: ± 2ºC, S_1, S_2: 10% variation from established value and S_3: 20% variation from established value. Analytical data are checked selectively and randomly. Selected and random checks are completed on approximately 10% of the samples. A standard is analyzed as an unknown every 10 samples" (GeoMark Procedures, pers. comm.).

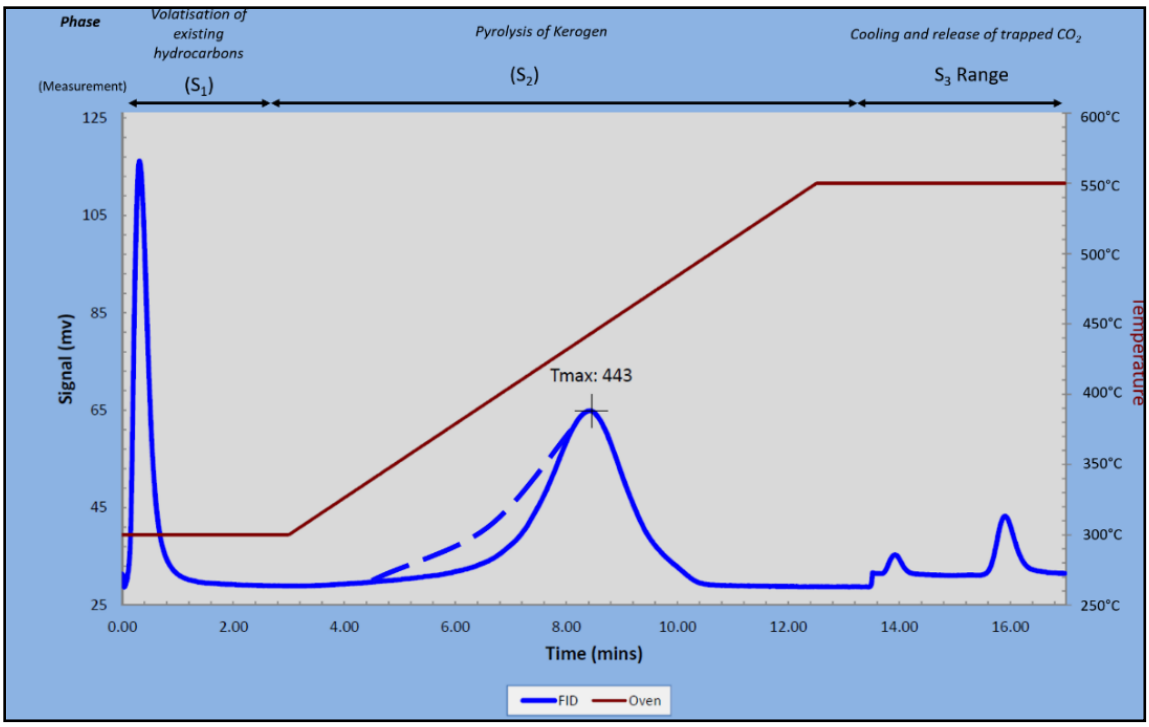

Figure 9: Cycle of Pyrolysis phases (adapted from Tyson, 1995 and Tissot and Welte, 1984). Note that FID = Flame Ionisation Detector and FID response is recorded. Also, the effect of a Low Temp S2 Shoulder on a sample is indicated by a dashed line. In the absence of contaminants, the peak would be symmetrical in signal amplitude over time.

3.3.2 Data presentation and analysis

3.3.2.1 S_1

S_1 is the measure, in milligrams, of hydrocarbon initially present in the sample (Tyson, 1995). This corresponds to the first pyrolysis peak indicated and depicts the concentration of volatile hydrocarbons in milligrams of hydrocarbon per g of sample. Specifically, this is a measurement of free hydrocarbons - i.e. those previously cracked from kerogen during hydrocarbon maturation, those introduced from a separate petroleum system, or those introduced during recovery and storage of samples.

3.3.2.2 S_2

S_2 is the measure, in milligrams, of hydrocarbons evolved from the thermal alteration of kerogen (Tyson, 1995). This is the second peak indicated by the RockEval method, and essentially depicts convertibility of non-volatile organic material (kerogen) to oil and gas. The value is normalised to sample weight. Where a "Low Temp. S_2 Shoulder" warning is given by the apparatus, cracking of heavier hydrocarbons (from contamination) is indicated.

3.3.2.3 S_3

S_3, measured in milligrams, is the concentration of carbon dioxide released during pyrolysis of kerogen per gram of sample. This results from the thermal breakdown of "oxygenated organic compounds", and are considered largely unreliable in cases of high carbonate content (Tyson, 1995).

3.3.2.4 T_{MAX}

T_{MAX} is the oven temperature, in °C, at the point at which the S_2 peak is measured, indicative of the temperature of maximum hydrocarbon evolution from kerogen (Tyson, 1995). This parameter can be used as a proxy for the thermal maturity of the sample, but it is important to note that the turbine drilling method, as used in well 18/25-1 and 27/13-1 may induce temperatures in excess of 400°C at the drill bit, possibly affecting T_{MAX} values during RockEval pyrolysis.

3.3.3 Derived Data Presentation and Analysis

3.3.3.1 Hydrogen Index

Per Tyson (1995), one of the most reliable parameters for determining source rock potential is the Hydrogen index (milligrams of hydrocarbon evolved during kerogen breakdown, divided by wt. % TOC, x 100 -mg HC/g TOC), as given by Equation 1:

$$\text{HI} = \frac{S2}{TOC} x\ 100$$

Equation 1: Hydrogen Index from Rock-Eval pyrolysis results

Hydrogen Index (HI) describes the amount of hydrogen relative to the amount of (organic) carbon in a sample and can be used as a proxy for the hydrogen: carbon atomic ratio.

3.3.3.2 Oxygen Index

This is a ratio of CO_2 (using the S_3 value from RockEval) to TOC and is calculated using Equation 2:

$$OI = \frac{S3}{TOC} x\ 100$$

Equation 2: Oxygen Index, as calculated using pyrolysis and LECO analysis results.

Oxygen Index (OI) describes the amount of oxygen relative to the amount of hydrocarbon in a sample and can be used as a proxy for the oxygen:carbon atomic ratio.

3.3.3.3 Organic matter typing - modified van-Krevelen diagram (HI vs. OI)

The HI and OI values are used in place of the hydrogen/carbon elemental ratio used in a van Krevelen diagram to produce a *pseudo* van Krevelen diagram. These can also be used to assess thermal maturity, using a modified van Krevelen diagram calibrated to vitrinite reflectance.

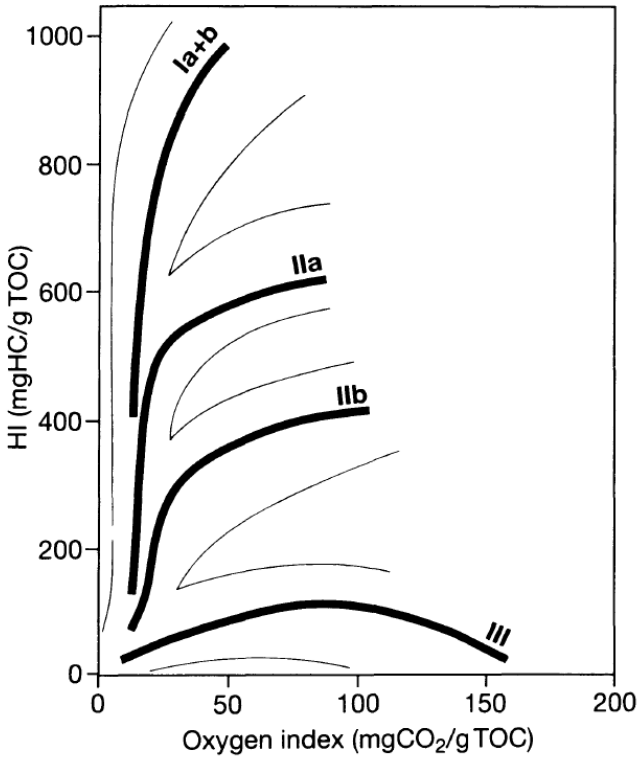

Figure 10: Modified van Krevelen diagram showing zones for typing kerogen types based on HI vs. OI content. The typing boundaries vary depending on interpretation – this is from Tyson (1995), but many will replace IIb with III and III with IV.

Table 5: Kerogen Types (Tyson, 1995)

Kerogen Type Designation	Deposited Material	Depositional Environment
I	Mainly algae	Lacustrine
II	Mostly plankton/some algae	Marine
III	Mostly woody plant material	Terrestrial
IV	Reworked or oxidised material	Mixed/changeable

3.3.3.4 Normalised Oil Content

Normalised Oil Content (NOC), measured in µg HC/ g TOC is an indication of maturity (or level of contamination) of a source, which indicates the quantity of free hydrocarbons in a sample compared to the amount of TOC, given by the equation

Equation 3: Normalised Oil Content

$$NOC = \frac{S1}{TOC}\ x\ 100$$

NOC is used to assess thermal maturity and presence of contamination (from drilling fluids) or migrated oil from a separate source, based on the following criteria (from Ruble, 2012):

- <50 indicates low hydrocarbon potential *OR* over mature source rock,
- 50-100 indicates mature source rock,
- >100 indicates productive source rock *OR* contamination.

3.3.3.5 Kerogen Quality

Langford and Blanc-Valleron (1990) proposed kerogen typing by plotting TOC against S_2, with the typing boundaries calibrated to the HI of a consistent database of mudstone samples.

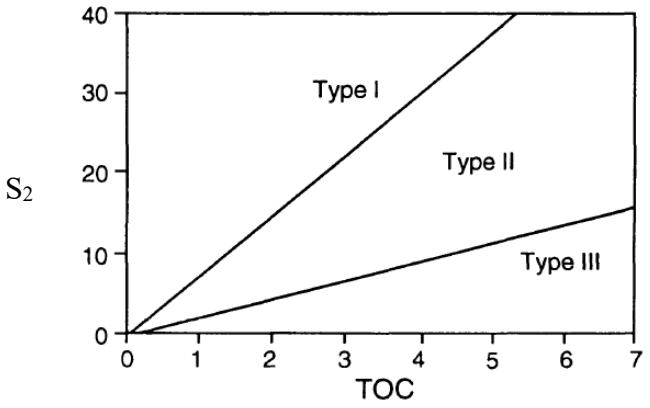

Figure 11: Kerogen typing plot, after Langford and Blanc-Valleron, 1990.

3.3.3.6 Kerogen type and thermal maturity – (HI vs. T_{MAX})

Plotting HI vs. T_{MAX} gives both a typing and a calibrated vitrinite reflectance equivalent (R_0), giving an indication of both capability to produce hydrocarbons and thermal maturity of kerogen (Jarvie and Baker, 1984; Delvaux *et al.,* 1990). This method is only suitable for samples with a TOC of > 0.5%, due to interference from siliciclastics matrices retaining pyrolyzed hydrocarbons. One advantage of this plot is that it abandons the sometimes-misleading oxygen index and provides an estimate of maturity (R_0 value, Figure 12).

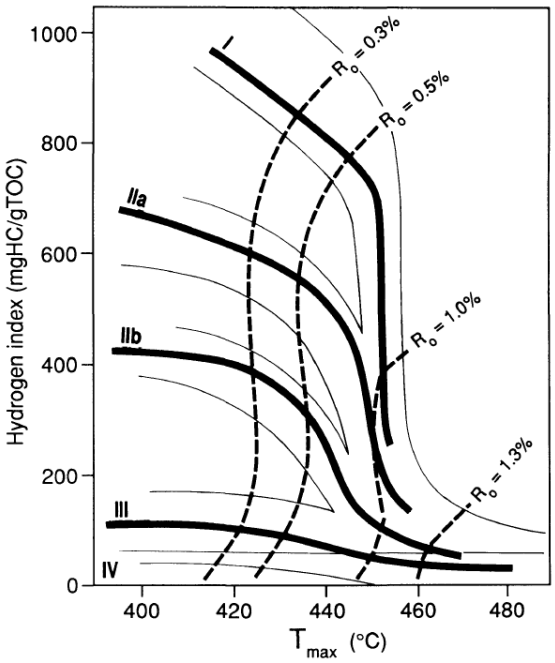

Figure 12: HI vs. Tmax diagram, as suggested by Delvaux (1990) to assess typing and maturity without the use of Oxygen Index.

3.3.3.7 Production Index

Production Index, given by Equation 4, is used to assess thermal maturity. Immature samples will feature a ratio of <0.1, while mature samples will feature a ratio of 0.1 – 0.4. Any greater than 0.4 may indicate contamination or very rich source rock.

Equation 4: Production Index

$$PI = \frac{S1}{S1 + S2}$$

3.4 X-RAY FLUORESCENCE: MAJOR ELEMENTS

Using a Thermo Scientific Niton XL3t 950 XRF Analyzer (Figure 13 and Figure 15) in a shielded housing (Figure 14 and Figure 15), major element (Fe, O, K, Si, Mg and Al) concentrations were determined.

In this apparatus, X-rays are directed at the sample, which results in secondary radiation – i.e. the emission of a photon (fluorescence). This photon has an energy and wavelength specific to the emitter's elemental composition and can be used to identify the element (Beckhoff *et al.*, 2006).

X-Ray Fluorescence methods are non-destructive, merely displacing electrons from the atomic orbits. This displacement causes another electron to drop in orbit to fill its place, releasing energy in the form of a photon. This photon and its energy are detectable by the XRF equipment, resulting in the derivation of the wavelength of the photon. The wavelength of fluorescent radiation is calculated using Planck's Law, below, to define elemental abundances.

$$\lambda = h \cdot c / E$$

Equation 5: Planck's Law, as used to calculate wavelength.

Where

λ =	observed wavelength
h =	Planck's Constant
c =	speed of light
E =	energy of the charged atomic oscillator.

3.4.1 Method

3.4.1.1 Preparation

Given the environmental health and safety concerns using X-Rays, a radiation detector badge is worn before entering the analysis laboratory and an electronic x-ray detector is kept close to the operator. Also, the XRF apparatus is never operated without the shielding housing in place. Samples were rinsed and picked of contaminants, then dried and crushed using a mortar and pestle. Lab cleanliness standards are adhered to in order to minimize sample contamination as they are crushed to a fine powder within a mortar and pestle. Surfaces are regularly wiped clean with Kimwipes, gloves are worn, paper sheets are used to line workspace and are disposed of between samples, 1:1 de-ionised water and alcohol mixture is used to clean pestle and mortar between samples, and a new TF 240-255 polypropylene film is used to protect the detector from samples. When analysing samples, the pre-set analysing program "Cu/Zn Mining" was used on both uncrushed and crushed samples. Sampling time was 180 seconds per sample. Samples had previously been separated by size – for XRF analysis only the >7500 μm fraction was used.

Figure 13: Niton XRF system (top left) in carrying case with accessories such as a battery (bottom right) and sample containers (bottom left). Image Credit: D. O'Connor.

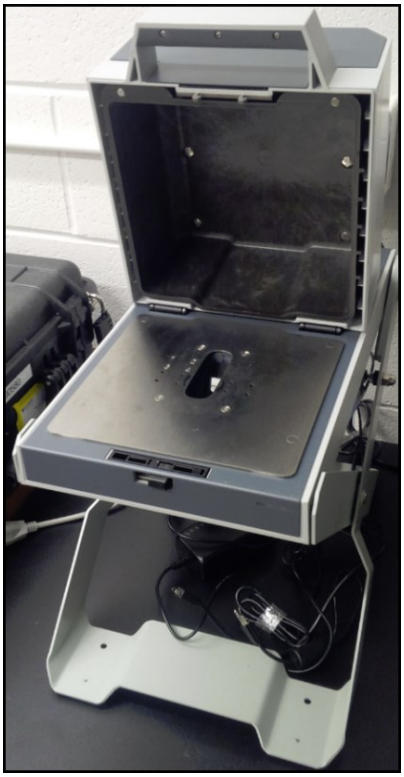

Figure 14: Shielded base station housing for Niton XRF system (image credit: D. O'Connor).

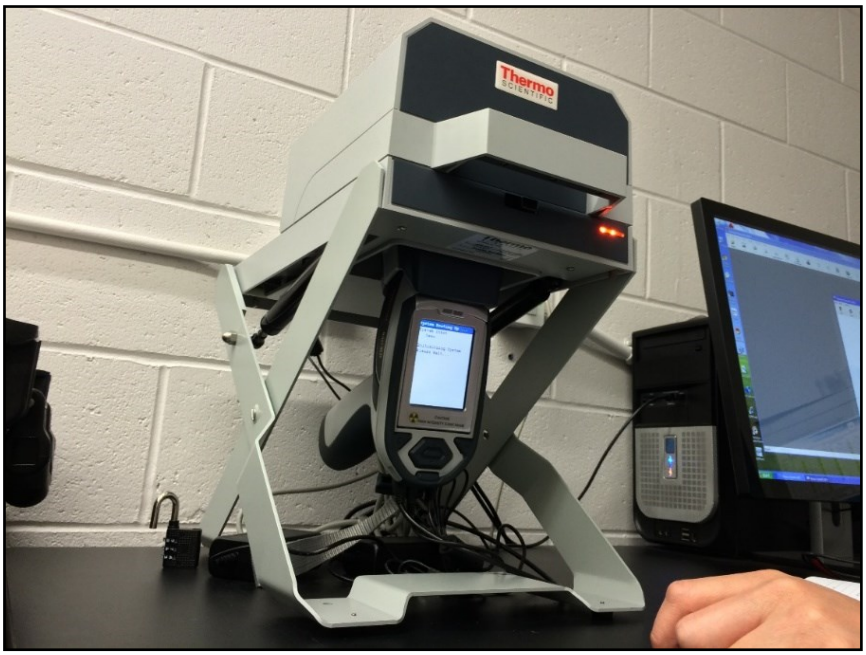

Figure 15: Thermo Scientific XRF and shielding housing setup at Dalhousie University Basin and Reservoir Laboratory.

3.4.1.2 Initialization and operation

Before any samples being placed in the housing, the apparatus runs a self-audit to check basic functionality (e.g. internal voltages, etc.). A written log of each sample analysed is kept, alongside a digital file containing results on the connected desktop computer. Samples are analysed twice, first using the options “Sample Type -> Soils Minerals -> Mining Cu2n”.

3.4.1.3 Uncertainty and Error in X-Ray Fluorescence Analysis

Uncertainty in XRF analysis occurs when sampling for a broad spectrum of elements due to mass attenuation of secondary X-rays, *i.e.* those emitted by the sample after bombardment. In this case, readings are missed as frequency responses do not arrive at the sensor within the XRF analyser. The effect of mass attenuation on results can be mitigated

through empirical (post-processing) methods. In this project, standards were analysed, and oxide concentrations stoichiometrically derived then compared against expected values.

Variable grain size in a sample is known to negatively affect the outcome of standards analysis, and it is recommended to use only crushing fraction smaller than 63 µm (Knight *et al.*, 2013). In accordance with this, samples were crushed then separated by grain size with a stainless-steel mesh.

XRF precision is also affected by random variations in matrix absorption effects, where the sample matrix scatters the source radiation. These are corrected within the analysis unit using "instrument dependent factors, calibration references and correction algorithms" (Natural Resources Canada, 2013), namely Compton Normalisation.

3.4.1.3.1 Precision

Precision is the measurement of repeatability around a most probable value, and the Niton equipment at Dalhousie University is designed to automatically report 2-sigma precision alongside each elemental concentration result, representing an error band of ±2 S.D., representing a 95% confidence interval.

3.4.1.3.2 Accuracy

Accuracy, the degree to which the analysis result conforms to the actual value of the sample, is assessed by comparing measured results to known values from the similar measurement of a reference standard. With the values in hand, we apply the method in Section 3.4.1.3.3 to correct values.

3.4.1.3.3 Standard Selection

Five standards are available to choose from at Dalhousie University (see Figure 16: Standards available for use at Dalhousie University. Till-4 was utilised in this study (photo credit: Darragh O'Connor), of which one was chosen (Till-4) as it contained the appropriate abundances of target oxides. The reference standard was used in duplicate analysis (Table 7).

Figure 16: Standards available for use at Dalhousie University. Till-4 was utilised in this study (photo credit: Darragh O'Connor)

Till-4 is a standard collected and certified by Natural Resources Canada in accordance with the Canadian Certified Reference Materials Project from either Scisson's Brook, New Brunswick (designated 21C) or a Molybdenite occurrence near Hull, Quebec (designated 31G). These standards were originally described using neutron activation and powder x-ray diffraction to diagnose the following elemental abundances:

Table 6: Summary of major and minor elements (expressed as %) and "Total" elements (expressed as µg/g [ppm], unless otherwise noted) in Standard "Till-4" (Lynch, 1996).

Major and Minor Element	Oxide %
SiO2	65.0
Al2O3	14.4
Fe2O2(T)	5.63
MgO	1.26
K2O	3.25
TiO2	0.81

Established standard values and observed results from the standard analysis were compiled to calculate a correction factor: alongside accepted elemental concentrations (Table 6), measurements of standards at Dalhousie were compiled in the following manner:

1. Oxides of interest were listed in column one: accepted concentrations listed in column two,
2. List new analyses of the standard (analysed concentration calculated to oxide %),
3. Calculate the mean for all standard analyses,
4. Calculate the standard deviation,
5. Calculate the % error for each oxide ((1 - (mean reading/known standard)) *100%),
6. Calculate the correction factor (known standard/mean reading),
7. Apply correction factor to each of the oxides of interest.

Resultant Correction factors are in Table 7:

Table 7: Correction Factors and % Errors of XRF apparatus calculated by standards analysis of "Till-4."

	Till-4 (known standard)	Till-4 (Reading 1)	Till-4 (Reading 2)	Till-4 (Reading 3)	Till-4 (Reading 4)	Mean Till-4 reading	Standard deviation	% Error	Correction Factor	n
SiO_2	65	53.88	53.07	52.52	53.08	53.14	0.56	18.25	1.22	4
TiO_2	0.81	0.68	0.67	0.68	0.69	0.68	0.01	16.19	1.19	4
Al_2O_3	14.4	8.93	8.65	8.59	8.74	8.73	0.15	39.39	1.65	4
Fe_2O_2(total)	5.63	6.03	6.04	6.00	6.01	6.02	0.02	-6.96	0.93	4
MnO	0.06	0.05	0.05	0.04	0.05	0.05	0.00	21.99	1.28	4
MgO	1.26	0.69	0.51			0.60	0.13	52.50	2.11	4
CaO	1.25	1.25	1.27	1.23	1.26	1.25	0.02	-0.20	1.00	4
K_2O	3.25	2.72	2.73	2.70	2.77	2.73	0.03	15.97	1.19	4
P_2O_5	0.2	0.35	0.40	0.36	0.39	0.37	0.02	-86.67	0.54	4

3.4.2 Data presentation and analysis

3.4.2.1 Sandclass classification

Herron's (1988) Sandclass plot distinguishes sample lithology based on the geochemistry of four oxides: Fe_2O, K_2O, SiO_2, and Al_2O_3. Resultant plots distinguish between Fe-shale, shale, Fe-sand, wacke, litharenite, arkose, sub-arkose, sub-litharenite and quartz arenite and are, therefore, a proxy for lithologic description where it is impossible, e.g. in cuttings samples where outcrop cannot be examined.

3.5 CARBON ISOTOPE ANALYSIS

3.5.1 Concept

Stable carbon isotopes include ^{12}C and ^{13}C (another carbon isotope, ^{14}C, is unstable and decays with a half-life of 5,730 years). The preserved signature in the geological record varies due to fractionation by natural processes such as population of carbonate producers, transgressive-regressive cycles, carbon export to sediments via organic matter, variation of continental weathering, input of volcanogenic CO_2 (simply: addition of "light" CO_2, sequestration of "heavy" CO_2) (e.g. Silva *et al.,* 2015 and references therein). Stable isotope chemostratigraphy assesses the change in the isotopic fractionation of a specific element across a sedimentary record. This fluctuation is the result of a change in environmental conditions (e.g. perturbations of the global carbon cycle) and the abundance of photosynthesizing organisms which affect isotope availability (e.g. high primary productivity in the photic zone will preferentially remove ^{12}C from the water column and deposit it in the benthic layer). $\delta^{13}C$ (*delta 13-Carbon,* the ratio of ^{12}C to ^{13}C) can also be used as a simple chemostratigraphic tool, both alone (Silva *et al.* 2015) and in conjunction with other methods such as Gamma Ray readings (West Virginia University, 2015).

3.5.2 Method

3.5.2.1 Analysis

The carbonate fractions were analysed by Continuous Flow–Isotope Ratio Mass Spectrometry (CF-IRMS) (Figure 17). The samples were first crushed at Dalhousie University, then dispatched to the IsoAnalytical Laboratories (UK) where they were weighed into clean Exetainer™ tubes and then flushed with 99.995 % helium. After

flushing, phosphoric acid was added to the samples, they were heated at 90ºC for 3 hours and then left to react with the acid overnight to allow complete conversion of carbonate to CO_2. CO_2 was sampled into a continuously flowing helium streamed using a double holed needle and resolved on a packed column gas chromatograph. The resultant chromatographic peak was carried forward into the ion source of a Europa Scientific 20-20 IRMS. Reference and control materials were prepared the same way. IA-R022 has been calibrated against and is traceable to NBS-18 and NBS-19 (limestone, $\delta^{13}C_{V\text{-}PDB}$ = +1.95 ‰). IA-R066 has been calibrated against and is traceable to NBS-18 and IAEA-CO-1 (Carrara marble, $\delta^{13}C_{V\text{-}PDB}$ = +2.5 ‰). NBS-18, NBS-19, and IAEA-CO-1 are inter-laboratory comparison standard materials distributed by the International Atomic Energy Agency (IAEA).

For Elemental Analysis- Isotope-Ratio Mass Spectrometry (EA-IRMS) analysis of the kerogen-only fraction (Figure 18), weighed sub-samples were taken from the sample vials, placed in universal tubes, acidified with 2M hydrochloric acid, mixed, heated in the oven at 60 °C for 2 hours and left for 24 hours to allow all carbonate to be liberated as CO_2. The sample fractions were then isolated by centrifugation, and the acid was subsequently decanted. Thereafter, the samples were washed twice using distilled water and centrifugation. After acid washing, the fractions were oven dried at 60 °C. Tin capsules containing a sample or reference material are loaded into an auto-sampler on a Europa Scientific elemental analyser, with the furnace temperature held at 1000 °C and combusted in an oxygen rich environment (Iso-Analytical Laboratory Report 160212-5, 2016). The exhaust gas is reacted in a series of catalysts (e.g. chromate, silver wool) to oxidise

hydrocarbons and remove sulphur and halides, purifying the CO_2 stream. After purification, the remaining gas stream enters a Europa Scientific 20-20 IRMS ion source.

3.5.3 Data presentation and analysis-

$\delta^{13}C$, as determined by Iso-Analytical Laboratories, is calculated per Equation 6, where Vienna Peedee Belemnite (V-PDB) is calculated from a known value for the check sample being used.

$$\delta^{13}C = \left(\frac{\left(\frac{^{13}C}{^{12}C}\right)[sample]}{\left(\frac{^{13}C}{^{12}C}\right)[V-PDB]} - 1 \right) * 1000\ ‰$$

Equation 6: Equation to acquire $\delta^{13}C$ using obtained ratios of samples and standards, where V-PDB is reference standard Vienna Peedee Belemnite, as described in Section 3.5.4.1.3.

As analytical precision is better than 0.1‰, error bars are omitted. Results are presented on two scales, including results from kerogen and carbonate fraction bulk analyses.

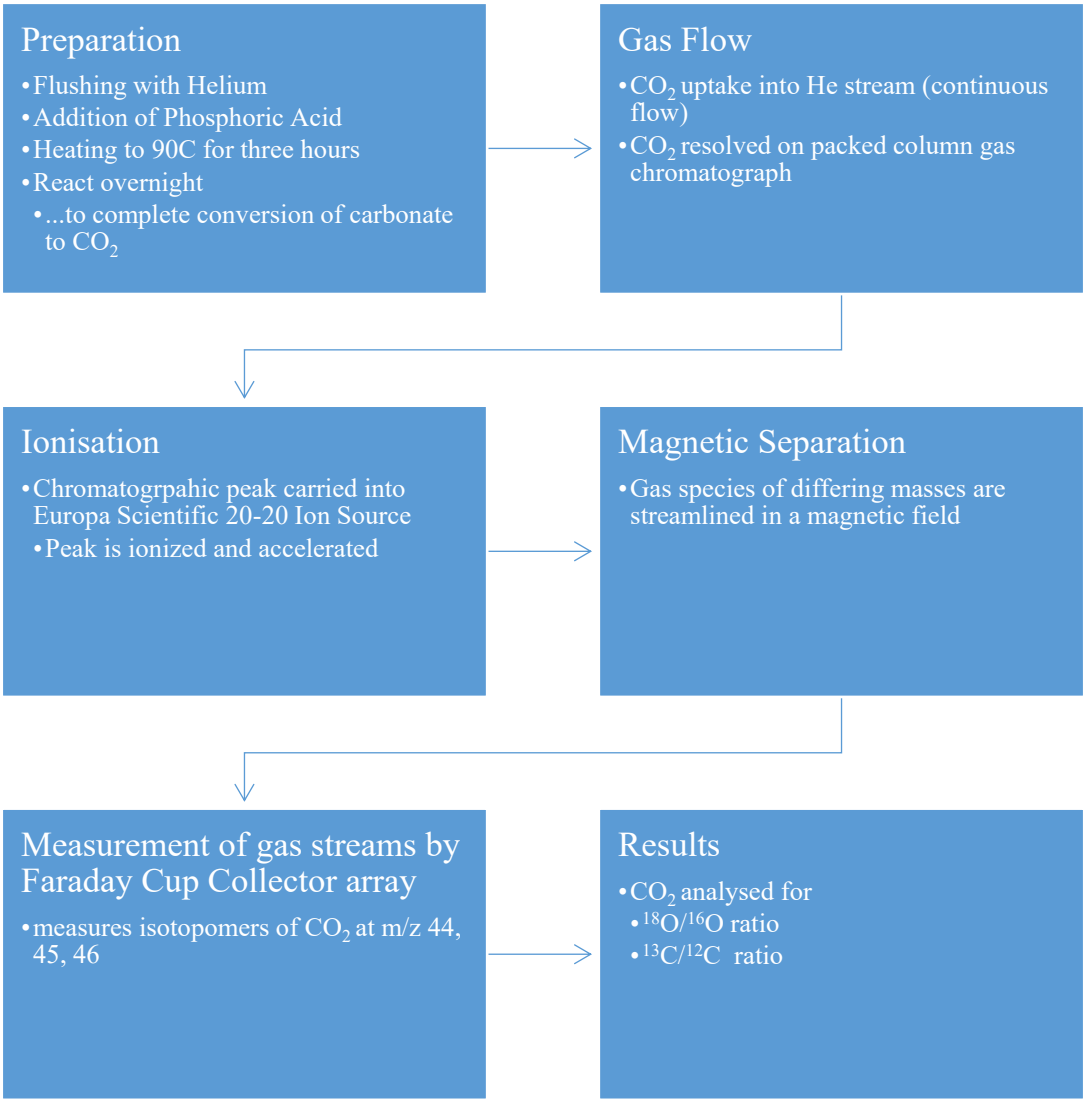

Figure 17: Continuous Flow Isotope Ratio Mass Spectrometry operation flow chart (From Iso-Analytical Laboratory Report 160212-5, 2016)

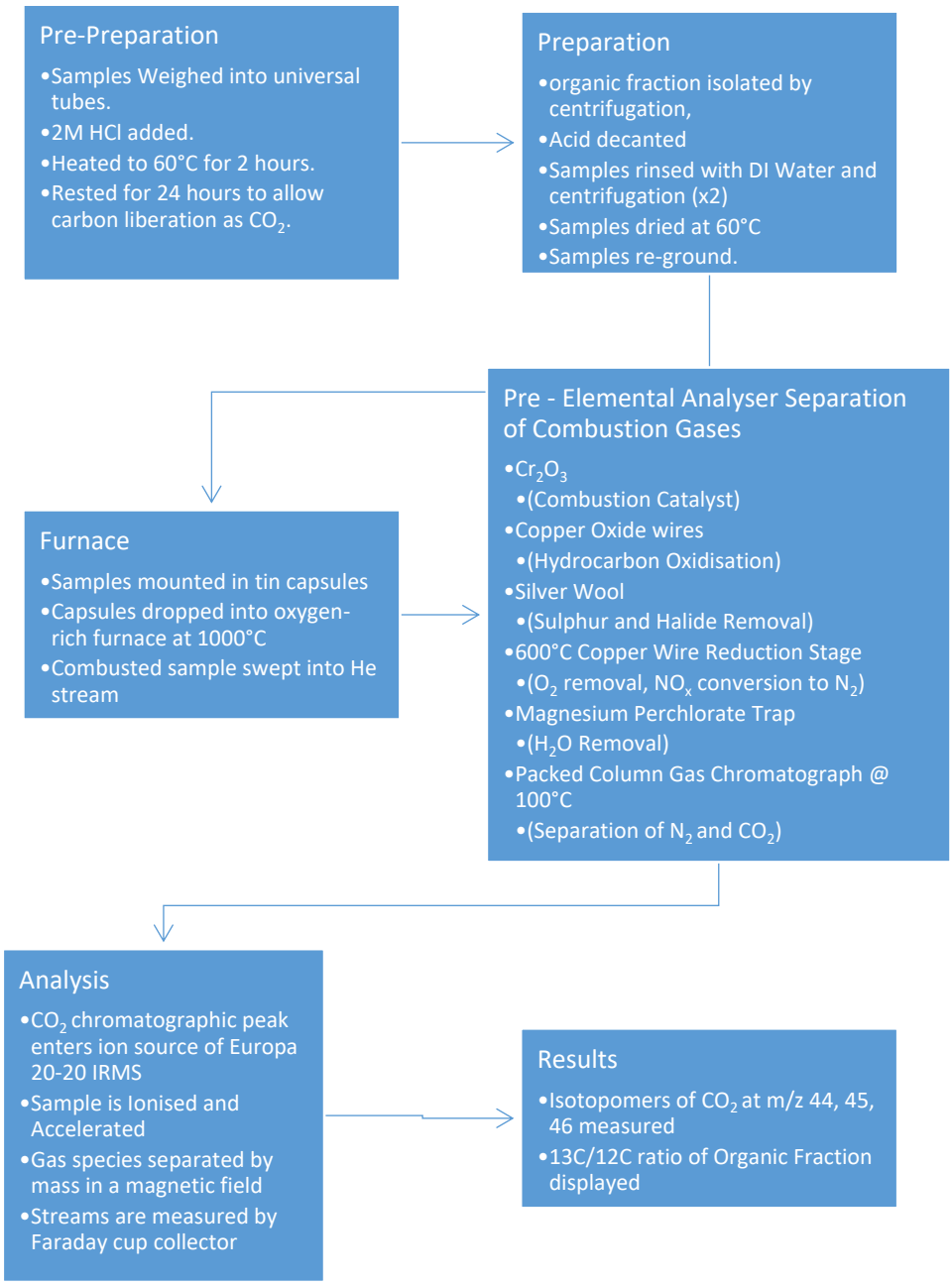

Figure 18: Elemental Analysis Isotope Ratio Mass Spectrometry operation flow chart (From Iso-Analytical Laboratory Report 160212-5, 2016)

3.5.4.1 Uncertainty and Error in Analysis

3.5.4.1.1 Precision

Analytical precision, as defined in Section 3.4.1.3.1, at Iso-Analytical Laboratories is reported to be between 0.00% in the case of NBS-18 and 4.56% in the case of IA R040 Dolomite (Table 8).

3.5.4.1.2 Accuracy

Accuracy was determined at Iso-Analytical Laboratories by running duplicates sample analyses after every fifth sample. In addition, reference standards are analyzed at the beginning and end of each 5-sample batch (*pers. comm.* Iso-Analytical Laboratory Report 160212-5). The accuracy of results (as defined in Section 3.4.1.3.2) is deemed not to require correction, based on a comparison of Correction Factors of 0.96 – 1.0 (Table 8 and Table 9).

3.5.4.1.3 Standard Selection

Vienna Peedee Belemnite (V-PDB) is regularly used as a reference standard for $\delta^{13}C$ (Fry, 2006) and has been designated as the baseline reference for stable carbon isotope analysis (Coplen, 1983). Due to V-PDB's high $\delta^{13}C$ value, most samples will register a negative value. Per Iso-Analytical Analysis reports, check samples and other in-house standards were calibrated to V-PDB, such as the reference material used during kerogen $\delta^{13}C$ analysis: IA-R001 (wheat flour, $\delta^{13}C_{V\text{-}PDB}$ = -26.43 ‰). For quality control purposes,

analysis of check samples IA-R001, IA-R005 (beet sugar, $\delta^{13}C_{V\text{-}PDB}$ = -26.03 ‰) and IA-R006 (cane sugar, $\delta^{13}C_{V\text{-}PDB}$ = -11.64 ‰) was carried out between samples. IA-R001, IA-R005 and IA-R006 are calibrated against and traceable to IAEA-CH-6 (sucrose, $\delta^{13}C_{V\text{-}PDB}$ = -10.43 ‰). IAEA-CH-6 is an inter-laboratory comparison standard distributed by the International Atomic Energy Agency (IAEA). To ensure the precision of laboratory analyses, duplicate samples were analysed every fifth sample. Based on the unpublished analysis and the data presented here, analytical precision is better than ±0.1‰.

Table 8: Standards Analysis within Iso-Analytical results

	IA-R022 Calcium Carbonate		**NBS-18 Calcite**		**IA-R066 Chalk**		**IA-R040 Dolomite**	
	$\delta^{13}C_{V\text{-}PDB}$ (‰)	**$\delta^{18}O_{V\text{-}PDB}$ (‰)**	**$\delta^{13}C_{V\text{-}PDB}$ (‰)**	**$\delta^{18}O_{V\text{-}PDB}$ (‰)**	**$\delta^{13}C_{V\text{-}PDB}$ (‰)**	**$\delta^{18}O_{V\text{-}PDB}$ (‰)**	**$\delta^{13}C_{V\text{-}PDB}$ (‰)**	**$\delta^{18}O_{V\text{-}PDB}$ (‰)**
	-28.49	-22.62	-5.01	-23.38	2.31	-1.56	-0.73	-17.29
	-28.60	-22.69	-5.05	-23.31	2.35	-1.48	-0.75	-17.31
	-28.64	-22.70	-4.98	-22.93	2.31	-1.56	-0.77	-17.10
	-28.64	-22.67	-5.00	-23.18	2.35	-1.48	-0.72	-17.14
	-28.66	-22.63	-5.10	-23.28	2.29	-1.53		
	-28.66	-22.73	-5.07	-23.26	2.36	-1.47		
	-28.63	-22.61	-4.93	-23.07	2.36	-1.56		
	-28.61	-22.72	-4.95	-23.19	2.31	-1.53		
	-28.66	-22.65	-4.96	-23.16	2.29	-1.55		
	-28.64	-22.67	-5.06	-23.24	2.30	-1.56		
	-28.66	-22.83	-4.96	-23.16	2.36	-1.52		
	-28.59	-22.65	-5.06	-23.24	2.37	-1.45		
	-28.60	-22.72						Sample Tranche 1
	-28.59	-22.61						Sample Tranche 2
	-28.62	-22.62						Sample Tranche 3
	-28.59	-22.61						Sample Tranche 4
	-28.62	-22.62						
min	**-28.66**	**-22.83**	**-5.10**	**-23.38**	**2.29**	**-1.56**	**-0.77**	**-17.31**
max	**-28.49**	**-22.61**	**-4.93**	**-22.93**	**2.37**	**-1.45**	**-0.72**	**-17.10**
mean	**-28.62**	**-22.67**	**-5.01**	**-23.20**	**2.33**	**-1.52**	**-0.74**	**-17.21**
st dev	**0.04**	**0.06**	**0.06**	**0.12**	**0.03**	**0.04**	**0.02**	**0.10**
n	**17**	**17**	**12**	**12**	**12**	**12**	**4**	**4**
expected	**-28.63**	**-22.69**	**-5.01**	**-23.20**	**2.33**	**-1.52**	**-0.71**	**-17.18**
% error	**0.048**	**0.099**	**0.000**	**0.000**	**0.000**	**0.000**	**-4.560**	**-0.179**
Correction Factor	**1.00**	**1.00**	**1.00**	**1.00**	**1.00**	**1.00**	**0.96**	**1.00**

Table 9: Check standard analysis of samples sent to Iso-Analytical Laboratories

	IA-R001 Wheat Flour □13CV-PDB (‰)	IA-R005 Beet Sugar □13CV-PDB (‰)	IA-R006 Cane Sugar □13CV-PDB (‰)
	-26.41	-25.97	-11.59
	-26.34	-25.99	-11.53
	-26.50	-26.00	-11.88
	-26.25	-26.02	-11.93
	-26.43	-25.98	-11.68
	-26.34	-26.02	-11.67
	-26.41	-26.06	-11.68
	-26.44	-26.02	-11.64
	-26.37	-26.03	-11.67
	-26.36	-25.98	-11.68
	-26.40	-25.97	-11.59
	-26.47	-25.99	-11.53
	-26.39		
	-26.31		
	-26.37		
	-26.41		
	-26.45		
	-26.41		
	-26.34		
min	-26.50	-26.06	-11.93
max	-26.25	-25.97	-11.53
Mean	-26.39	-26.00	-11.67
1 s.d.	0.06	0.03	0.12
n	19	12	12
Accepted	-26.43	-26.03	-11.64
% error	0.149	0.108	-0.284
Correction Factor	1.00	1.00	1.00

CHAPTER 4: RESULTS

4.1 TOC CONTENT

4.1.1 Well 18/25-1

TOC in well 18/25-1 varies from 0.8–5.2 wt. % (Figure 19 and Table A12). The base of the studied portion of the well, corresponding to the Broadford Beds Formation Equivalent and the lower portion of the Lower Jurassic Undifferentiated, presents low TOC values, reaching up to 1.8 %. The highest TOC values are observed in the middle part of the Portree Shale Formation Equivalent, dated from the Lower–Middle Toarcian (around 2700 m), reaching up to 5.2 %. The upper part of this unit also presents high TOC values, ~ 3 %. This entire interval is more than 90 m thick. Carbonate contents vary between 9.4–66 %. The lowest values are recorded in the lower part of the Portree Shale Formation Equivalent.

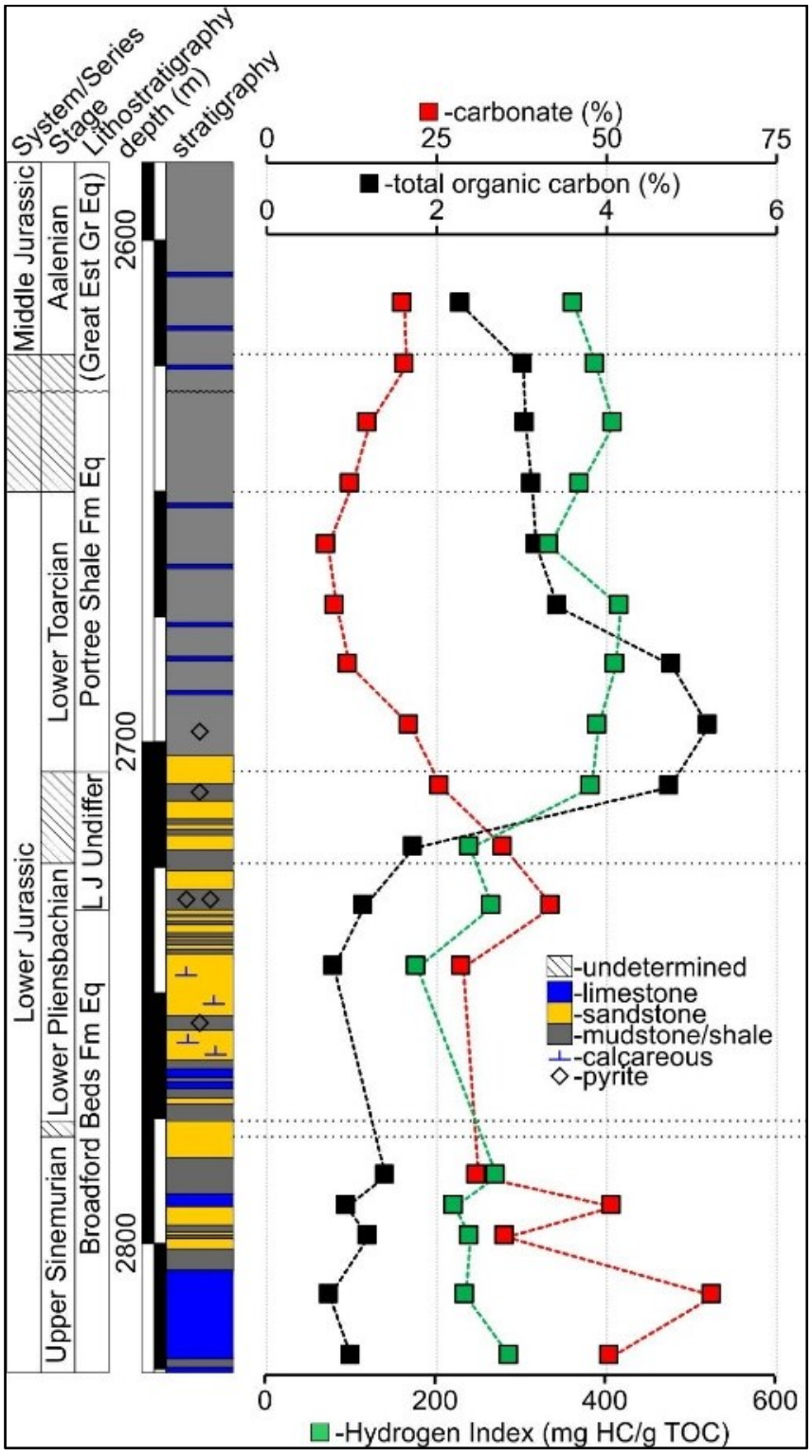

Figure 19: Total Organic Carbon and percentage carbonate (top axis) and Hydrogen Index (mg HC/g TOC, bottom axis) from LECO analysis, well 18/25-1. of the top of Broadford Beds Formation Equivalent, Lower Jurassic Undifferentiated (L J Undiffer), Portree Shale Formation Equivalent and Middle Jurassic (Great Estuarine Group Equivalent) units in the well 18/25-1 (Corrib Gas field), Slyne Basin, offshore Ireland (after Enterprise Oil, 2000; Millennia, 2004). Est – Estuarine; Fm-Formation; Eq-Equivalent.

4.1.2 Well 27/13-1

TOC in well 27/13-1 varies from 0.61–5.14 wt. % (Figure 20 and Table A13). Much of the studied portion of the well, corresponding to the Lias Formation, presents a range of TOC values, reaching from 0.61 wt.% up to 5.14 wt.%. The sample with the highest TOC value dated from the Pliensbachian (2345 m). The upper well section (Dogger Formation.) also presents high TOC values, ~ 3 wt.%.

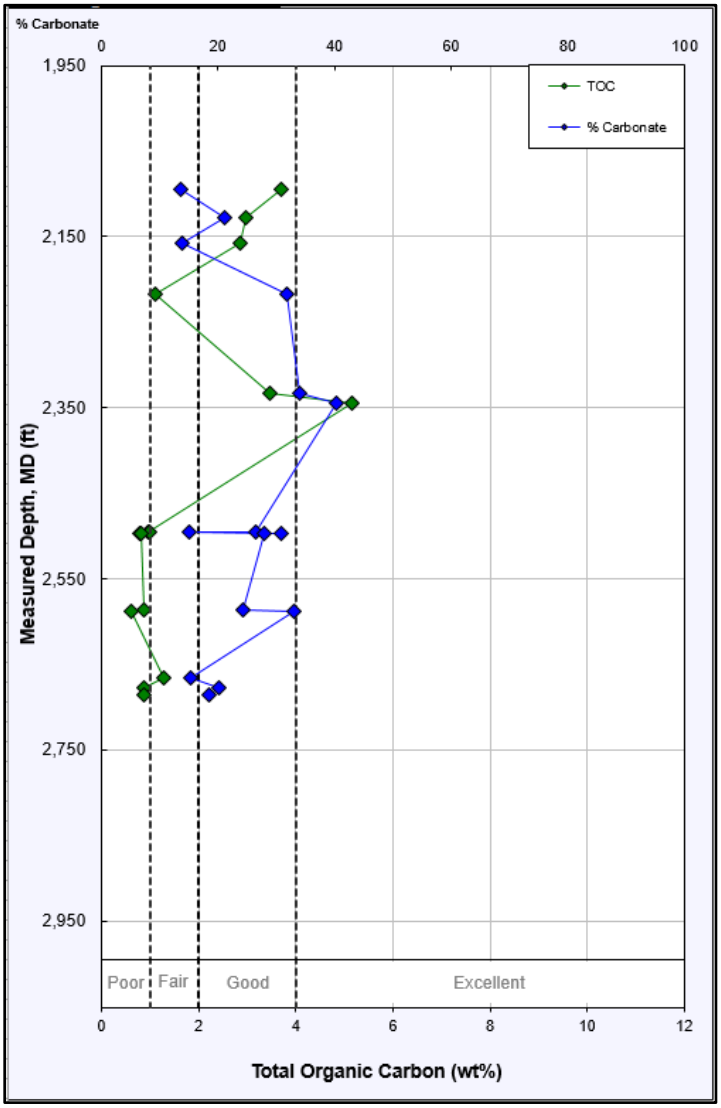

Figure 20: Total Organic Carbon (bottom axis) and percentage carbonate (top axis) results from LECO TOC analysis of well 27/13-1.

4.2 ROCK-EVAL PYROLYSIS

4.2.1 Well 18/25-1 - Summary

S_1, S_2, and S_3 results from well 18/25-1 vary between 1.36–8.28 mg HC/g rock, 1.44–20.36 mg HC/g rock, and 0.57–1.05 mg CO_2/g rock, respectively (Table A12). T_{MAX} ranges from 434–446 °C (Figure 25 and Table A12). HI and OI vary between 179–418 mg HC/g TOC and 12–95 mg CO2/g TOC (Figure 26). A low temperature S_2 shoulder (Figure 9) presented in multiple results.

4.2.1.1 Source Potential Logs

Oil potential of samples in this well range from poor to fair in the lower seven samples, with a marked increase in potential at 2,709 m (Figure 21). All samples above and including this one present good to excellent oil potential (S_2: mg HC/g rock).

HI (S_2/TOC) ranges from 179–418 mg HC/g TOC (Figure 22 and Table A12) and OI ranges from 12–95 mg CO2/g TOC (Table A12). A low temperature S_2 shoulder (Figure 9) was present in multiple results.

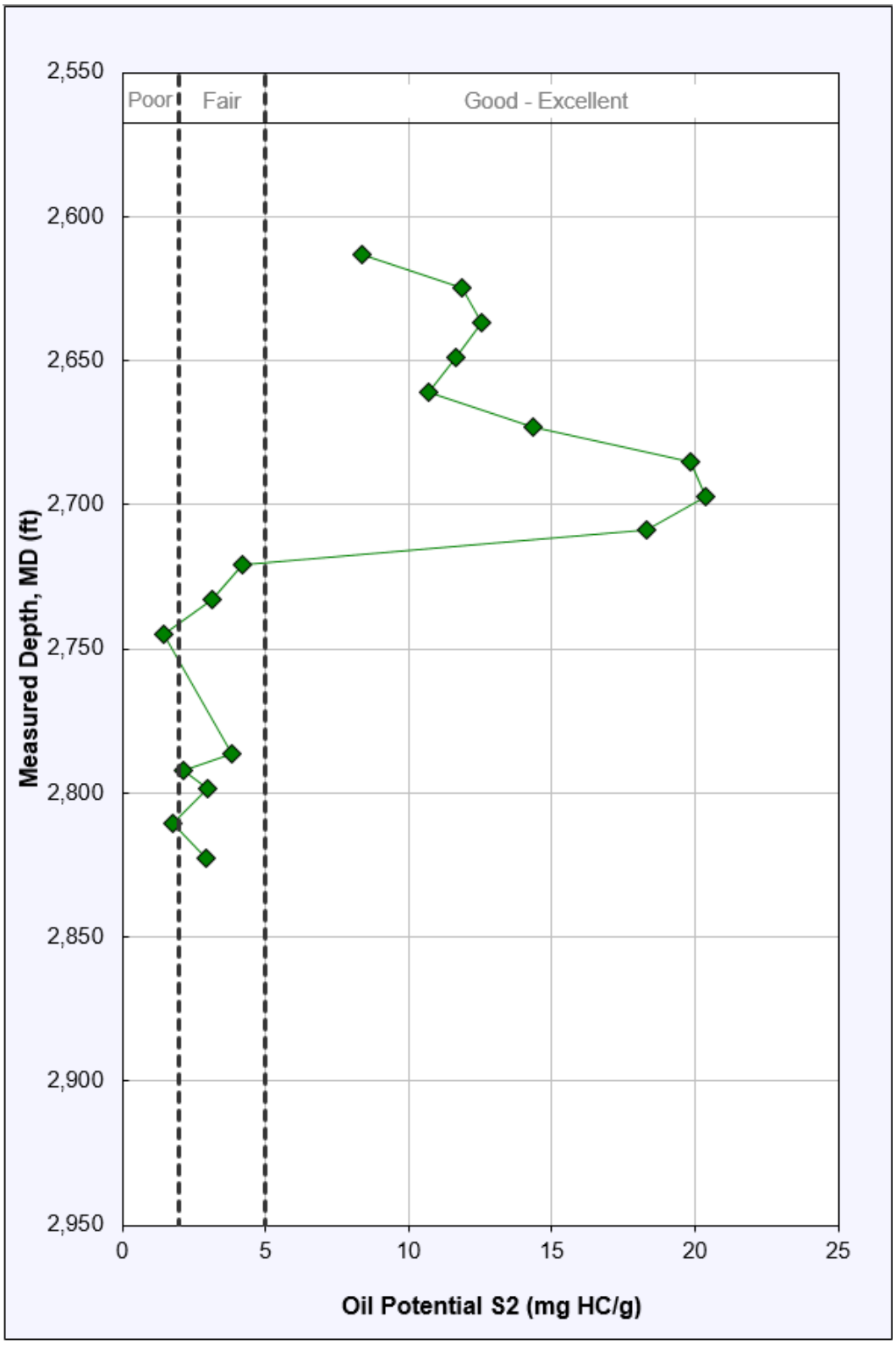

Figure 21: Oil Potential of sampled section in well 18/25-1, depicting two samples of poor S2 potential, five of fair S2 potential and the remainder of good - excellent S2 potential.

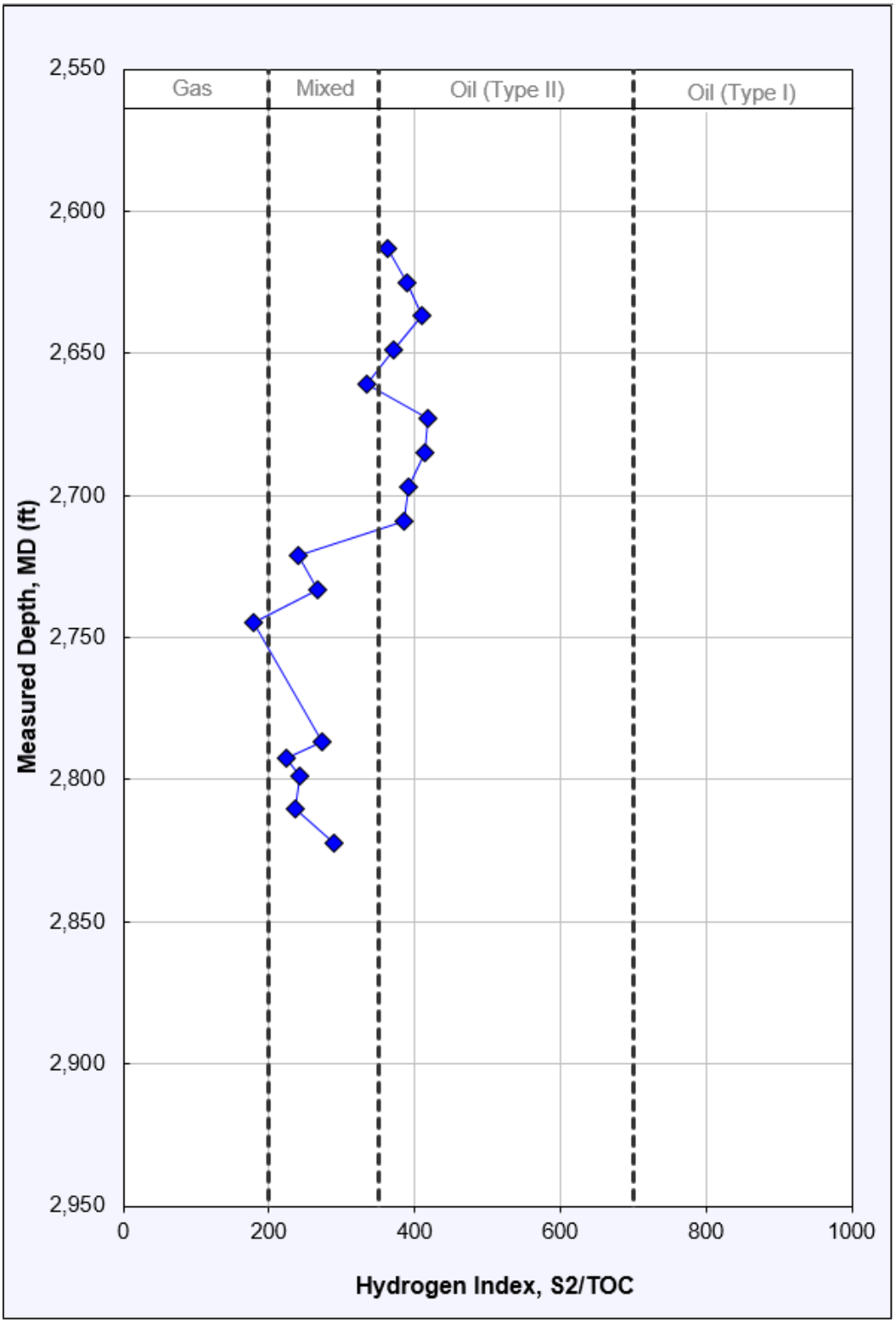

Figure 22: Depth vs Hydrogen Index (S2 / TOC) in well 18/25-1 indicating source type to be of mixed Type II/Type III generative capability.

4.2.1.2 Hydrocarbon Indicator and Maturity Logs

All samples from this well analysed for Normalised Oil Content (NOC, derived from S_1/TOC), display a high value indicating that all are within the oil/gas production window or contamination in the case of incomplete rinsing (Figure 23).

Production Index analysis (S_1/S_1+S_2) indicates that samples below 2,709 m vary between 0.3 and 0.59, while those above vary between 0.27 and 0.33 – a much narrower spread (Figure 24). The well section above 2,709 m straddles the distinction between oil prone and gas prone, while all samples deeper than 2,709 m are characteristic of a gas prone source rock.

Vitrinite reflectance equivalent ranges from 0.65 to 0.87 and tracks roughly in line with T_{MAX}, indicating generation capability to be within the oil generation zone (Figure 25). Note that Measured vitrinite reflectance is not available within this well.

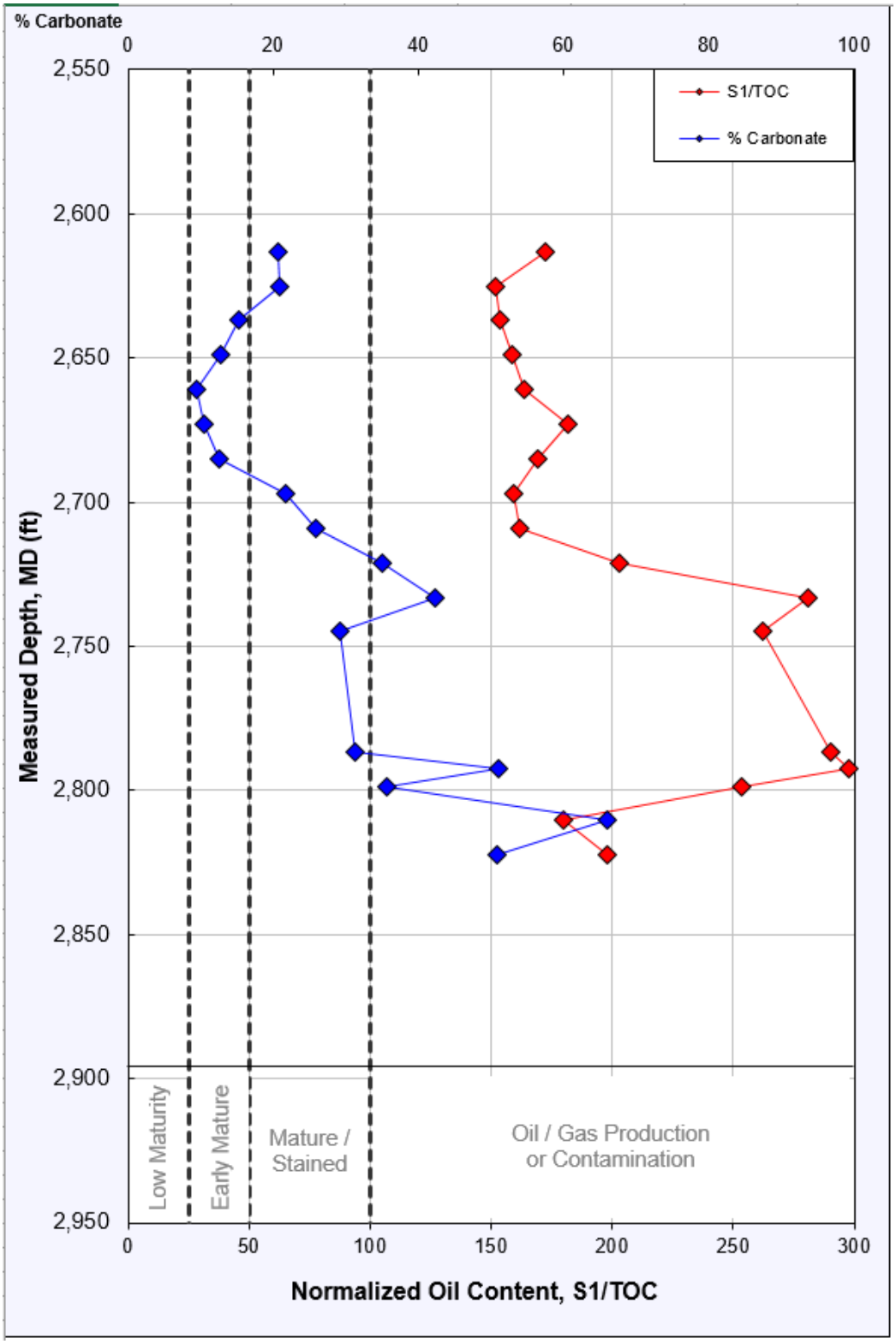

Figure 23: Normalised Oil Content (S1 / TOC) plot for samples from well 18/25-1, with % carbonate. Note that all samples fall within the production (or contamination) range of NOC

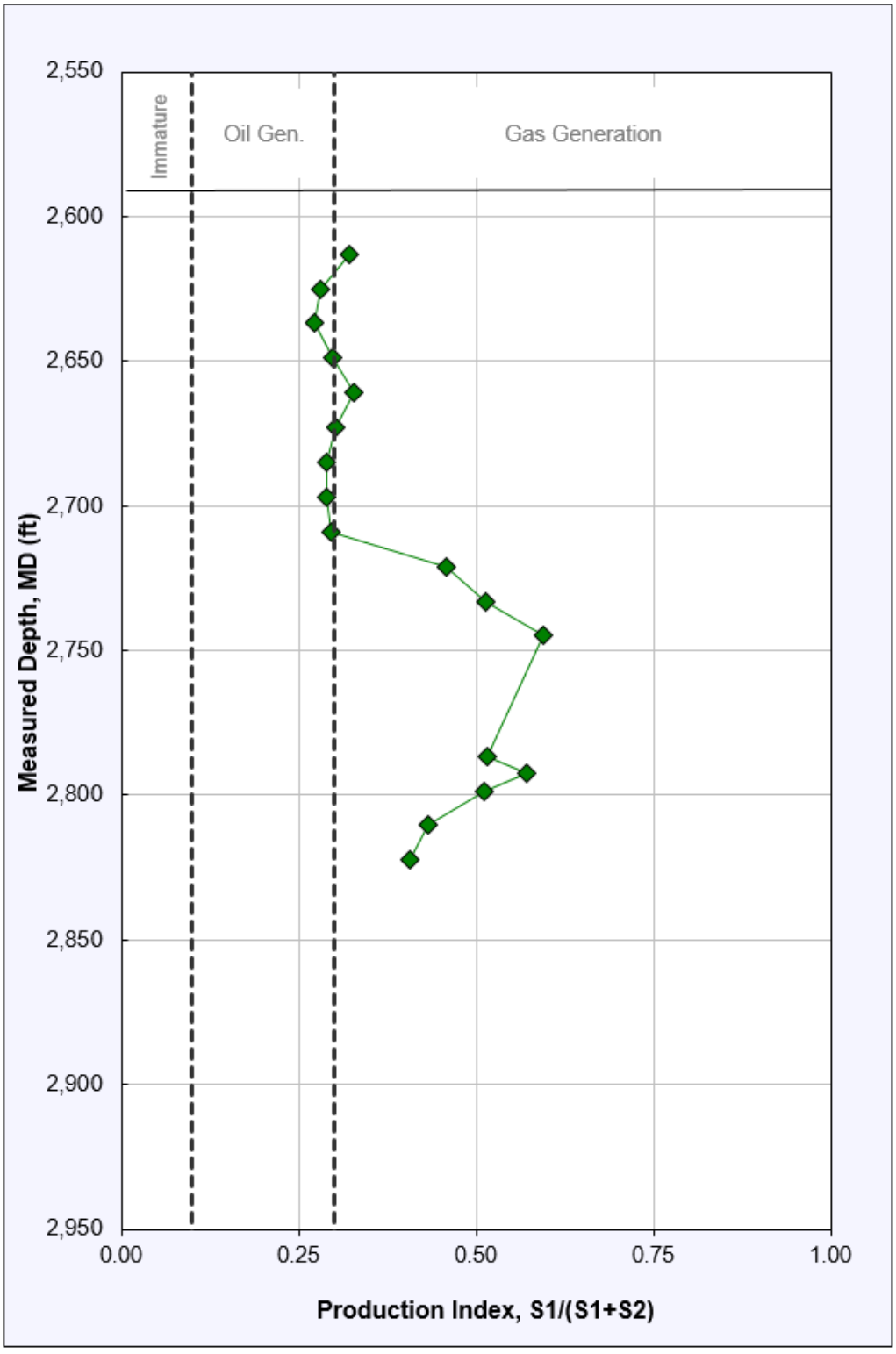

Figure 24: Production Index for samples from well 18/25-1. While upper samples fall within the oil/gas generation zone, lower samples fall within the gas zone, indicating a lower H:O ratio.

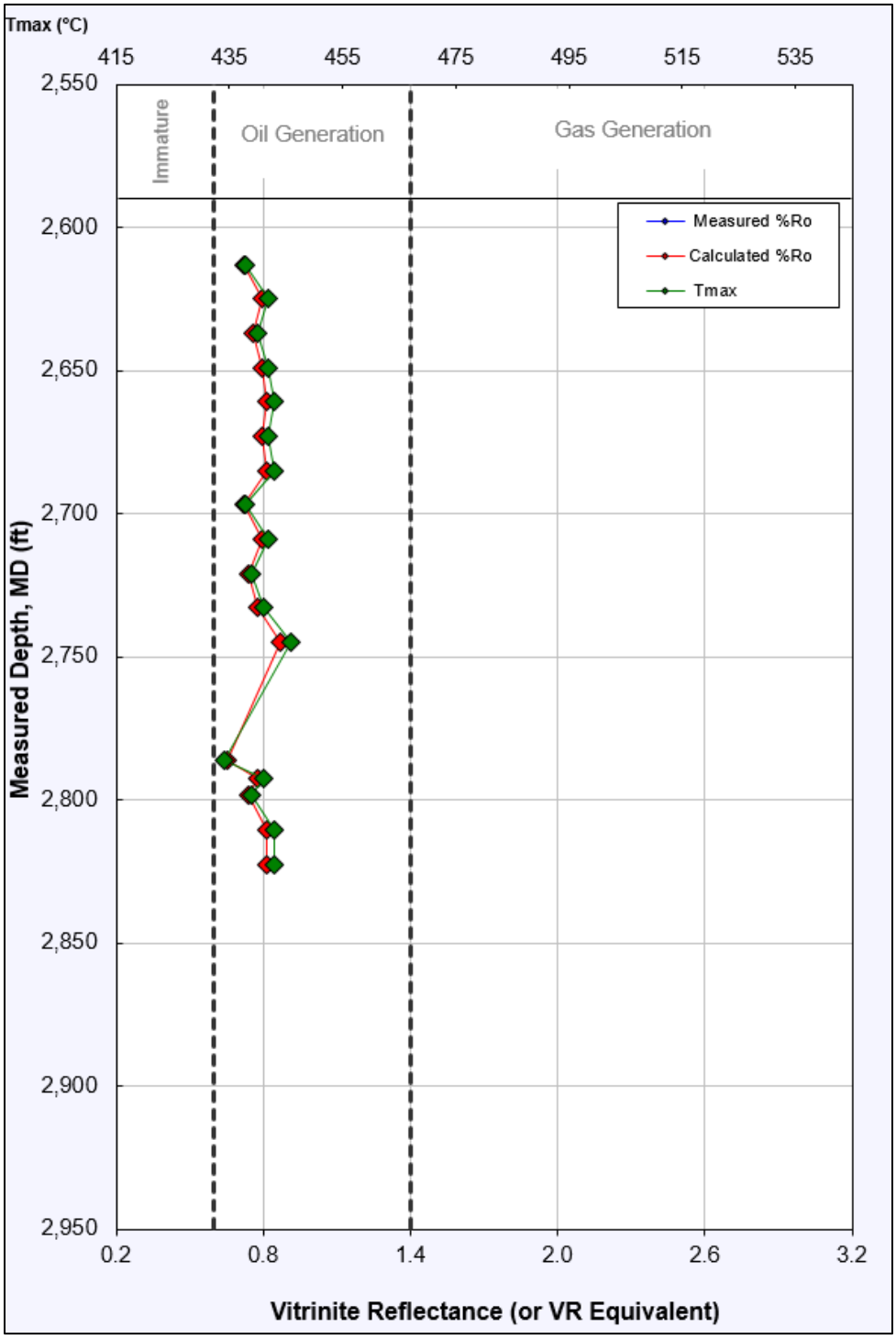

Figure 25: Maturity Indicators (Depth vs Tmax, and calculated vitrinite reflectance) plot of samples from Well 18/25-1. Note that all samples appear to the lower end of the oil generation window.

4.2.1.3 Pseudo Van Krevelen Plots

As seen in Figure 26, results from this well indicate Type II and type III kerogens. A clear distinction is seen in how results are generally close based on depth: samples from above 2,709 m cluster around a Type II kerogen composition, while those from below cluster together towards the Type II/Type III kerogen designation boundary. Two samples from this well were not flagged as having a Low Temp S_2 Shoulder (2,697 m and 2,709 m).

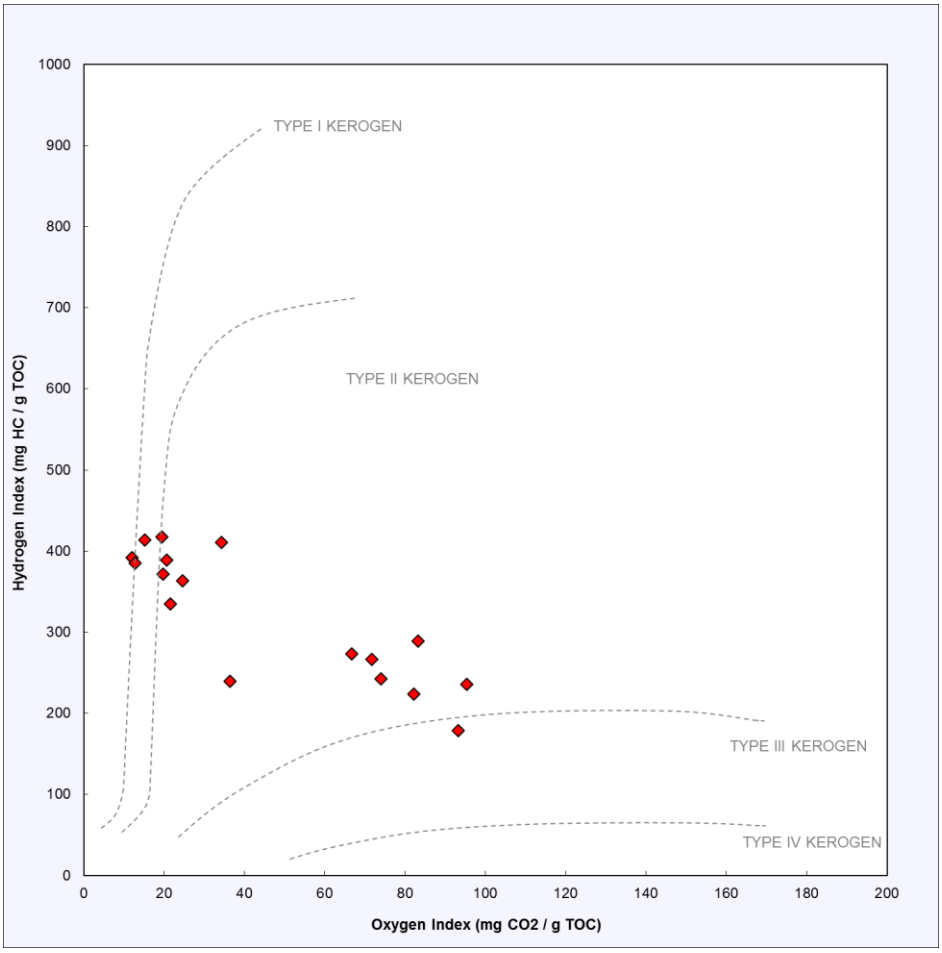

Figure 26: Cross-Plot of HI vs. OI in samples from well 18/25-1. Samples returned were dominantly Type II, with shallower samples grouping in Type II / III and deeper samples plotting Type II and one outlier in the Type III designation.

4.2.1.4 Kerogen Quality Plots

Using a different style of kerogen typing, Figure 27 shows analysis results to be skewed further in favour of Type II/Type III classification. Shallower samples (above 2,709 m) appear to fall within the Type II Oil-Prone Usually Marine section, while deeper samples cluster together in the Mixed Type II/Type III Oil/Gas Prone designation due to lower TOC and Remaining Hydrocarbon Potential.

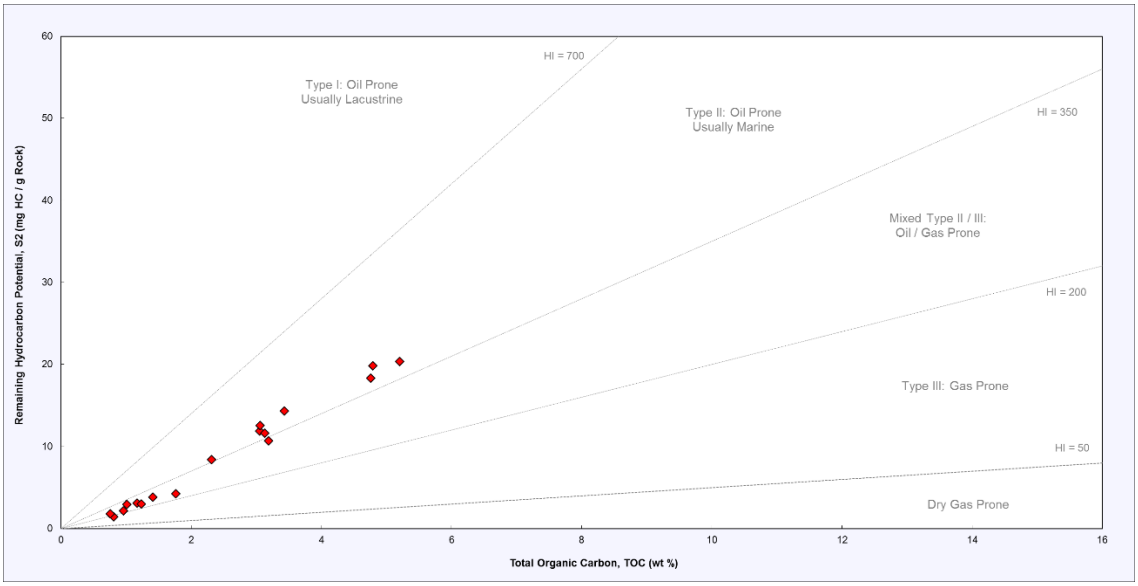

Figure 27: Kerogen Quality Plot of samples from well 18/25-1.

4.2.1.5 Kerogen Type and Maturity Plots

Figure 28 shows a final kerogen typing plot. As HI falls between 179 and 418, and T_{MAX} ranges from 434 to 446, most samples plot as Type II kerogens within the oil generation window of vitrinite reflectance equivalent (%Ro). Five samples (2,625 m, 2,637 m, 2,673 m, 2,685 m, and 2,709 m) fall within the Type II kerogen zonation, again within the oil generation windows regarding %Ro. Grouping is again apparent as samples above 2,709 m cluster together closer to the Type II kerogen boundary, while those from deeper than 2,709 m fall almost centrally within the Type II-III kerogen zone.

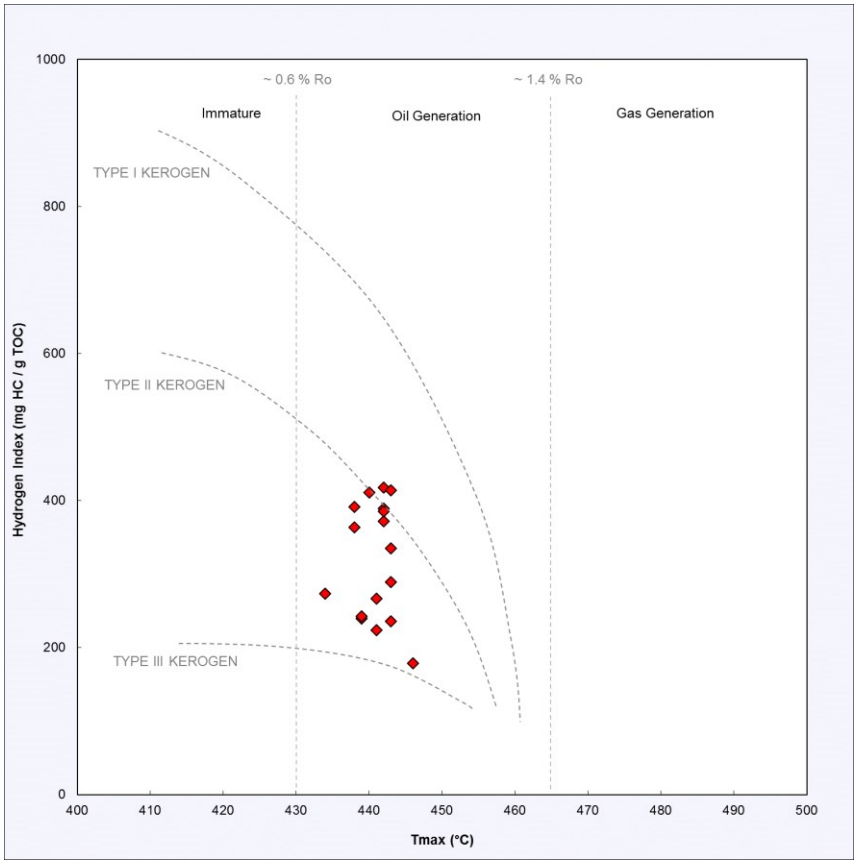

Figure 28: Kerogen type and maturity plot of Lower Jurassic samples from well 18/25-1.

4.2.1.6 Kerogen Conversion and Maturity Plots

Plotting Production Index (PI) against T_{MAX} as in Figure 29 indicates that all samples fall within the oil zone or oil generation window, and none indicate staining, contamination or low-level conversion.

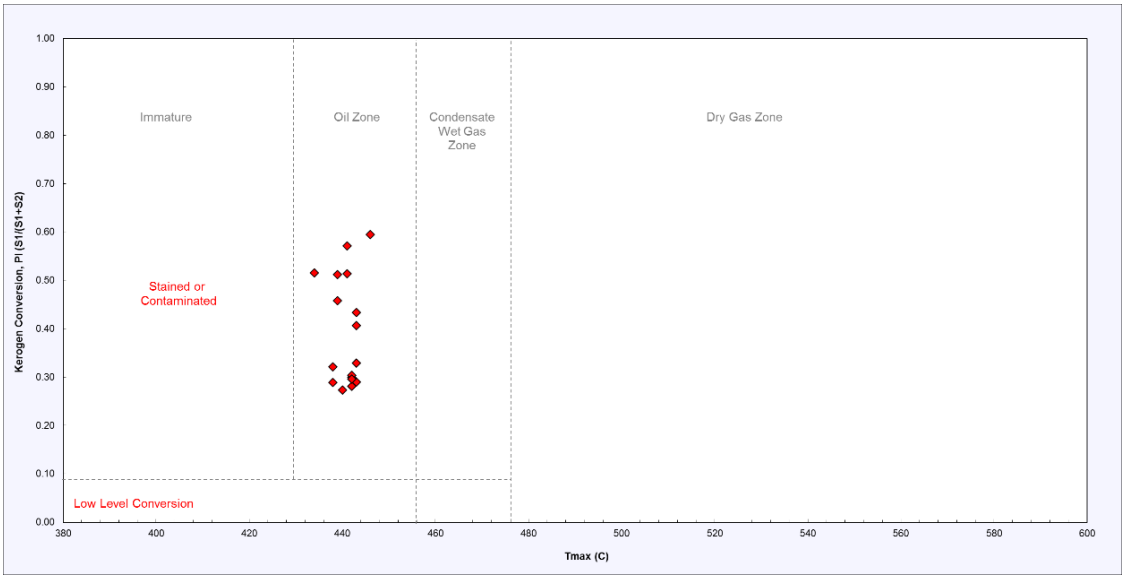

Figure 29: Kerogen Conversion and Maturity data for samples from well 18/25-1.

4.2.2 Well 27/13-1 – Summary

S_1, S_2, and S_3 results from well 27/13-1 vary between 0.07–2.77 mg HC/g rock, 0.06–22.17 mg HC/g rock, and 0.17–1.02 mg CO_2/g rock, respectively (Table A13). T_{MAX} in cuttings range from 428–438 °C, with void readings in all four core samples (Figure 25 and Table A13). and OI ranges from 20–490 mg CO2/g TOC (Table A12).

Most of the samples present a low-temperature S_2 shoulder.

4.2.2.1 Source Potential Logs

Oil potential of samples in this well range from poor in the lowermost samples, to good – excellent in the upper portions of the well (Figure 30). All samples, except for one outlier, above and including sample 2,494 m present good to excellent oil potential (S_2: mg HC/g rock).

HI (S_2/TOC) ranges from 7–431 mg HC/g TOC (Figure 31 and Table A13), placing shallower samples, from 2,095 m to 2,345 m in the oil zone (with one outlier in the gas zone), and deeper cuttings in the gas zone.

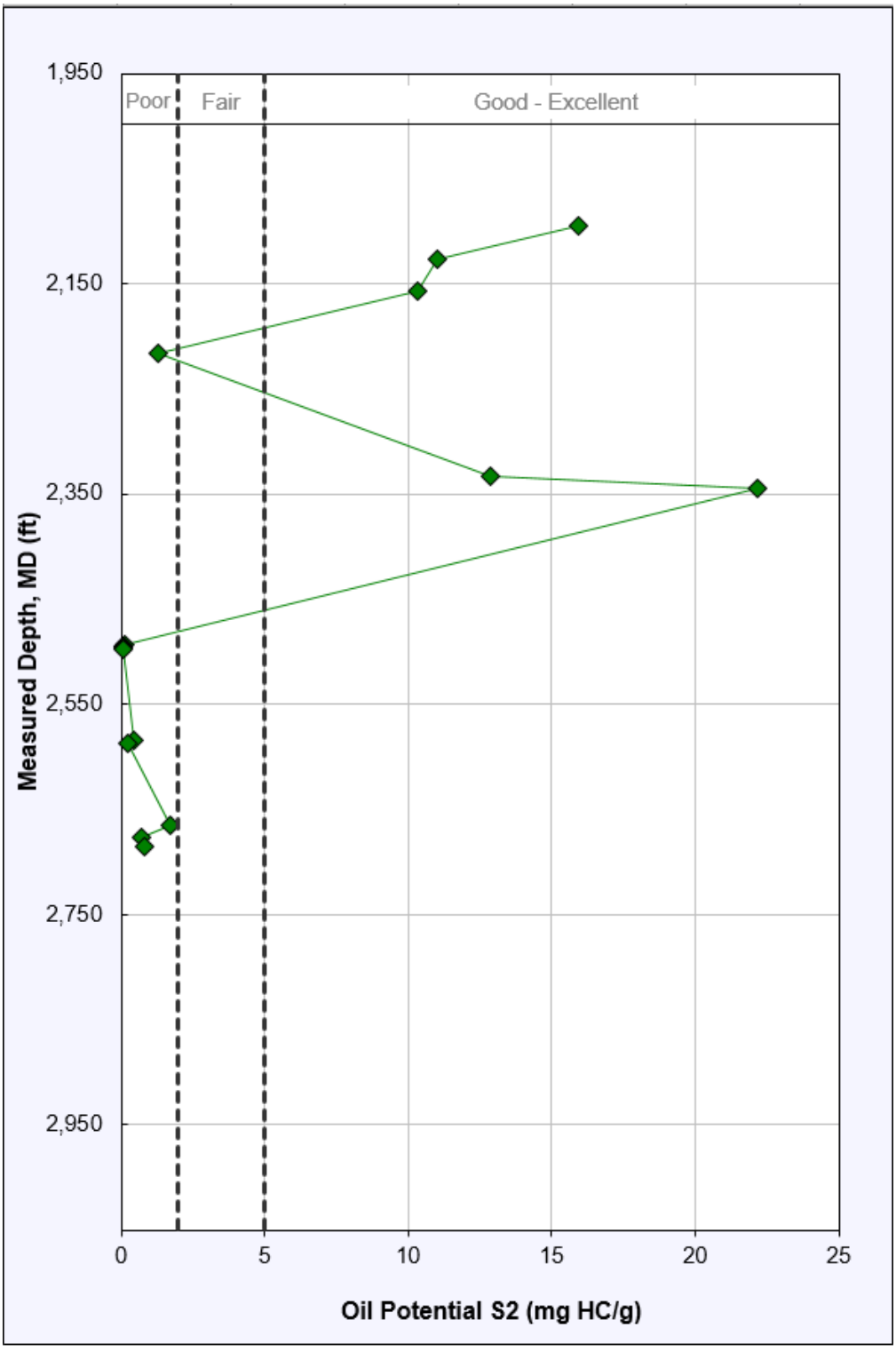

Figure 30: Oil Potential (S2) log for samples from well 27/13-1.

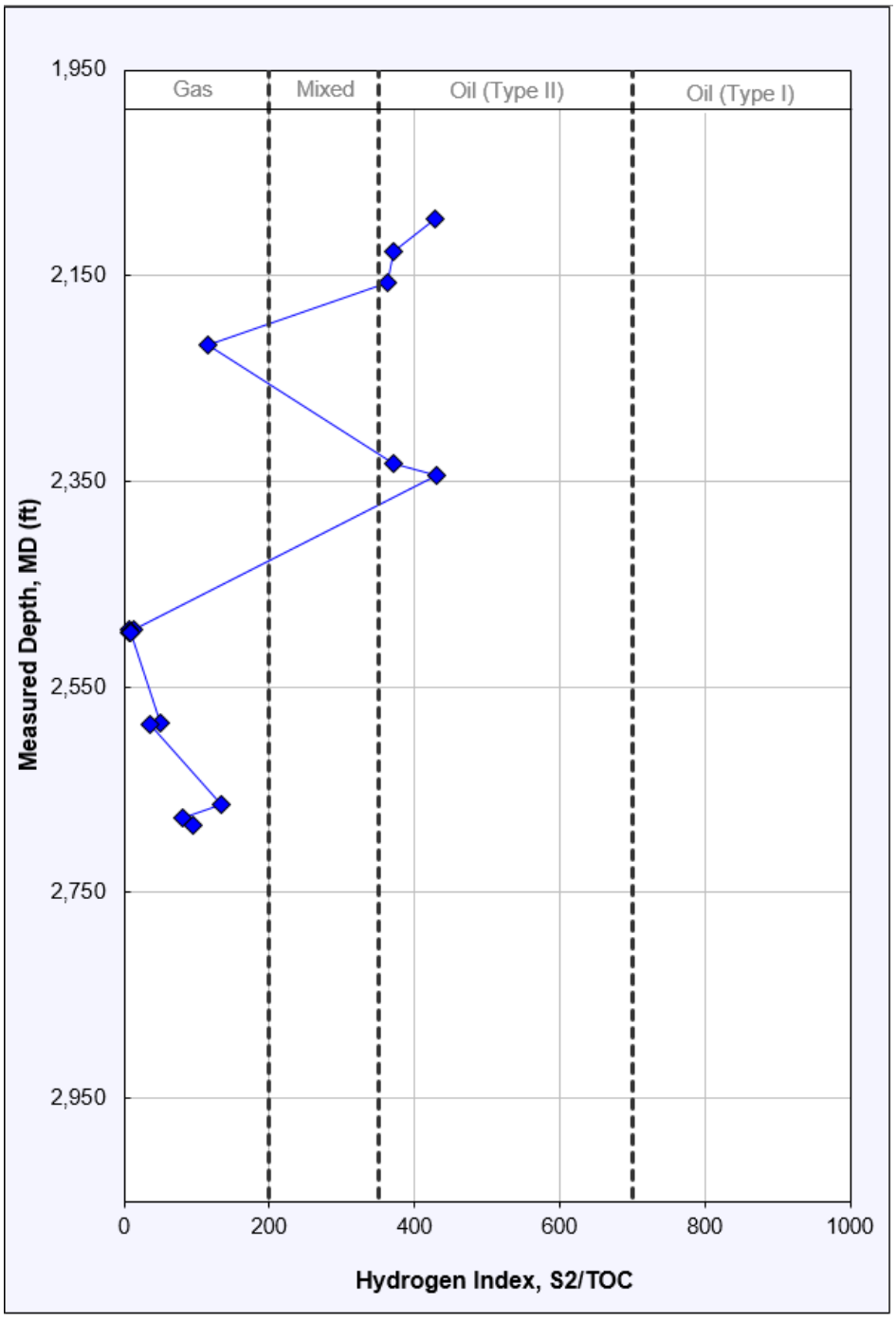

Figure 31: Hydrogen Index (S2 / TOC) source potential log for samples from well 27/13-1.

4.2.2.2 Hydrocarbon Indicator and Maturity Logs

Samples analysed for NOC indicate both Low Maturity and Early Maturity, with some indicating either maturity or staining/contamination from drilling muds. (Figure 32).

PI analysis indicates that cuttings samples range from immature to early gas generation zones, while core samples give results within the gas generation zone and may present unreliability (Figure 33). The cuttings from above 2,345 m straddle the distinction between immature and oil prone, while deeper samples are somewhat more varied.

While measured vitrinite reflectance is not available within this well section, vitrinite reflectance equivalents range from 0.54 to 0.72, tracking roughly in line with T_{MAX}, indicating generation capability to be within the oil generation zone and in one case immature (Figure 34). Samples between 2,350 m and 2,575 m fall off the scale due to void T_{MAX} readings in core samples (i.e. core samples did not register a T_{MAX} reading considered reliable by GeoMark Laboratories).

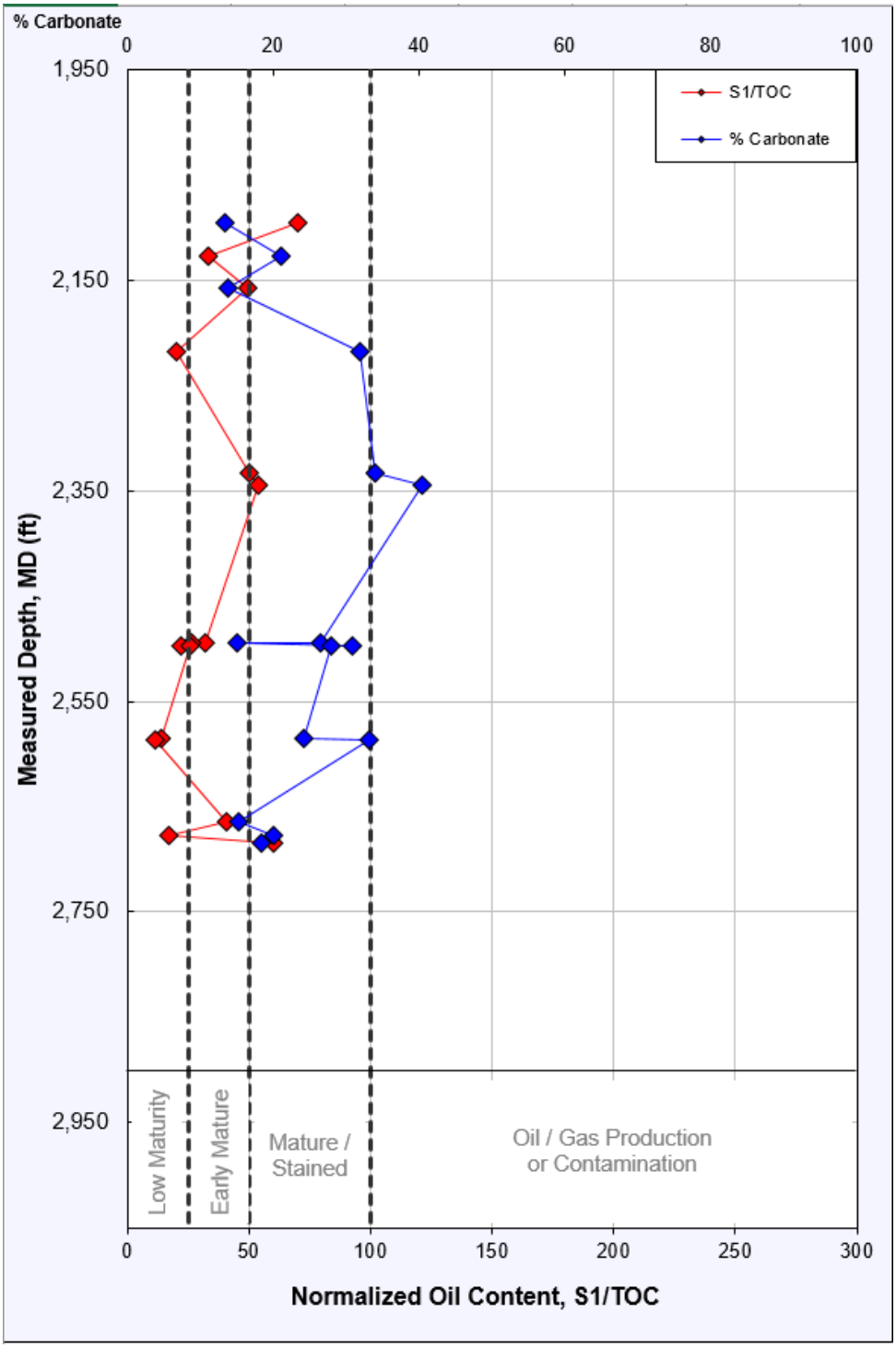

Figure 32: Normalised Oil Content and % carbonate. Samples straddle Low Maturity and Early Maturity, with some indicating either maturity or staining.

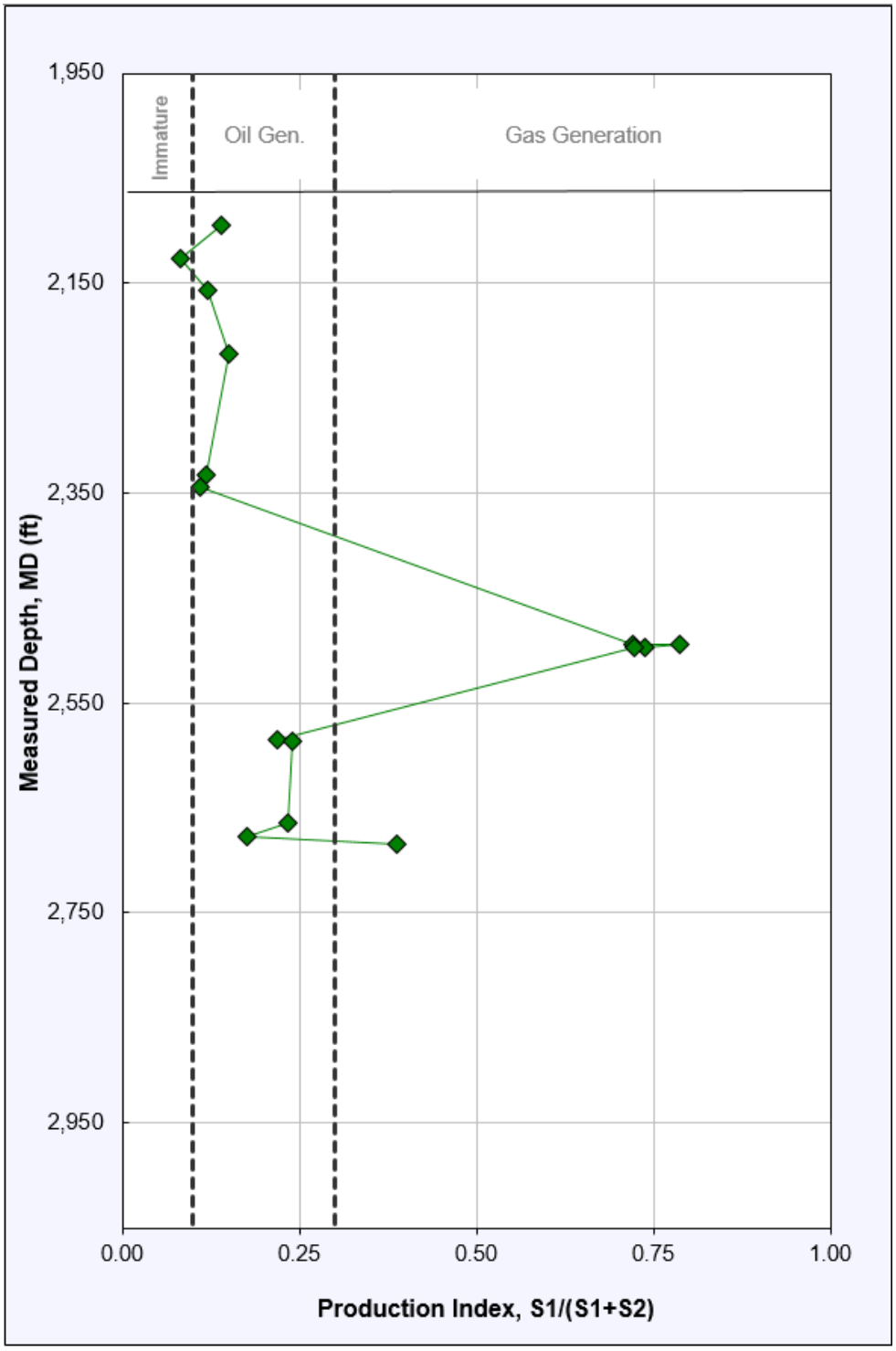

Figure 33: Production Index Plot. While most samples range from immature to early gas generation, the cluster of samples within the gas generation zone originate from core and may present unreliability.

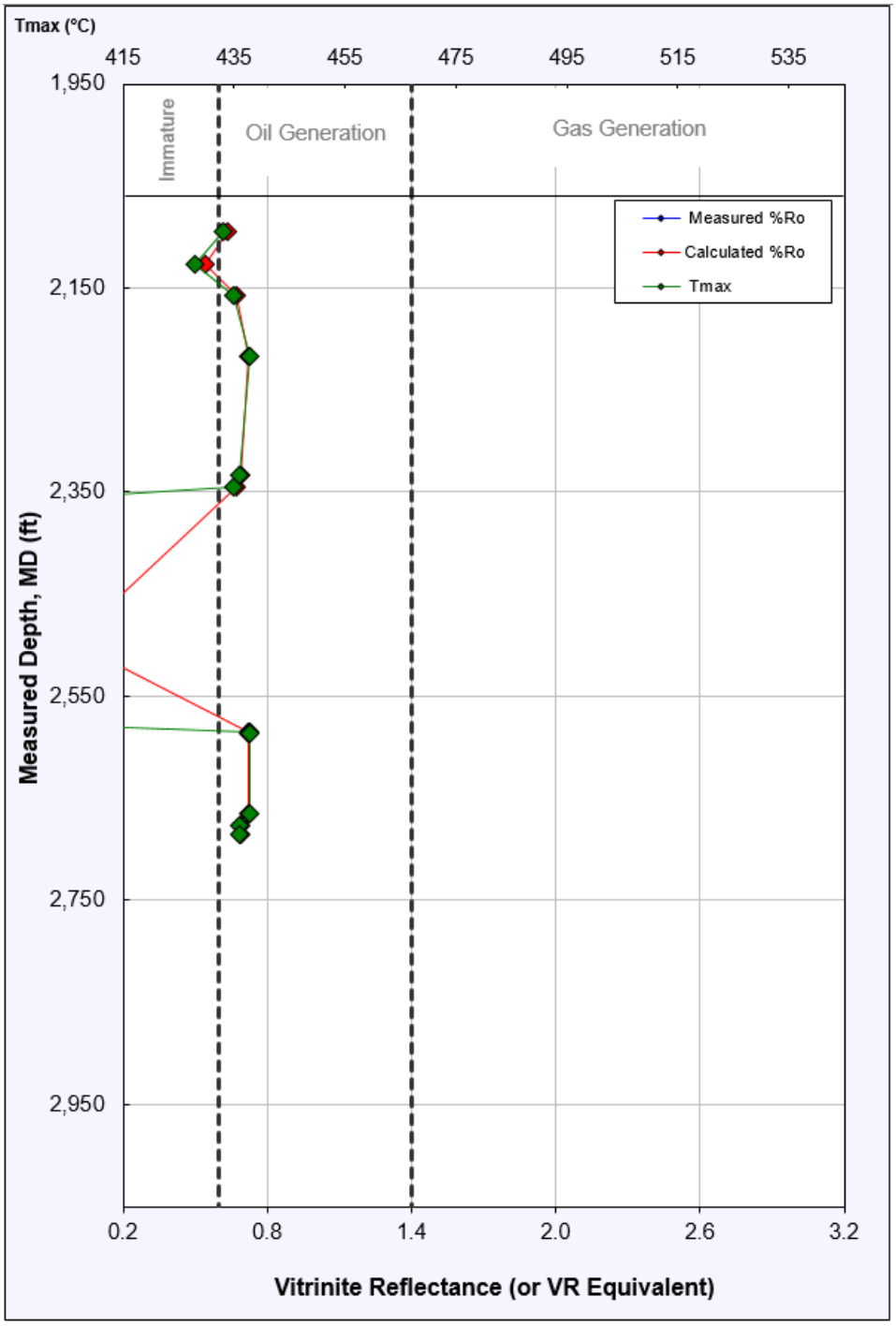

Figure 34: Maturity Indicator Source Potential logs for samples from well 27/13-1. Samples between 2,350 m and 2,575 m fall off the scale due to erroneous Tmax readings in core samples (i.e. core samples did not register a Tmax)

.

4.2.2.3 Pseudo Van Krevelen Plots

Figure 35 outlines results from this well, indicating a dominantly Type II kerogen and a scatter of samples with lower HI and OI results around Type II/III/IV kerogen. A cluster is seen at the Type II kerogen definition line, while results from core samples cluster at the baseline having produced low OI results.

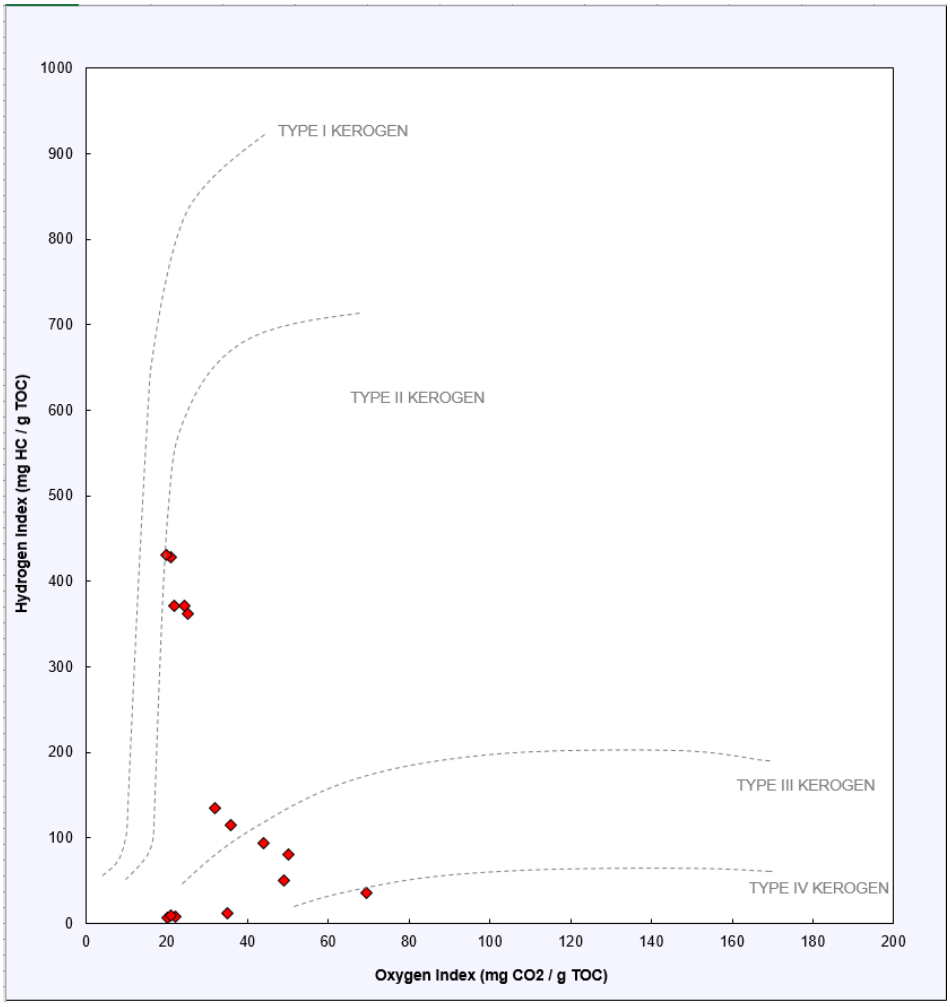

Figure 35: Pseudo Van Krevelen Diagram (HI vs. OI) of samples from well 27/13-1. Note that while most samples plot within Type II/Type III, core samples returned low HI and plotted anomalously as Type IV kerogen (possibly due to sample degradation).

4.2.2.4 Kerogen Quality Plots

Figure 36 displays a Kerogen Quality Plot for cuttings and core samples from well 27/13-1. Using this depiction of Remaining Hydrocarbon Potential vs. TOC, high-ratio results appear in Type II: Oil-Prone, Usually Marine classification.

Other samples display an HI too low to plot accurately, falling into the Type III: Gas Prone and Dry Gas Prone designations. This is due to lower TOC and Remaining Hydrocarbon Potential. Note that these samples clustered at the baseline may be unreliable due to low TOC readings.

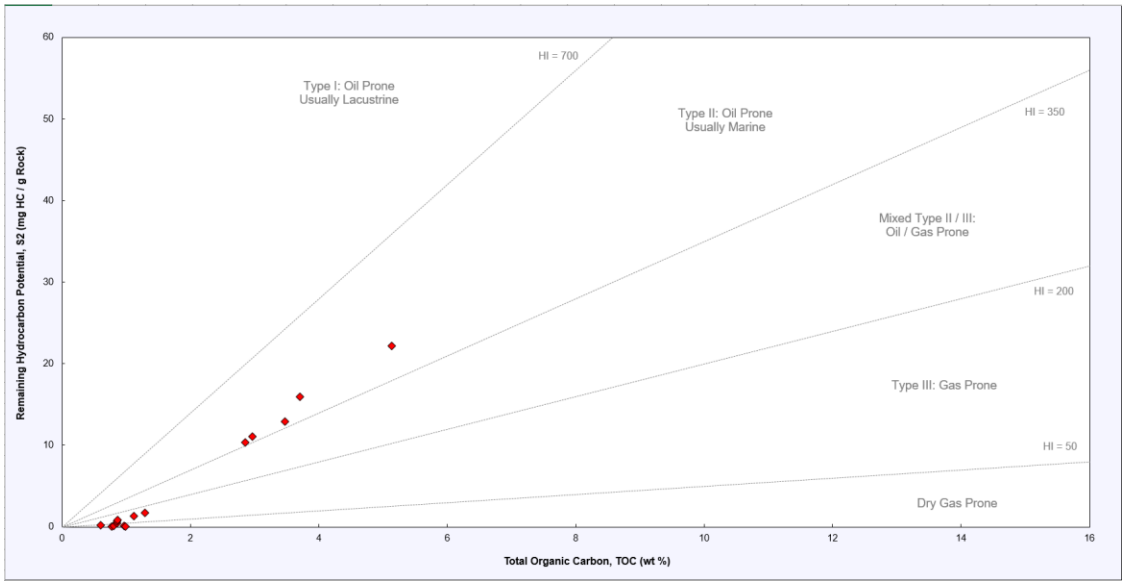

Figure 36: Kerogen quality plot for cuttings and core samples from well 27/13-1.

4.2.2.5 Kerogen Type and Maturity Plots

Figure 37 indicates kerogen typing using HI, T_{MAX}, and the derived %Ro. Core samples, due to returning void T_{MAX} results, do not appear on this chart. As HI falls between 36 and 431, and T_{MAX} ranges from 428 – 438, samples plot in two distinct groups as Type II and Type III kerogens. Except for one immature result, all samples plot above 0.6 %Ro, within the oil generation window.

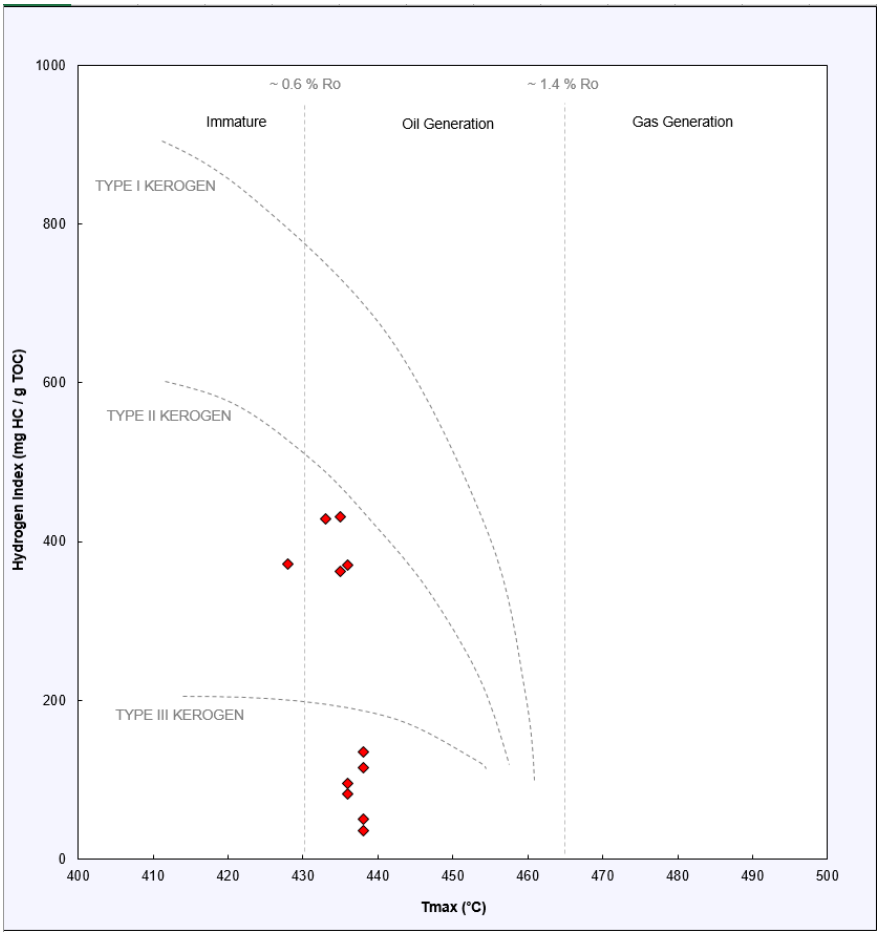

Figure 37: Cross-plot of HI vs. Tmax in samples from well 27/13-1 (note that core samples are omitted due to null Tmax readings). All samples plot close to a given Ro% value of 1.5% (marginally mature), and within Type II/Type III source rock potential zones.

4.2.2.6 Kerogen Conversion and Maturity Plots

A PI vs T_{MAX} plot, as in Figure 38 indicates that almost all samples fall within the oil zone or oil generation window, with one indication of Low-Level Conversion or contamination. As this uses T_{MAX} values, core results are not included.

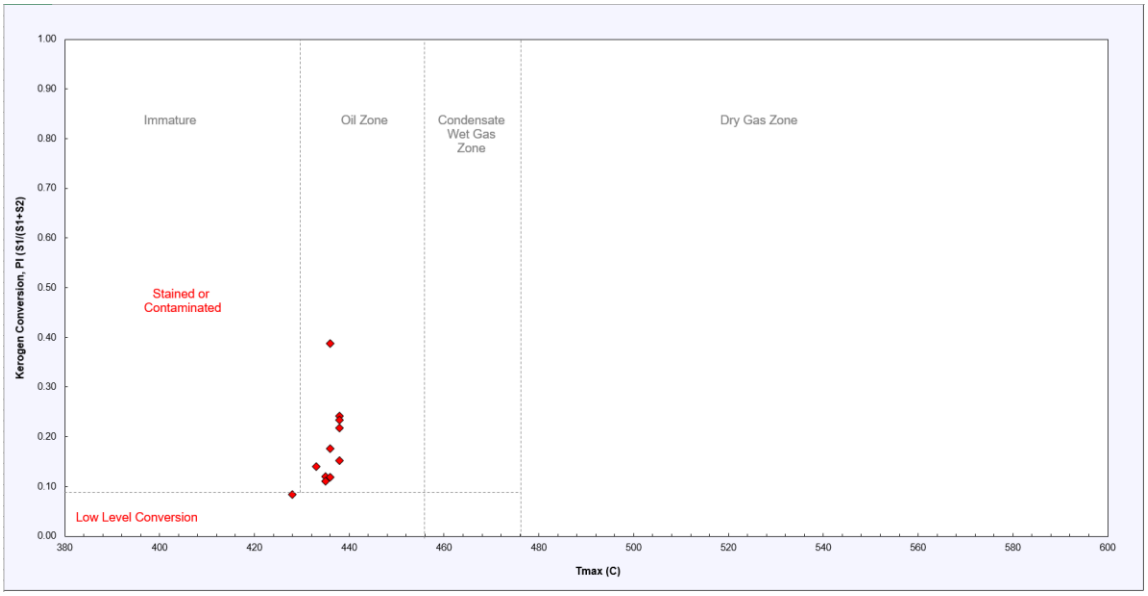

Figure 38: Kerogen Conversion and Maturity Plot for well 27/13-1.

4.3 XRF

4.3.1 Well 18/25-1

4.3.1.1 Sandclass lithological discrimination

Sandclass (Herron, 1998) analysis (Figure 39) indicates that all samples from the well 18/25-1 fall into the shale category. There appear to be two distinct groupings, which can be split into samples shallower and including 2,709 m, and those deeper than 2,709 m: cuttings from deeper than 2,709 m appear closer to the wacke shale/wacke discrimination boundary.

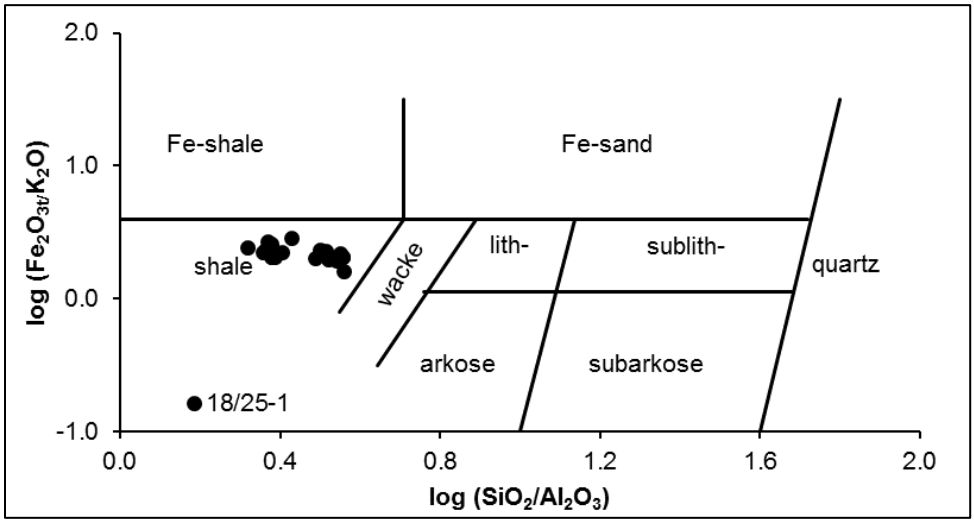

Figure 39: Sandclass plot of samples from well 18/25-1

4.3.2 Well 27/13-1

4.3.2.1 Sandclass lithological description

Samples from well 27/13-1 plot primarily as shale on the Sandclass diagram (Herron, 1998) (Figure 40), with three outliers appearing slightly enriched in iron and plotting as Fe-shale. Sample results are tightly grouped in the shale subdivision.

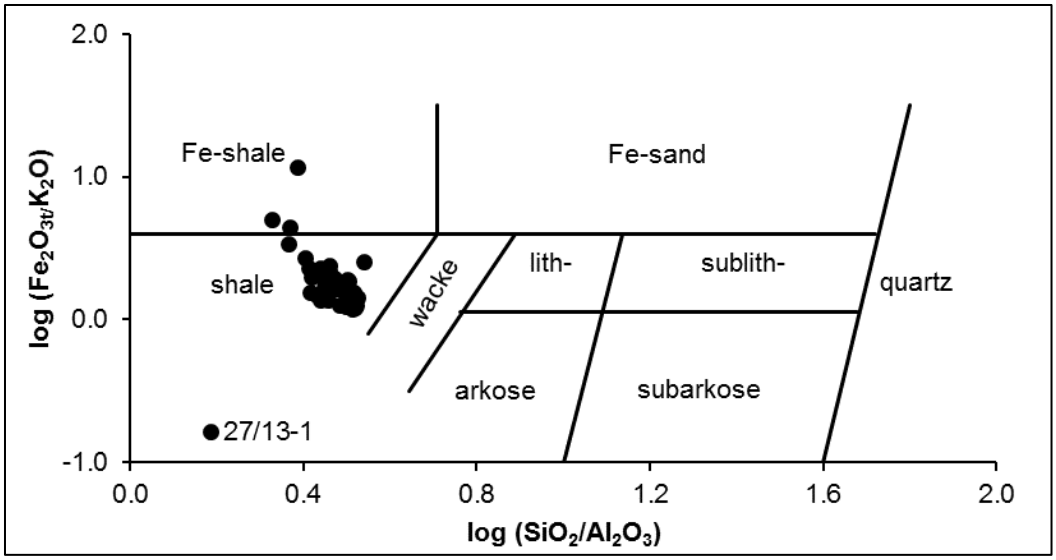

Figure 40: SandClass plot of cuttings and core samples taken from well 27/13-1.

4.4 $\delta^{13}C$ RESULTS

4.4.1 Well 18/25-1

In well 18/25-1, $\delta^{13}C$ in carbonates and kerogen varies from -5.16 to 2.22 ‰ and -28.23 to 25.52 ‰, respectively (Figure 41 and Table A13). $\delta^{13}C$ in carbonates and TOC varies from -5.16 to 2.22 ‰ and -28.23 to -25.52 ‰, respectively (Figure 41and Table A12). A negative shift (~ 4.5 ‰) in the carbonate record is observed from the bottom of the well until around 2750 m. This interval is dated as uppermost Sinemurian–?lowermost Pliensbachian. $\delta^{13}C_{carb}$ tends to present more positive values in the portion of the core dated from the Pliensbachian. Closer to 2725 m, $\delta^{13}C$ exhibits a sharp negative shift, around 5 ‰ in carbonates and 2.7 ‰ in TOC. This negative trend spans over more than 75m, corresponding to the Lower Toarcian. Above this interval, both isotopic records tend to more positive values, during the upper part of the Toarcian and lower part of the Aalenian. $\delta^{18}O_{carb}$ varies between -3.35 to -9.06. The lowest values are observed in the inferred Pliensbachian–Lower Toarcian transition.

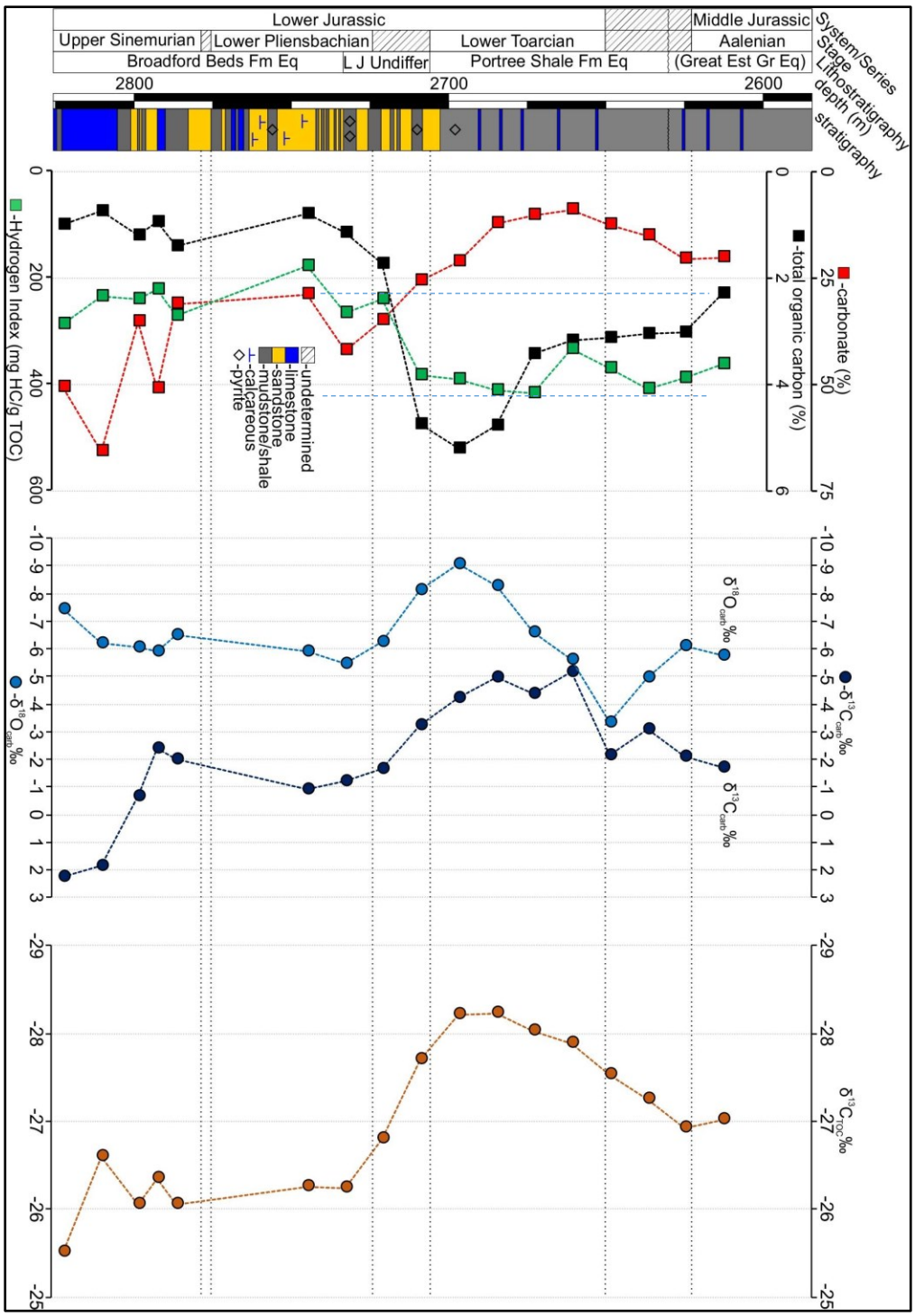

Figure 41: Well 18/25-1: Detailed log, total organic carbon, carbonate content, HI, carbonate δ13C and δ18O and δ13CTOC variation of the top of Broadford Beds Formation Equivalent, Lower Jurassic Undifferentiated (L J Undiffer), Portree Shale Formation Equivalent and Middle Jurassic (Great Estuarine Group Equivalent) (Corrib Gas field), Slyne Basin, offshore Ireland (after Enterprise Oil, 2000; Millennia, 2004). Est – Estuarine; Fm-Formation; Eq.-Equivalent.

4.4.2 Well 27/13-1

In well 27/13-1, $\delta^{13}C$ in carbonates and kerogen varies from -3.98 ‰ to -0.14 ‰ and -29.54 ‰ to 24.18 ‰, respectively (Figure 42 and Table A13). A negative trend (~ 4 ‰) is observed in the carbonate fraction at the top of the studied section from 2217 m, placed in the uppermost Pliensbachian. Notably, this trend is not observed in kerogen: $\delta^{13}C$ in carbonates tends to present more positive values in the portion of the core dated from the Pliensbachian.

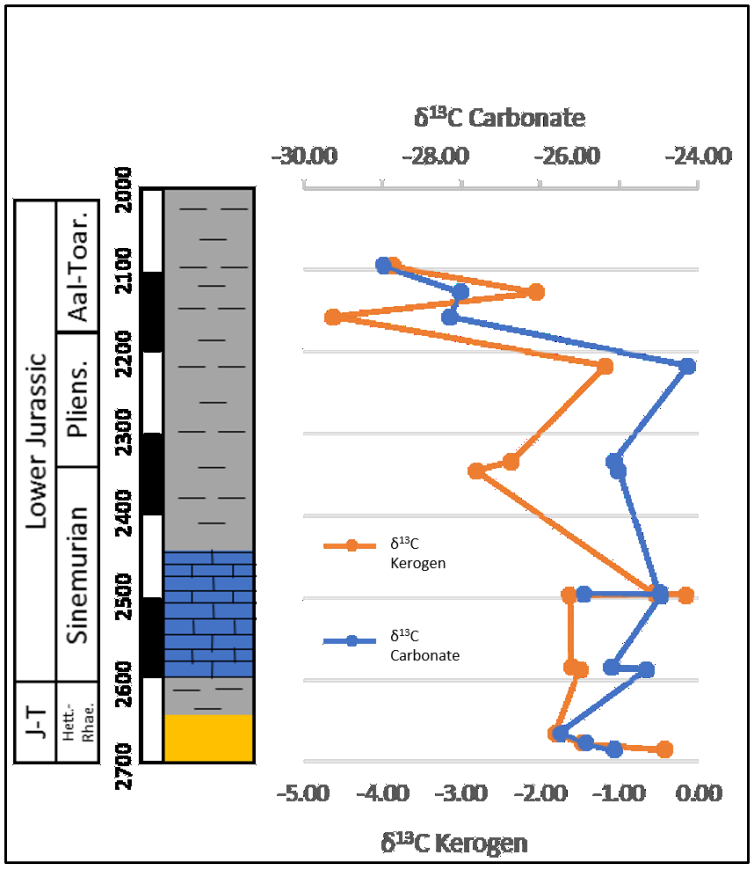

Figure 42: $\delta^{13}C$ record of carbonate and kerogen in well 27/13-1.

4.5 δ ^{18}O RESULTS

$\delta^{18}O$ in well 18/25-1 varies between -3.35 and -9.06 ‰ in well 18/25-1 (Figure 43) and between -3.93 and -7.99 ‰ in well 27/13-1.

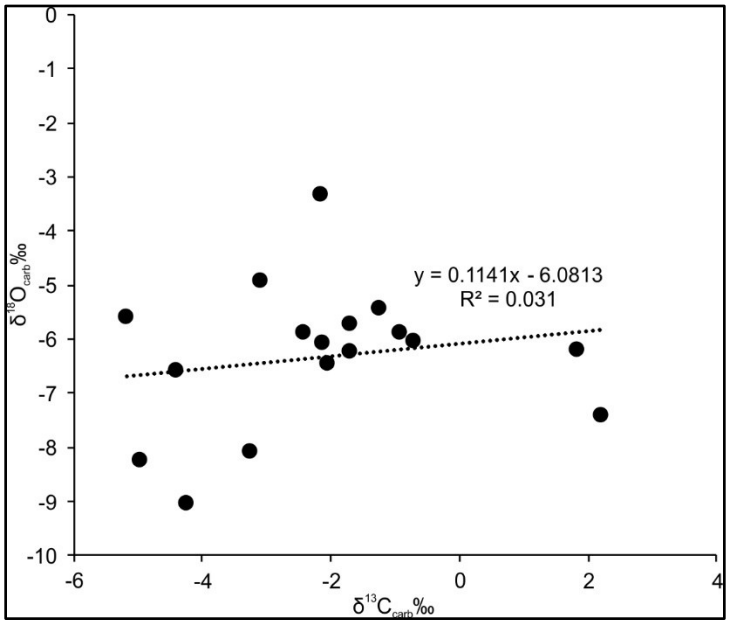

Figure 43: $\delta^{13}C$ versus $\delta^{18}O$ cross plot of the analysed samples from the top of Broadford Beds Formation Equivalent, Lower Jurassic Undifferentiated, Portree Shale Formation Equivalent and Middle Jurassic (Great Estuarine Group Equivalent) units in the well 18/25-1, Slyne Basin, offshore Ireland.

CHAPTER 5: DISCUSSION

5.1 SOURCE ROCK ANALYSIS OF THE STUDIED WELLS

The TOC and Rock-Eval Pyrolysis results from well 18/25-1 describes the Pabba Shale Equivalent (Late Sinemurian-Pliensbachian) and Portree Shale Equivalent (Toarcian) as a mature source rock in this sector of the Slyne Basin (Sections 4 and 4.2). The Late Pliensbachian interval is not identified in this well.

The Maturity Report (Enterprise Energy Ireland, 2003) for well 18/25-1 indicated that:

- Upper Jurassic sediments are early mature for oil generation,
- Middle Jurassic sediments are early to middle mature for oil generation,
- Lower Jurassic sediments are middle to late mature for oil generation and approaching the gas window.

In this study, the latter has been confirmed and kerogen has been identified as being of generally Type II/Type III (section 4.2). Using typical interpretations, this can be related to a marine depositional setting (Tyson, 1995).

5.1.1 Source rock distribution in the Slyne Basin

The Bandon discovery located south of the Corrib gas field in the Slyne Basin, (Serica Energy, Ireland Slyne Basin Licence FEL 1/06, Dancer *et al.*, 2005; Wrigley *et al.*, 2014) is thought to be sourced from Lower Jurassic shales. In well 27/4-1z, similar Lower Jurassic source rock intervals have been dated from the Late Pliensbachian (TOC ~ 5 wt.% and HI ~ 400 mg HC/g TOC) and Lower Toarcian (TOC ~ 3.5 wt.% and HI ~ 450 mg HC/g TOC), although immature (e.g. Serica Energy, 2014). In well 27/13-1, located further

south, the Pliensbachian (TOC = < 6.5 wt.% and HI 205-377 mg HC/g TOC) and the Lower Toarcian (TOC < 7.8 wt.% and HI 330–550 mg HC/g TOC) were also identified as source rocks (Scotchman, 2001 and references therein). Despite the differences in TOC and occurrence, the kerogen types associated with each source rock interval for the entire Slyne Basin remain type II-III (gas-oil prone) for the Pliensbachian and type II (oil-prone) for the Toarcian and Aalenian. The same trends are observed elsewhere around this region (e.g. Fleet *et al.*, 1987; Scotchman, 2001).

TOC and Rock-Eval Pyrolysis results from well 18/25-1 indicates the Portree Shale Formation Equivalent (Lower Toarcian) as a mature source rock (TOC ~ 5 wt.%, HI ~ 400 mg HC/g TOC, and T_{max} ~ 434–446 °C) in this sector of the Slyne Basin. However, the data obtained from well 27/13-1 is much less conclusive. While TOC analysis indicates that source rock is present, ranging from poor to excellent quality (up to 5.14 wt. % TOC), the variation in data over such low-resolution sampling reduces the ability to identify potentially highly productive zones in terms of potential to produce hydrocarbon. In the lower section of the well, samples cluster with a low HI (<200 mg HC/g TOC; Figure 31) indicating possible gas generation potential. Samples from the upper section indicate predominantly oil-prone characteristics, ranging from immature to just within the oil generation window. T_{MAX} in this well indicates that samples are within production windows of both oil and gas source rocks (428 – 438 °C). Kerogen types associated with each aforementioned source rock interval bear similarities across the entire Slyne Basin; type II-III (gas-oil prone) for the Pliensbachian and type II (oil-prone) for the Toarcian and Aalenian. The same trends are observed elsewhere around this entire region (e.g. Fleet *et al.*, 1987; Scotchman, 2001) indicating that results are consistent with previous studies.

5.2 THE $\delta^{13}C$ AND $\delta^{18}O$ RECORD OF THE SLYNE BASIN

The Lower Jurassic interval is characterized by the occurrence of several CIEs and associated organic matter preservation intervals (OMPIs, Silva *et al.*, 2011). The origin, extent, duration, causes and consequences of these CIEs are still under intense scrutiny (Silva, 2015a, 2015b; Suan, 2015; Krencker, 2015; Gómez, 2016; Masetti, 2016).

The $\delta^{13}C$ record of organic matter obtained from well 18/25-1 presents positive values during the Upper Sinemurian, a negative trend followed by a positive trend during the uppermost Sinemurian–Lower Pliensbachian, a negative trend during the lowermost Lower Toarcian, and then the return to more positive $\delta^{13}C$ values (Figure 44).

Ultimately, this study finds that the $\delta^{13}C$ record of well 18/25-1 records the Raricostatum Zone positive CIE, the Sinemurian-Pliensbachian Boundary Event, and the negative CIE associated with the T-OAE, despite stratigraphic uncertainty, coarse sampling resolution, and possible diagenetic effects (see section 5.2.1). The T-OAE positive CIE it is not clearly defined in the obtained dataset (e.g. Jenkyns and Clayton, 1986; Jenkyns, 1988; 2010; Hesselbo, 2000a; 2000b; Jenkyns *et al*., 2001; 2002; Hesselbo *et al*., 2007; Korte and Hesselbo, 2011; Jenkyns and Weedon, 2013; Duarte *et al*., 2014; Suan *et al.*, 2015; Gómez *et al*., 2016). No clear CIE, and therefore no clear OAE, is seen in our dataset from well 27/13-1. For further discussion of these CIEs, see sections 5.2.2, 5.2.3, and 5.2.4, below.

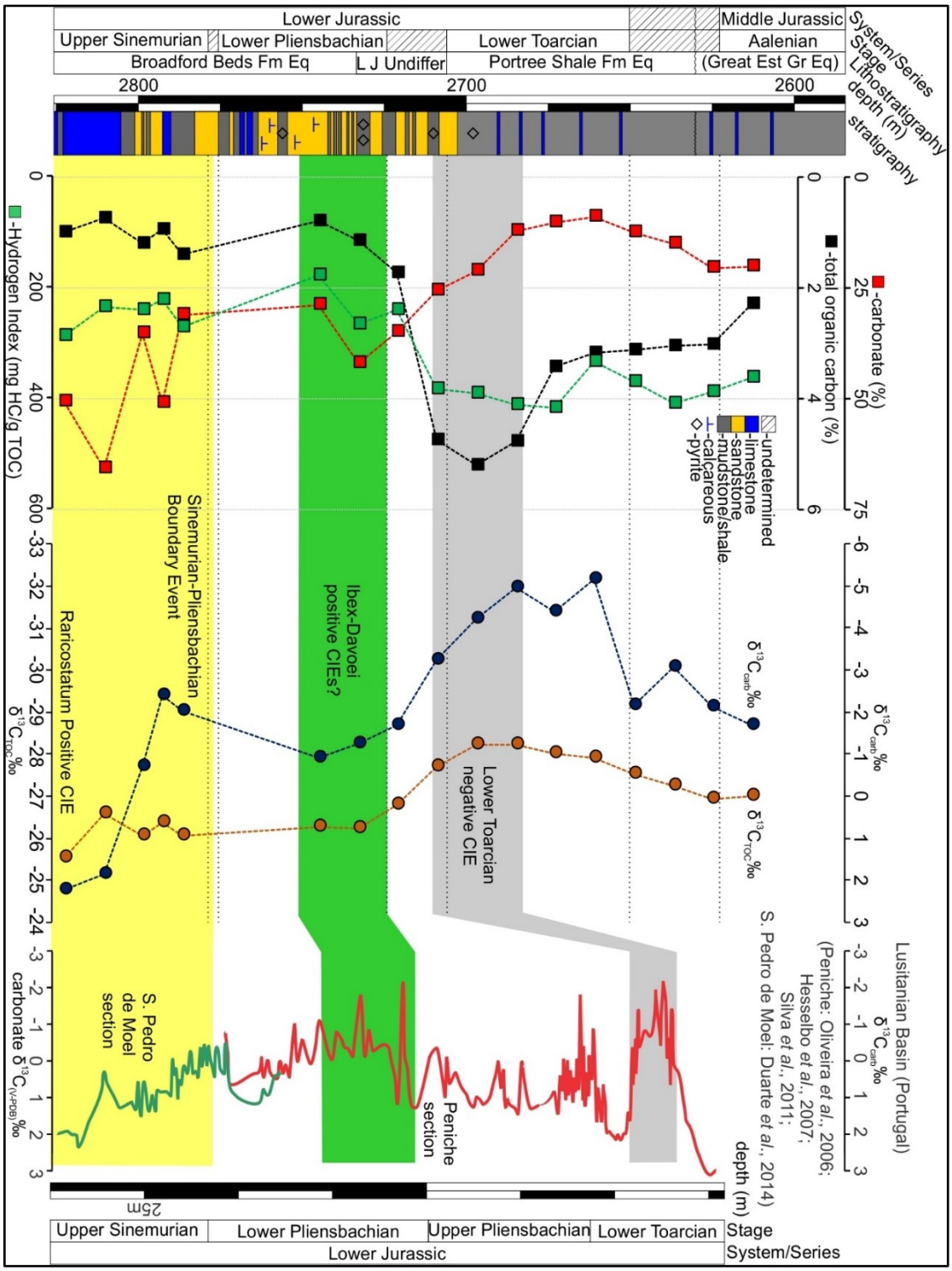

Figure 44: Detailed log and δ13C variation of the top of Broadford Beds Formation Equivalent, Lower Jurassic Undifferentiated, Portree Shale Formation Equivalent and Middle Jurassic (Great Estuarine Group Equivalent) units in the well 18/25-1 (Corrib Gas field), Slyne Basin, offshore Ireland (after Enterprise Oil, 2000, Millennia, 2004) and comparison with the detailed δ13C record of the Lusitanian Basin (Portugal) (modified from Silva and Duarte, 2015 and references therein). Est – Estuarine; Fm-Formation; Eq.-Equivalent.

5.2.1 Primary Signal vs Diagenetic Signal

The effects of early marine diagenesis on carbonate $\delta^{13}C$ and $\delta^{18}O$ are not yet fully understood (see Swart, 2015). Inorganic aragonite and high-Mg calcite cements tend to have more positive $\delta^{13}C$ than normal skeletal aragonite (Braithwaite and Camoin, 2011). Notwithstanding, early cementation influenced by the products linked with microbial organic matter decay (resulting in the production of CO_2 depleted in ^{13}C) may result in lower $\delta^{13}C$ values (e.g. Marshall, 1992; Swart and Merlim, 2000; Dickson *et al.,* 2008; Coimbra *et al.,* 2009; Silva *et al.,* 2011; Duarte *et al.,* 2014). The supply of oxidants (from both mixing and biological activity) controls the extent of the degradation of organic matter and it has been established that oxidation of organic matter does not impact $\delta^{13}C$ significantly in carbonate-rich rocks (Swart, 2015). On the other hand, the occurrence of diagenetic components influenced by organic matter oxidation might be significant in intervals of low or non-deposition and where carbonates are a minor component (Swart, 2015). The $\delta^{18}O$ of this cement is also likely to be vary depending on the nature of the original grains and the temperature of precipitation: colder environments would result in more positive $\delta^{18}O$ values (e.g. Swart and Merlim, 2000).

Upon deeper burial, the temperature effect is further recorded on the carbonate $\delta^{18}O$, leading to lighter values due to the higher temperatures. $\delta^{13}C$ is more resistant to change during late stage diagenesis, as it has very low thermal dependency and requires a high degree of water-rock interaction (Marshall, 1992; Jacobsen and Kaufman, 1999). However, the presence of high pCO_2 and low $\delta^{13}C$ fluids, a situation observed elsewhere during late stage diagenesis, can alter carbonate $\delta^{13}C$ towards lighter values (Derry, 2010).

The high carbonate content of the analysed samples (9.41 % - 65.98 %) and the low TOC contents of the Sinemurian-Pliensbachian interval suggests that the $\delta^{13}C$ trend reflects the primary oceanographic signal, even if the absolute values are slightly modified. The lack of correlation between $\delta^{13}C$ and $\delta^{18}O$ supports this interpretation (Figure 43). Due to the low carbonate content (arguably the reflection of the T-OAE carbonate production crisis – Suan, 2008) and organic matter richness, the isotopic trend of carbonates in Lower Toarcian interval is interpreted to present a higher degree of diagenetic alteration, a warning when interpreting results. It is important to note that diagenesis can be as a result of water flow-through from any source: marine, lacustrine or meteoric (Swart, 2015) and a narrow sedimentary basin such as the Slyne Basin may be influenced be all three.

5.2.2 Raricostatum Zone positive CIE

The Sinemurian time interval records several carbon isotopic excursions (Jenkyns *et al.*, 2002). The most notable, so far, has been the one observed in the Obtusum Subzone (Riding *et al.*, 2013, Jenkyns and Weedon, 2013; Masetti *et al.*, 2016). On the other hand, some studies point out a more common positive trend of this time interval, namely the occurrence of positive CIE in the Turneri (Lower Sinemurian, e.g. Jenkyns and Weedon, 2013; Porter *et al.*, 2014) and Raricostatum zones (e.g. Korte and Hesselbo, 2011, Jenkyns and Weedon, 2013; Duarte *et al.*, 2014; Gómez *et al.*, 2016), which coincides with a warming event (Gómez *et al.*, 2016). Despite the biostratigraphic uncertainty associated with the record and the marked lithological contrast, I suggest that the more positive $\delta^{13}C$ values observed in Upper Sinemurian sediments in the studied well correspond to the Raricostatum Zone positive CIE (Figure 44).

5.2.3 Sinemurian-Pliensbachian Boundary Event

The Sinemurian-Pliensbachian Boundary Event spans from the uppermost Sinemurian to the Lower Pliensbachian (Hesselbo 2000b; Korte and Hesselbo, 2011; Jenkyns and Weedon, 2013; Duarte *et al.*, 2014; Gómez *et al.*, 2016) and it is expressed in the $\delta^{13}C$ carbonate dataset of well 18/25-1. The uppermost Sinemurian–Lower Pliensbachian negative CIE is concomitant with the final stages of the Late Sinemurian warming and subsequent cooling (Korte and Hesselbo, 2011; Gómez *et al.*, 2016) and deposition and preservation of organic matter in a transgressive context (Duarte *et al.*, 2010; 2014). Korte and Hesselbo (2011) suggested a connection between that n-CIE and with the events that eventually led to the T-OAE.

Several authors noted a positive $\delta^{13}C$ CIE in the later part of the Lower Pliensbachian (Ibex and Davoei zones) in datasets from Portugal (e.g. Suan *et al.*, 2010; Silva *et al.*, 2011, Silva *et al.*, 2015), Spain (e.g. Rosales *et al.*, 2006; Almendáriz *et al.*, 2012) Italy (Morettini *et al.*, 2002) and the UK (van de Schootbrugge *et al.*, 2005, Korte and Hesselbo, 2011). In addition, the upper Davoei–lower Margaritatus Chronozone interval is characterized by a positive εNd excursion (Dera *et al.*, 2009b, 2015), increased kaolinite content (Dera *et al.*, 2009a), rise in seawater temperatures in the NW Tethys (van de Schootbrugge *et al.*, 2005; Rosales *et al.*, 2006; Gómez *et al.*, 2016), organic matter preservation (Duarte *et al.*, 2010; Silva and Duarte., 2015; Silva *et al.*, 2015), Tethyan/Boreal faunal exchanges (e.g. Aberhan and Baumiller, 2003; Dommergues *et al.*, 1997, 2009; Schweigert, 2005; Arias, 2006), and an interpreted rising in sea level (Haq *et al.*, 1988). Dera *et al.* (2009b, 2015) suggested that incursion of warm water masses from equatorial Tethys was a factor conditioning sedimentation and the distribution of climatic belts during the Lower Jurassic. It is

important to note that the Upper Pliensbachian positive CIE and concomitant OMPI (Silva *et al.*, 2011, Silva and Duarte, 2015, and references therein) is not observed (at least to the extent that the current biostratigraphic knowledge allows) in this well. Silva and Duarte (2015) argued that extreme climate warming was the driver of organic matter deposition during most of the Pliensbachian, coupled with high oceanic productivity and intermittently thermo-stratified epeiric seas.

5.2.4 Toarcian Oceanic Anoxic Event and the negative CIE

The Toarcian time interval features variations in the $\delta^{13}C$ record (Figure 44). One of the most significant is the negative CIE followed by a positive CIE linked with the T-OAE (Jenkyns and Clayton, 1986; Jenkyns, 1988; 2010; Jenkyns *et al.*, 2001; Hesselbo *et al.*, 2000a; 2007). This event is characterized by widespread anoxia (Jenkyns and Clayton, 1986; Jenkyns, 1988, 2010, Hesselbo *et al.*, 2000a; van de Schootbrugge *et al.*, 2013), global warming (e.g. Danise *et al.*, 2013; Gómez *et al.*, 2016), ocean acidification (e.g. Suan *et al.*, 2010), a 2nd-order mass extinction event in benthic and pelagic groups (e.g. Danise *et al.*, 2013, Gómez and Arias, 2010), deposition of organic-rich sediments (e.g. Fleet *et al.*, 1987; Baudin *et al.*, 1990; Prauss *et al.*, 1991; Murphy *et al.*, 1995; Röhl *et al.*, 2001), and a major perturbation of the global carbon cycle, recorded in carbonates, fossil wood and kerogens (e.g., Jenkyns, 1988; 2010, Jenkyns *et al.*, 2001; Hesselbo *et al.*, 2000a, 2007; Gómez *et al.*, 2008; Suan *et al.*, 2008a; 2008b; 2010; 2011; Bodin *et al.*, 2010; Gómez and Arias, 2010; Caruthers, *et al.*, 2011; Pittet *et al.*, 2014; French *et al.*, 2014; Kafousia *et al.*, 2014; Suan *et al.*, 2015; Gómez *et al.*, 2016). In more detailed datasets with higher resolution analyses, it is possible to observe two sharp negative CIEs, one associated

with the Pliensbachian-Toarcian boundary and another one with the uppermost Tenuicostatum-lower Falciferum zones of the Lower Toarcian interval (e.g. Hesselbo *et al.*, 2007; Suan *et al.*, 2010). The latter is one of the longest CIEs observed in the Mesozoic. The dataset (Figure 44) shows the combined occurrence of a broad negative CIE (around 125m thick, between 2600–2725 m) associated with high TOC, S_2, and HI. The onset of this CIE is most likely coincidental with the T-OAE CIE, corresponding to the highest TOC and lowest $\delta^{13}C$ interval of the studied section in well 18/25-1, between ~ 2680–2715 m. The assumed ~25 m thickness of the T-OAE CIE deposits in the Slyne Basin agrees with the $\delta^{13}C$ expression of this interval in the Mochras borehole (Wales, e.g. Jenkyns *et al.*, 2001), Yorkshire (UK, Krencker, *et al.*, 2015), Portugal (Hesselbo *et al.*, 2007), and Morocco (Bodin *et al.,* 2010). The low $\delta^{13}C_{TOC}$ (<–30 ‰) values typically recorded during the T-OAE are not observed in the dataset (see, for example, Röhl *et al*., 2001; Suan *et al.,* 2015). This may be the result of burial diagenesis, petroleum generation and the low sampling resolution of this dataset, which is probably too coarse to capture abrupt short-term variations.

After this interval, TOC contents remain relatively high and $\delta^{13}C_{TOC}$ trend reflects a slight enrichment in ^{13}C (Figure 44), although not defining the abrupt positive CIE seen in the upper half of the Falciferum Zone, Lower Toarcian (Jenkyns, 1988; Jenkyns *et al.,* 2001). The high TOC, elevated HI content, and $\delta^{13}C$ trend reflects the occurrence of lipid-rich organic matter in the kerogen assemblages and the existence of conditions prone to organic matter preservation post negative CIE. A similar phenomenon is seen in SW Germany and France, where an expanded interval with high TOC and relatively low $\delta^{13}C$ is recorded for most of the Lower–Middle Toarcian, with only the lowermost part corresponding the T-

OAE CIE (Prauss *et al.*, 1991; Röhl *et al.*, 2001; van Breugel *et al.*, 2006; Hermoso *et al.*, 2013; Suan *et al.*, 2015). Röhl *et al.* (2001) suggested that stressed oxygen conditions (anoxia punctuated by brief periods of oxygenation) were prevalent from the mid-Semicelatum Subzone (Tenuicostatum Zone) to the upper Bifrons Zone in the German sections. Hermoso *et al.* (2013) proposed that, in the Paris Basin, these post-OAE black shales were driven by third-order sea-level changes (i.e. exposure of shelf deposits through sea level change of 0.5 Ma – 3 Ma duration; Haq et al., 1988; Jaquin and de Graciansky, 1998). It appears that after the "global" T-OAE negative CIE, local and regional conditionings (including diagenesis) have an important role governing the $\delta^{13}C$ of either carbonate and organic matter in the Slyne Basin. This observation supports Suan *et al*. (2015) inference that the amplitude and shape of the CIE recorded by $\delta^{13}C_{TOC}$ across the T-OAE are strongly dependent on palaeogeographic gradients in productivity and oxygenation. The Slyne Basin record also provides further evidence that increased rates of organic matter burial might have been one of the main drivers behind the $\delta^{13}C$ rebound after the negative CIE (Jenkyns, 1988).

5.3 XRF ANALYSIS

Given that drill cuttings were finely crushed prior to storage, geological identification of samples was impossible on site. As such, XRF elemental composition analysis proved useful to ensure that shale samples were collected for this project. All samples within the set plotted in the shale and Fe-shale subsections of Herron's (1998) Sandclass lithological diagram showing that shales were selected for other laboratory analyses. Unfortunately, variable TOC across all samples presents uncertainty related to dilution, preventing further investigation of these wells using this instrument without sample purification.

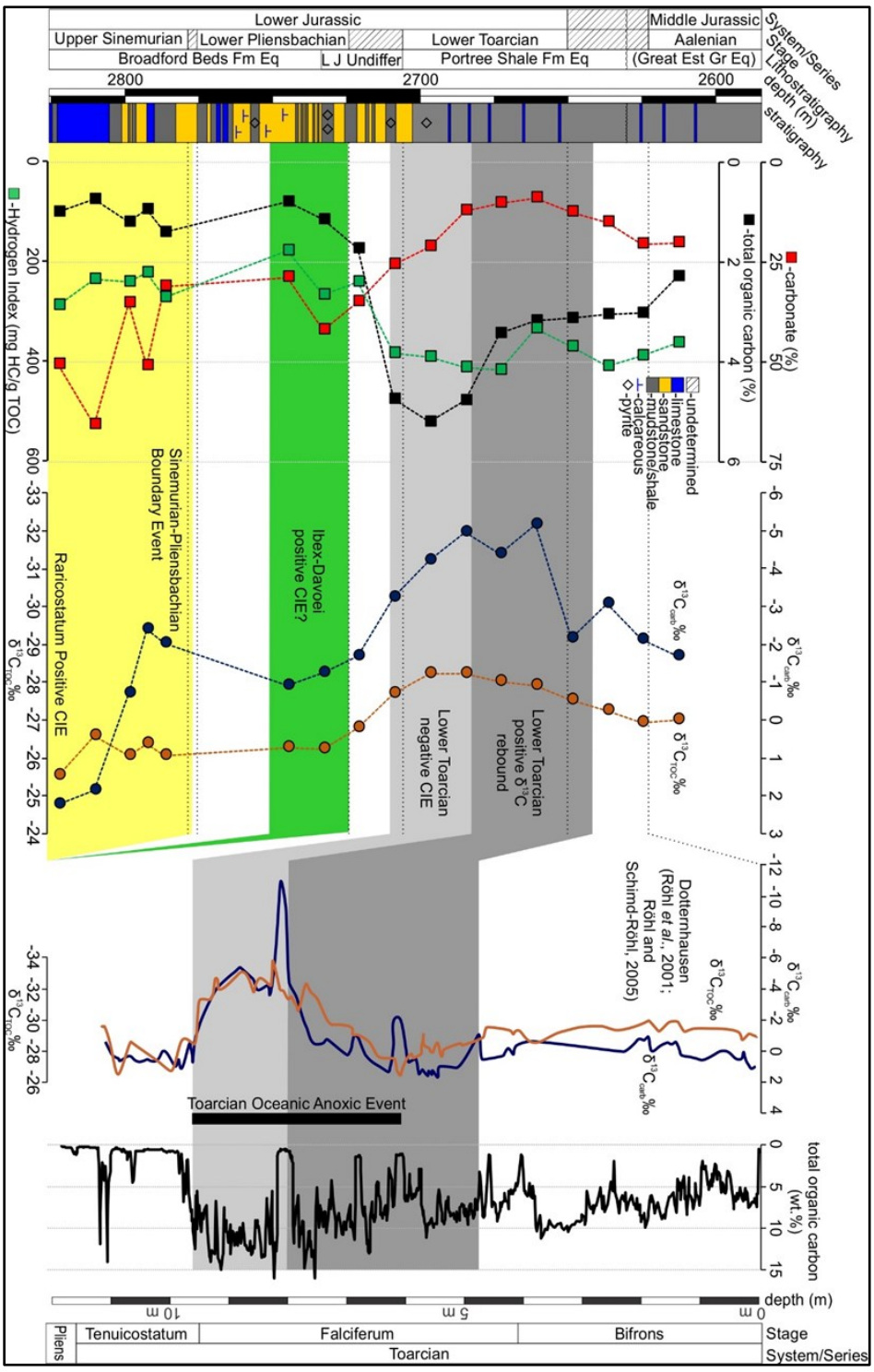

Figure 45: Detailed log and δ13C variation of the top of Broadford Beds Formation Equivalent, Lower Jurassic Undifferentiated, Portree Shale Formation Equivalent and Middle Jurassic (Great Estuarine Group Equivalent) units in the well 18/25-1 (Corrib Gas field), Slyne Basin, offshore Ireland (after Enterprise Oil, 2000, Millennia, 2004) and comparison with the detailed Toarcian δ13C record from SW Germany (e.g. Röhl et al., 2001). Pliens – Pliensbachian; Est – Estuarine; Fm-Formation; Eq.-Equivalent.

CHAPTER 6: CONCLUSIONS AND FUTURE WORK

6.1 SUMMARY

The new TOC, Rock-Eval pyrolysis, $\delta^{13}C$ and XRF datasets from the Slyne Basin 18/25-1 and 27/13-1 wells are a major contribution to the study and recognition of several Lower Jurassic CIEs and associated source rock intervals, despite the biostratigraphic uncertainty and low resolution of the datasets. The Lower Toarcian is confirmed as a mature source rock. Despite the diagenetic artefacts and coarse resolution, the dataset allows expanding the recognition of several carbon cycle perturbations to a portion of the Northern European epicontinental area that was not previously investigated using carbon stable isotopes. The resulting record enables the correlation to of the Raricostatum Zone positive CIE, the Sinemurian-Pliensbachian Boundary Event, and the negative CIE associated with the T-OAE. The T-OAE positive CIE, however, it is not clearly resolved in the obtained dataset.

Cuttings from both wells often presented a Low Temp S_2 shoulder because heavier, free hydrocarbons and non-hydrocarbons (resins, asphaltenes) vaporise or crack only at higher temperatures and are included in the S_2 peak, resulting in reduced S_1, artificially elevated S_2, and potentially suppressed T_{max} values (e.g. Clementz, 1979). Comparing high TOC unaffected with affected samples, this effect seems to have little impact in the dataset. Low TOC samples (Broadford beds), on the other hand, are more affected, as demonstrated by the larger dispersion of T_{max} data, although still comparable with the high TOC samples. Even considering this effect, these present a clear distinction between the Broadford Beds type II-III kerogens (even if S_2 is artificially elevated) and the Pabba/Portree Shales and informal Middle Jurassic B (Great Estuarine Group Equivalent) type II kerogen (Table

A13). T_{MAX} indicates that this portion of the well is mature, within the oil generation window (Tissot and Welte, 1984).

Ultimately, this study aids in the valuable understanding of the extent and causes of the events that led to the T-OAE. It is also a contribution to lowering the risk of hydrocarbon exploration efforts in Ireland's offshore, allowing the integration with known time-equivalent source rock outcrops on Atlantic conjugate margins, for example, Canada, UK, Morocco, Portugal, and Spain.

6.2 SIGNIFICANCE OF ANALYSES

Stable isotope analysis is crucial for inferring the influence of OAEs on a depositional system, as it traces the change in carbon reservoirs, such as atmospheric and ocean-dissolved CO_2. A major negative excursion in the $\delta^{13}C$ record indicates a significant input of isotopically light CO_2 – regardless of the source (volcanogenic, methane hydrate release), as seen in the dataset, represents a possible trigger for major palaeoclimate change. Stable isotope data have not previously been published on analyses of bulk sediment samples of Toarcian age offshore Ireland. The presentation of RockEval pyrolyses confirms that Lower Jurassic intervals host hydrocarbon source rocks in significant thicknesses. As they have been found to be dominantly oil-prone, they should continue to prove highly prospective for exploration companies focusing on Ireland's Atlantic margins.

By using stable isotope data alongside data such as Rock-Eval pyrolysis and total organic carbon values, a better understanding of processes acting upon organic matter preservation at the time of deposition offshore Ireland has been produced. The addition of these data

sets represents a significant contribution to the study and recognition of several Lower Jurassic CIEs and their associated source rock intervals.

6.3 Future Work and Recommendations

If stable isotope analyses are collected from existing sample sets and future wells, they may be combined into a highly accurate chemostratigraphic tool useful for identifying depositional sequences of interest across the entire margin, bypassing any difficulties with biostratigraphic and lithostratigraphic nomenclatures. In addition, palynofacies and calcareous nannofossil research currently underway could be in future implemented into the results presented here to improve correlation of wells within the Slyne Basin.

In future wells exploring the Jurassic oil system, a greater understanding of the T-OAE and the influence on global climate and carbon burial may be achieved by more rigorous depth control such as the acquisition of core or sidewall cores, avoiding the pitfalls of cuttings collection. Such investigation would reduce the uncertainty surrounding the reported depth of samples and ensure the validity of stable isotope analysis curves. In addition, given the shortage of material for sampling, a study of wireline log combinations (e.g. ΔLogR method by Passey, 1990) will add to our understanding TOC levels beyond the scope and resolution of this dataset. Finally, a sequence stratigraphic compilation, using wells with suspected and confirmed hydrocarbon source rocks of Lower Jurassic age across the Atlantic Margins will provide widespread basin correlation and understanding of the extent of high-TOC intervals (Pederson, P.K., *pers. comm.*).

REFERENCES

Aberhan, M., and Baumiller, T.K. 2003. Selective Extinction among Early Jurassic bivalves: A consequence of anoxia. Geology, **31**: 1077-1080.

Ainsworth, N.R. 1990. Uppermost Rhaetian to Lower Bajocian Ostrocode from the Porcupine, Slyne, Erris and Donegal Basins, offshore west Ireland. Bulletin of the Geological Survey of Ireland. **4:**169-200.

Al-Suwaidi, A.H., Angelozzi, G.N., Baudin, F., Damborenea, S.E., Hesselbo, S.P., Jenkyns, H.C., Mancenido, M.O., and Riccardi, A.C. 2010. First record of the Early Toarcian Oceanic Anoxic Event from the Southern Hemisphere, Neuquén Basin, Argentina. Journal of the Geological Society. **167**: 633-636.

Arias, C. 2006. Northern and Southern Hemispheres ostracod palaeobiogeography during the Early Jurassic: Possible migration routes. Palaeogeography, Palaeoclimatology, Palaeoecology. 233: 63 – 95.

Arthur, M.A., Dean, W.E., and Pratt, L.M. 1988. Geochemical and climatic effects of increased marine organic carbon burial at the Cenomanian/Turonian boundary. Nature. **355**: 714-717.

Arthur, M.A., Jenkyns, H.C., Brumsack, H.-J., and Schlanger, S.O. 1990. Stratigraphy, Geochemistry, and Paleoceanography of Organic Carbon-Rich Cretaceous Sequences. *In* Cretaceous Resources, Events and Rhythms. *Edited by* Ginsburg, R.N. and Beauloin, B. Klwer Academic Publishers. *pp*. 75-119.

Bailey, T.R., Rosenthal, Y., McArthur, J.M., van de Schootbrugge, B., and Thirlwall, M.F. 2003. Paleoceanographic changes of the Late Pliensbachian–Early Toarcian interval: a possible link to the genesis of an Oceanic Anoxic Event. Earth and Planetary Science Letters. **212**: 307–320.

Barbu, V. 2014. Valanginian isotopic and palaeoecological signals from the Bucegi Mountains, Southern Carpathians, Romania. *In* Isotopic Studies in Cretaceous Research. *Edited by* Bojar, A.-V., Melinte-Dobrinescu, M.C. and Smit, J. Geological Society, London, Special Publications. **382**: 5-29.

Baudin, F., Herbin, J.-P., Bassoullet, J.-P., Dercourt, J., Lachkar, G., Manivit, H., and Renard, M. 1990. Distribution of organic matter during the Toarcian in the Mediterranean Tethys and Middle East. *In* Deposition of organic facies. Edited by Huc, A.Y. American Association of Petroleum Geologists, Studies in Geology **30:** 73–92.

Baudin, F., Bulot, L.G., Cecca, F., Coccioni, R., Gardin, S., and Renard, M. 1999. Un équivalent du "Niveau Faraoni" dans le bassin du Sud-Est de la France, indice possible d'un événement anoxique fini-hauterivien étendu à la Téthys méditerranéenne. Bulletin de la Société Géologique de France. **170**(4): 487–498

Baudin, F. 2005. A Late Hauterivian short-lived anoxic event in the Mediterranean Tethys: The 'Faraoni Event'. Comptes Rendus Geoscience. **337:** 1532-1540.

Baudin, F., and Riquieri, L. 2014. The Late Hauterivian Faraoni 'Oceanic Anoxic Event': an update. Bulletin de la Société Géologique de France. **185**: 359-377.

Bassoulet, J.-P., Elmi, S., Poisson, A., Cecca, F., Bellion, Y., Guiraud, R., and Baudin, F. 1993. Middle Toarcian (184–182 Ma). *In:* Atlas Tethys Paleoenvironmental Maps. *Edited by* Dercourt, J., Ricou, L.E., Vrielynck, B. pp. 63–80. Beicip-Franlab, Rueil-Malmaison.

Beckhoff, B., Kanngießer, B., Langhoff, N., Wedell, R., and Wolff, H. 2006. Handbook of Practical X-Ray Fluorescence Analysis. Springer Berlin Heidelberg.

Belaid, A., Krooss, B.M., and Littke, R. 2010. Thermal history and source rock characterization of a Paleozoic section in the Awbari Trough, Murzuq Basin, SW Libya. Marine and Petroleum Geology. **27**: 612-632.

Berner, R.A. 2003. The long-term carbon cycle, fossil fuels and atmospheric composition. Nature. **426:** 323-326.

Bodin, S., Mattioli, E., Fröhlich, S., Marshall, J.D., Boutib, L., Lahsini, S., and Redfern, J. 2010. Toarcian carbon isotope shifts and nutrient changes from the Northern margin of Gondwana (High Atlas, Morocco, Jurassic): Palaeoenvironmental implications. Palaeogeography, Palaeoclimatology, Palaeoecology. **297**: 377-390.

Bond, D.P.G., and Wignall, P.B. 2014. Large igneous provinces and mass extinctions: an update. *In* Volcanism, Impacts and Mass Extinctions: Causes and Effects. *Edited by* Keller, G., and Kerr, A.C. Geological Society of America Special Papers. **505:** 29-55.

Braithwaite, C.J.R., and Camoin, G.F. 2011. Diagenesis and sea-level change: lessons from Moruroa, French Polynesia. Sedimentology. **58:** 259–284.

Bréhéret, J.-G. 1995. L'Aptien et l'Albien de la fosse Vocontienne (des bordures au bassin) Evolution de la sedimentation et enseignements sur les événements anoxiques. Ph.D. Thesis, François Rabelais University, Tours.

Caruthers, A.H., Gröcke, D.R., and Smith, P.L. 2011. The significance of an Early Jurassic (Toarcian) carbon-isotope excursion in Haida Gwaii (Queen Charlotte Islands), British Columbia, Canada. Earth and Planetary Science Letters. **307**: 19-26.

Caston, V. 1995. The Helvick oil accumulation, Block 49/9, North Celtic Sea Basin. *In* the Petroleum Geology of Ireland's Offshore Basins. *Edited by* Croker, P.F. and Shannon, P.M. Geological Society, London, Special Publications. **93**: 209–225. doi:10.1144/GSL.SP.1995.093.01.15.

Caswell, B.A., Coe, A.L., and Cohen, A.S. 2009. New range data for marine invertebrate species across the early Toarcian (Early Jurassic) mass extinction. Journal of the Geological Society. **166**: 859-872.

Clementz, D. M. 1979. Effects of oil and bitumen saturation on source-rock pyrolysis. Bulletin of the American Association of Petroleum Geologists. **63:** 2227-2232.

Cohen, A.S., Coe, A.L., Harding, S.M., and Schwark, L. 2004. Osmium isotope evidence for the regulation of atmospheric CO2 by continental weathering. Geology. **32:** 157–160.

Cohen, A.S., Coe, A.L., and Kemp, D.B. 2007.The Late Palaeocene-Early Eocene and Toarcian (Early Jurassic) carbon isotope excursions: a comparison of their time scales, associated environmental changes, causes and consequences. Journal of the Geological Society. **164**: 1093-1108.

Cohen, K.M., Finney, S.C., Gibbard, P.L., and Fan, J.X. 2013; updated 2016. The ICS International Chronostratigraphic Chart. **36**:199-204.

Coimbra, R., Immenhauser, A., and Olóriz, F. 2009. Matrix micrite $\delta^{13}C$ and $\delta^{18}O$ reveals synsedimentary marine lithification in Upper Jurassic Ammonitico Rosso limestones (Betic Cordillera, SE Spain). Sedimentary Geology. **219**: 332–348.

Cope, J.C. 1997. The Mesozoic and Tertiary History of the Irish Sea. *In* Petroleum Geology of the Irish Sea and Adjacent Areas. *Edited by* Meadows, N.S., Trueblood, S.P., Hardman, M. and Cowan, G. Geological Society of London Special Publications. **124:** 47-59.

Coplen T.B., Kendall C., and Hopple J. 1983. Comparison of stable isotope reference samples. Nature. **302**: 236–238.

Dancer, P.N., Algar, S.T., and Wilson, I.R. 1999. Structural evolution of the Slyne Trough. In Petroleum Geology of Northwest Europe: Proceedings of the 5th Conference. Edited by Fleet, A.J., and Boldy, S.A.R. The Geological Society. pp. 445-453.

Dancer, P.N., Kenyon-Roberts, S.M., Downey, J.W., Baillie, J.M., Meadows, N.S., and Maguire, K. 2005. The Corrib gas field, offshore west of Ireland. In Petroleum Geology: North-West Europe and Global Perspectives-Proceedings of the 6th Petroleum Geology Conference. Edited by Doré, A.G. and Vining, B.A. The Geological Society, London. pp. 1035-1046.

Danise, S., Twitchett, R.J., Little, C.T.S., and Clémence, M.-E. 2013. The Impact of Global Warming and Anoxia on Marine Benthic Community Dynamics: An Example from the Toarcian (Early Jurassic). PLoS ONE. **8:** 2.

Delvaux, D., Martin, H., Leplat, P., and Paulet, J. 1990. Geochemical characterization of sedimentary organic matter by means of pyrolysis kinetic parameters. *In* Advances in Organic Geochemistry. *Edited by* Durand, B. and Behar, F. Organic Geochemistry, Pergamon Press. **16:** 175-87.

Dera, G., Pellenard, P., Neige, P., Deconinck, J.-F., Pucéat, E., and Dommergues, J.-L. 2009. Distribution of clay minerals in Early Jurassic Peritethyan seas: Palaeoclimatic significance inferred from multiproxy comparisons. Palaeogeography, Palaeoclimatology, Palaeoecology. **271**: 39-51.

Dera, G., Pucéat, E., Pellenard, P., Neige, P., Delsate, D., Joachimski, M.M., Reisberg, L., and Martinez, M. 2009. Water mass exchange and variations in seawater temperature in the NW Tethys during the Early Jurassic: Evidence from neodymium and oxygen isotopes of fish teeth and belemnites. Earth and Planetary Science Letters. **286**: 198-207.

Dera, G., Neige, P., Dommergues, J.-L., Fara, E., Laffont, R., and Pellenard, P. 2010. High-resolution dynamics of Early Jurassic marine extinctions: the case of Pliensbachian–Toarcian ammonites (Cephalopoda). Journal of the Geological Society. **167:** 21-33.

Dera, G., Prunier, J., Smith, P.L., Haggart, J.W., Popov, E., Guzhov, A., Rogov, M., Delsate, D., Thies, D., Cuny, G., Pucéat, E., Charbonnier, G., and Bayon, G. 2015. Nd isotope contraints on ocean circulation, paleoclimate, and continental drainage during the Jurassic breakup of Pangea. Gondwana Research. **27**: 1599-1615.

Derry, L.A. 2010. A burial diagenesis origin for the Ediacaran Shuram–Wonoka carbon isotope anomaly. Earth and Planetary Science Letters. **294**: 152–162.

Dickson, J.A.D., Wood, R.A., Bu Al Rougha, H., and Shebl, H. 2008. Sulphate reduction associated with hardgrounds: Lithification afterburn! Sedimentary Geology. **205**: 34–39.

Dommergues, J.-L., Meister C., and Mouterde, R. 1997. Pliensbachien. *In* Groupe Français d'étude du Jurassique: Biostratigraphie du Jurassique ouest-européen et méditerranéen: zonations paralleles et distribution des invertébrés et microfossiles. *Edited by* Cariou, E. and Hantzpergue P. Bulletin des Centres de Recherche Exploration-Production Elf-Aquitaine, Mémoire. **17:** 15–23.

Dommergues, J.-L., Fara, E., and Meister, C. 2009. Ammonite Diversity and its palaeobiogeographical structure during the early Pliensbachian (Jurassic) in the western Tethys and adjacent areas. Palaeogeography, Palaeoclimatology, Palaeoecology. **280**: 64-77.

Doré, A.G., Corcoran, D.V., and Scotchman, I.C. 2002. Prediction of the hydrocarbon system in exhumed basins, and application to the NW European Margin. *In:* Exhumation of the North Atlantic Margin: Timing, Mechanisms and Implications for Petroleum Exploration. *Edited by:* Doré, A.G., Cartwright, J.A., Stoker, M.S., Turner, J.P. and White, N.J. Geological Society of London Special Publications. **196:** 401-429.

Duarte, L.V., Silva, R.L., Mendonça-Filho, J.G., Oliveira, L.C. 2010. Geochemical evidence of the Lower Jurassic of Peniche (Lusitanian Basin, Portugal): State of the art and future perspectives. In Proceedings of the tenth conference of geochemistry of countries of the Portuguese Language ("X Congresso de Geoquimica dos Paises de Lingea Portuguesa – XVI Semana de Geoquimica").

Duarte, L.V., Silva, R.L., Mendonça Filho, J.G., Poças Ribeiro, N., and Chagas, R.B.A. 2012. High-resolution stratigraphy, Palynofacies and source rock potential of the Água de Madeiros Formation (Upper Sinemurian) of the Lusitanian Basin, Portugal. Journal of Petroleum Geology **35:** 105–126.

Duarte, L.V., Comas-Rengifo, M.J., Silva, R.L., Paredes, R., and Goy, A. 2014. Carbon isotope stratigraphy and ammonite biochronostratigraphy across the Sinemurian-Pliensbachian boundary in the Western Iberian margin. Bulletin of Geosciences. **89**: 719-736.

Duncan, R.A., Hooper, P.R., Rehacek, J., Marsh, J.S., and Duncan, A.R. 1997. The timing and duration of the Karoo igneous event, southern Gondwana. Journal of Geophysical Research. **102**: 18,127-18,138.

Elf Aquitaine. Source rock potential. 1982. In Geological completion report for well 27/13-1, pp. 29-31.

Emerson, S.R., and Hedges, J.I. 2008. Chemical Oceanography and the Marine Carbon Cycle. Cambridge University Press, Cambridge.

Enterprise Oil, 2000. Well IRE 18/25-1 Geological Completion Report, pp. 47.

Enterprise Energy Ireland Ltd. 2003. Maturity evaluation of wells 18/20-1, 18/20-2, 18/20-2z and 18/25-1, Corrib Basin, Offshore Ireland.

Enterprise Energy Ireland Ltd. 2014. Corrib Offshore Environmental Impact Statement.

Espitalié, J., Laporte, J.L., Madec, M., Marquis, F., Leplat, P., Paylet, J., and Boutefeu, A. 1977. Rapid Method for Characterisation of Source Rocks and for Determination of Petroleum Potential and Degree of Evolution. Oil and Gas Science and Technology – IFP Review. **32**: 23-42.

Espitalié, J., Deroo, G., and Marquis, F. 1985. La pyrolyse Rock-Eval et ses applications: première partie. Revue de l'Institut Français du Pétrole. **40:** 563–579.

Fleet, A.J., Clayton, C.J., Jenkyns, H.C., and Parkinson, D.N. 1987. Liassic source rock deposition in western Europe. *In* Petroleum Geology of North West Europe. *Edited by* Brooks, J., and Glennie, K. Graham and Trotman. pp. 59-70.

Follmi, K.B., Bole, M., Jammet, N., Froidevaux, P., Godet, A., Bodin, S., Adatte, T., Matera, V., Fleitmann, D., and Spangenberg, J.E. 2012. Bridging the Faraoni and Selli oceanic anoxic events: late Hauterivian to early Aptian dysaerobic to anaerobic phases in the Tethys. Climate of the Past. **8:** 171-189.

French, K.L., Sepúlveda, J., Trabucho-Alexandre, J., Gröcke, D.R., and Summons, R.E. 2014. Organic geochemistry of the early Toarcian oceanic anoxic event in Hawsker Bottoms, Yorkshire England. Earth Planetary Science Letters. **390**: 116–127.

Fry, B. 2006. Isotope notation and measurement. In Stable Isotope Ecology. Springer education. **7**: 194-275.

Gale, A.S., Kennedy, W.J., Burnett, J.A., Caron, M., and Kidd, B.E. 1996. The Late Albian to Early Cenomanian succession at Mont Risou near Rosans (Drôme, SE France): an integrated study (ammonites, inoceramids, planktonic foraminifera, nannofossils, oxygen and carbon isotopes). Cretaceous Research. **17:** 515-506.

Gale, A.S. 2012. Early Cretaceous: rifting and sedimentation before the flood. *In:* Geological History of Great Britain and Ireland. *Edited by:* Woodcock, N. and Strachan, R. Blackwell Publishing.

Galimov, E.M. 2006. Isotope organic geochemistry. Organic Geochemistry. **37**: 1200–1262.

GeoArctic Limited. 2014. A new kinematic plate reconstruction between Ireland and Canada. Petroleum Infrastructure Programme Report **IS08/05:** 1-103.

Gómez, J.J., and Arias, C. 2010. Rapid warming and ostracods mass extinction at the Lower Toarcian (Jurassic) of central Spain. Marine Micropaleontology. **74**: 119-135.

Gómez, J.J., Comas-Rengifo, M.J., and Goy A. 2016. Palaeoclimatic oscillations in the Pliensbachian (Early Jurassic) of the Asturian Basin (Northern Spain). Climate of the Past. **12**: 1199-1214.

Gröcke, G.R., Hori, R.S., Trabucho-Alexandre, J., Kemp, D.B., and Schwark, L. 2011. An open ocean record of the Toarcian oceanic anoxic event. Solid Earth. **2**: 245-257.

Haq, G.U., Hardenbol, J., and Vail, P.R. 1988. Mesozoic and Cenozoic chronostratigraphy and cycles of sea-level change. In Sea-Level Changes – an integrated approach. Society of Economic Paleontologists and Mineralogists Special Publication. **42**: 71-108.

Herron, M.M. 1988. Geochemical classification of terrigenous sands and shales from core or log data. Journal of Sedimentary Petrology. **58**: 820–829.

Hermoso, M., Minoletti, F., and Pellenard, P. 2013. Black shale deposition during Toarcian super-greenhouse driven by sea level. Climate of the Past. **9:** 2703–2712.

Hesselbo, S.P., Meister, C., and Grocke, D.R. 2000a. A potential global stratotype for the Sinemurian-Pliensbachian boundary (Lower Jurassic), Robin Hood's Bay, UK: ammonite faunas and isotope stratigraphy. Geological Magazine. **137**: 601-607.

Hesselbo, S.P., Gröcke, D.R., Jenkyns, H.C., Bjerrum, C.J., Farrimond, P., Morgans Bell, H.S., and Green, O.R. 2000. Massive Dissociation of gas hydrate during a Jurassic oceanic anoxic event. Nature. **406**: 392-395.

Hesselbo, S.P., Jenkyns, H.C., Duarte, L.V., and Oliveira, L.C.V. 2007. Carbon-isotope record of the Early Jurassic (Toarcian) Oceanic Anoxic Event from fossil wood and marine carbonate (Lusitanian Basin, Portugal). Earth and Planetary Science Letters. **253**: 455-470.

Hoefs, J. 2015. Stable Isotope Geochemistry. Springer.

Jacobsen, S.B., and Kaufman, A.J. 1999. The Sr, C and O isotopic evolution of Neoproterozoic seawater. Chemical Geology. **161**: 37–57.

Jaquin, T., and de Graciansky, P.-C. Major transgressive/regressive cycles: the stratigraphic signature of European basin development. In Mesozoic and Cenozoic Sequence Stratigraphy of European Basin. SEPM (Society for Sedimentary Geology). Special Publication No. 60. pp. 15-29.

Jarvie, D., and Baker, D. 1984. Application of the Rock-Eval III Oil Show Analyzer to the Study of Gaseous Hydrocarbons in an Oklahoma Gas Well. *Presented at* the 187th American Chemical Society National Meeting, Geochemistry Division.

Jenkyns, H.C., and Clayton, C.J. 1986. Black shales and carbon isotopes in pelagic sediments from the Tethyan Lower Jurassic. Sedimentology. **33**: 87–106.

Jenkyns, H. C. 1988. The Early Toarcian (Jurassic) Anoxic Event: Stratigraphic, Sedimentary, and Geochemical Evidence. American Journal of Science. **288**: 101-151.

Jenkyns, H.C., Grocke, D.R., and Hesselbo, S.P. 2001. Nitrogen isotope evidence for water mass denitrification during the Early Toarcian (Jurassic) oceanic anoxic event. Paleoceanography. **16**: 593-603.

Jenkyns, H.C., Jones, C.E., Grocke, D.R., Hesselbo, S.P., and Parkinson, D.N. 2002. Chemostratigraphy of the Jurassic System: applications, limitations and implications for palaeoceanography. Journal of the Geological Society. **159**: 351-378.

Jenkyns, H. C. 2010. Geochemistry of Anoxic Events. Geochemistry, Geophysics, Geosystems. **11**: 1-30.

Jenkyns, H.C., and Weedon, G.P. 2013. Chemostratigraphy ($CaCO_3$, TOC, δ^{13}Corg) of Sinemurian (Lower Jurassic) black shales from the Wessex Basin, Dorset and palaeoenvironmental implications. Newsletters on Stratigraphy. **46**: 1-21.

Jones, D.M. 1992. A report on the Organic Geochemical Analysis of Cuttings and Core Material from Well 27/13-1. Report Commissioned by Enterprise Oil Based on PAD Samples. Newcastle Research Group in Fossil Fuels and Environmental Geochemistry, University of Newcastle upon Tyne.

Kafousia, N., Karakitsios, C., Mattioli, E., Kenjo, S., and Jenkyns, H.C. 2014. The Toarcian Oceanic Anoxic Event in the Ionian Zone, Greece. Palaeogeography, Palaeoclimatology, Palaeoecology. **393**: 135-145.

Kemp, D.B., Coe, A.L., Cohen, A.S., and Schwark, L. 2005. Astronomical pacing of methane release in the Early Jurassic period. Nature. **437**: 396-399.

Kemp, D.B., Coe, A.L., Cohen, A.S., and Weedon, G.P. 2011. Astronomical forcing and chronology of the early Toarcian (Early Jurassic) oceanic anoxic event in Yorkshire, UK. Paleoceanography. **26**: PA4210.

Kessler II, L.G., and Sachs, S.D. 1995. Depositional setting and sequence stratigraphic implications of the Upper Sinemurian (Lower Jurassic) sandstone interval, North Celtic Sea/St. George's Channel Basins, offshore Ireland. *In* The petroleum geology of Ireland's Offshore Basins, Geological Society of London Special Publication. *Edited by* Croker, P. F. and Shannon, P. M. **93**: 171-192.

Knight, R.D., Kjarsgaard, B.A., Plourde, A.P., and Moroz, M. 2013. Portable XRF spectrometry of reference materials with respect to precision, accuracy, instrument drift, dwell time optimization, and calibration. Geological Survey of Canada, Open File 7358.

Korte, C., and Hesselbo S.P. 2011. Shallow marine carbon and oxygen isotope and elemental records indicate icehouse-greenhouse cycles during the Early Jurassic. Paleoceanography. **26**: PA4219.

Krencker, F-N., Bodin, S., Suan, G., Heimhofer, U., Kabiri, L., and Immenhauser, A. 2015. Toarcian extreme warmth led to tropical cyclone intensification. Earth and Planetary Science Letters, **425**: 120-130.

Kuspert, W. 1982. Environmental changes during oil shale deposition as deduced from stable isotope ratios. *In* Cyclic and Event Stratification. *Edited by* Einsele, G. and Seilacher, A. Springer-Verlag, pp. 482-501.

Lafargue, E., Bertrand Braunschweig, C., and Wady Naanaa, H. 2003. Method for interpreting petroleum characteristics of geological sediments. United Stated Patent Office.

Langford, F.F., and Blanc-Valleron, M.-M. 1990. Interpreting Rock-Eval pyrolysis data using graphs of pyrolizable hydrocarbons vs. total organic carbon. The American Association of Petroleum Geologists Bulletin. **74:** 799-804.

Law, C.A. 1999. Evaluating source rocks. *In* Exploring for oil and gas traps—Treatise of Petroleum Geology/Handbook of Petroleum Geology. *Edited by* Beaumont, E.A. and Foster, N.H.: Tulsa, Okla., American Association of Petroleum Geologists.

Lynch, J.J. 1996. Provisional elemental values for four new geochemical soil and till reference materials, TILL-1, TILL-2, TILL-3 and TILL-4. Geostandards Newsletter. **20**: 277-287.

Magoon, L.B., and Beaumont, E.A. 1999. Petroleum systems. *In* American Association of Petroleum Geologists Treatise of Petroleum Geology: Exploring for oil and gas traps. *Edited by* Beaumont, E.A. and Foster, N.H. **3:** 3.1-3.34.

Marshall, J.D. 1992. Climatic and oceanographic isotopic signals from the carbonate rock record and their preservation. Geological Magazine. **129:** 143–160.

Masetti, D., Figus, B., Jenkyns, H.C., Barattolo, F., Mattioli, E., and Posenato, R. 2016. Carbon-isotope anomalies and demise of carbonate platforms in the Sinemurian (Early Jurassic) of the Tethyan region: evidence from the Southern Alps (Northern Italy). Geological Magazine.

Mattioli, E., Pittet, B., Riquier, L., and Grossi, V. 2014. The mid-Valanginian Weissert Event as recorded by calcareous nanoplankton in the Vocontian Basin. Palaeogeography, Palaeoclimatology, Palaeoecology. **414**: 472-485.

McElwain, J.C., Wade-Murphy, J., and Hesselbo, S.P. 2005. Changes in carbon dioxide during an oceanic anoxic event linked to intrusion into Gondwana coals. Nature. **435**: 479-482.

Miles, A. J. 1994. Glossary of Terms Applicable to the Petroleum System. *In*: The Petroleum System - from source to trap. *Edited by* Magoon, L. B., and Dow, W. G. AAPG Memoir. **60**: 643-644.

Millennia. 2004. Biostratigraphic Review of the Slyne and Erris Basins, West of Ireland. Petroleum Affairs Technical Division Data Repository.

Morettini, E., Santantonio, M., Bartolini, A., Cecca, F., Baumgartner, P.O., and Hunziker, J.C. 2002. Carbon isotope stratigraphy and carbonate production during the Early-Middle Jurassic: examples from the Umbria-Marche-Sabina Apennines (central Italy). Palaeogeography, Palaeoclimatology, Palaeoecology. **184**: 251-273.

Murphy, N. J., Sauer, M. J., and Armstrong, J. P. 1995. Toarcian source rock potential in the North Celtic Sea Basin, offshore Ireland. *In* The petroleum geology of Ireland's Offshore Basins, Geological Society of London Special Publication. *Edited by* Croker, P. F. and Shannon, P. M. **93**: 193-207.

Naylor, D., Shannon, P., and Murphy, N. 1999. Irish Rockall Basin region – a standard structural nomenclature system. Petroleum Affairs Division Special Publication 1/99.

Naylor, D. and Shannon, P.M. 1982. Northwest Irish Offshore Basins. *In* The geology of offshore Ireland and west Britain. Graham and Trotman, London. pp. 76-81.

Natural Resources Canada (NRCAN). 2014. XRF Analyzer Operator Certification News. (http://www.nrcan.gc.ca/mining-materials/non-destructive-testing/8580).

Oliveira, L.C., Duarte, L.V., Silva, R.L., and Rodrigues, R. 2014. Belemnite 18O and 13C Record of the Lusitanian Basin Pliensbachian carbonate series (Portugal). Goldschmidt Conference Abstract.

Pederson, T.F., and Calvert, S.E. 1990. Anoxia vs. Productivity: What Controls the Formation of Organic-Carbon-Rich Sediments and Sedimentary Rocks? AAPG Bulletin. **74**: 454-466.

Peters, K.E. 1986. Guidelines for Evaluating Petroleum Source Rock Using Programmed Pyrolysis. American Association of Petroleum Geologists Bulletin. **70**: 318-329.

Peters, K.E., Walters, C.C., and Molowan, J.M. 2005. The Biomarker Guide. Cambridge University Press, London.

Petroleum Affairs Division, 2006. Petroleum Systems Analysis of the Rockall and Porcupine Basins Offshore Ireland Digital Atlas - Special Publication **3**:06, Department of Natural Resources, Dublin Ireland.

Pittet, B., Suan, G., Lenoir, F., Duarte, L.V., and Mattioli, E. 2014. Carbon isotope evidence for sedimentary discontinuities in the lower Toarcian of the Lusitanian Basin (Portugal): Sea level change at the onset of the Oceanic Anoxic Event. Sedimentary geology. **303**: 1-14.

di Primio, R., Cramer, B., Zwach, C., Kroose, B.M., and Littke, R. 2008. Petroleum Systems. *In* Dynamics of Complex Intracontinental Basins. *Edited by* Littke, R., Bayer, U., Gajewski, D., and Nelskamp, S. Springer. pp. 411-432.

Porter, S.J., Smith, P.L., Caruthers, A.H., Hou, P., Grocke, D.R., and Selby, D. 2014. New high resolution geochemistry of Lower Jurassic marine sections in western North America: A global positive carbon isotope excursion in the Sinemurian? Earth and Planetary Science Letters. **397**: 19-31.

Potter, J., Richards, B.C., and Goodarzi, F. 1993. The organic petrology and thermal maturity of lower Carboniferous and Upper Devonian source rocks in the Liard basin, at Jackfish Gap-Yohin Ridge and North Beaver River, northern Canada: implications for hydrocarbon exploration. Energy Sources. **15**: 289-314.

Prauss, M., Ligouis, B., and Luterbacher, H. 1991. Organic matter and palynomorphs in the 'Posidonienschiefer' (Toarcian, Lower Jurassic) of southern Germany. *In* Modern and Ancient Continental Shelf Anoxia. *Edited by* Tyson, R.V. and Pearson, T.H. The Geological Society, Special Publications. **58:** 335-351.

Riding, J.B., Leng, M.L., Kender, S., Hesselbo, S.P., and Feist-Burkhardt, S. 2013. Isotopic and palynological evidence for a new Early Jurassic environmental perturbation. Palaeogeography, Palaeoclimatology, Palaeoecology. **374**: 16-27.

Riediger, C.L. 2002. Hydrocarbon source rock potential and comments on correlation of the Lower Jurassic Poker Chip Shale, west-central Alberta. Bulletin of Canadian Petroleum Geology. **50:** 263–276.

Röhl, H-J., Schmid-Röhl, A., Oschmann, W., Frimmel, A., and Schwark, L. 2001. The Posidonia Shale (Lower Toarcian) of SW-Germany: an oxygen-depleted ecosystem controlled by sea level and palaeoclimate. Palaeogeography, Palaeoclimatology, Palaeoecology. **169:** 273–299.

Rosales, I., Quesada, S., and Robles, S. 2006. Geochemical arguments for identifying second-order sea-level changes in hemipelagic carbonate ramp deposits. Terra Nova. **18**: 233-240.

Ruble, T., Drozd, R.J., and Heck, W.A. Undated Presentation: Practical Geochemical methods to assess unconventional reservoirs: A case study from the Permian Basin, Texas. Weatherford Laboratories Publication.

Sachse, V.F., Leythaeuser, D., Grobe, A., Rachidi, M., and Littke. R. 2012. Organic Geochemistry and Petrology of a Lower Jurassic (Pliensbachian) Petroleum Source Rock from Aït Moussa, Middle Atlas, Morocco. Journal of Petroleum Geology. **35:** 5–24.

Schlanger, S.O., and Jenkyns, H.C. 1976. Cretaceous oceanic anoxic events: causes and consequences. Geologie en Mijnbouw. **55:** 179-184.

Schweigert, G. 2005. The occurrence of the Tethyan ammonite genus Meneghiniceras (Phylloceratina: Juraphyllitidae) in the Upper Pliensbachian of SW Germany. Stuttgarter beiträge zur naturkunde. **356**: 1-16.

Scotchman, I.C., and Thomas, J.R.W. 1995. Maturity and hydrocarbon generation in the Slyne Trough, northwest Ireland. *In* the Petroleum Geology of Ireland's Offshore Basins. *Edited by* Croker, P.F., and Shannon, P.M. Geological Society Special Publication. **93**: 385-411.

Scotchman, I., 2001. Petroleum Geochemistry of the Lower and Middle Jurassic in Atlantic margin basins of Ireland and the UK. *In* the Petroleum Geology of Ireland's Offshore Basins. *Edited by* Croker, P.F., and Shannon, P.M. Geological Society, Special Publication **188**: 31-60.

Scotchman, I.C., Doré, A.G., and Spencer, A.M. 2016. Petroleum Systems and results of exploration on the Atlantic margins of the UK, Faroes and Ireland: what have we learnt? *In* Petroleum Geology of NW Europe: 50 Years of Learning – Proceedings of the 8th Petroleum Geology Conference. *Edited by* Bowman, M. and Levell, B. Geological Society of London.

Serica Energy. 2014. Rockall and Slyne Basin Opportunities, presented at Atlantic Ireland Conference, Dublin.

Shannon, P. M. 1991. The development of Irish offshore sedimentary basins. Journal of the Geological Society, London. **148**: 181-189.

Shannon, P. M. Corcoran, D.V., and Haughton, P.D.W. 2001. The petroleum exploration of Ireland's offshore basins: introduction. *In* the Petroleum Exploration of Ireland's Offshore Basins. *Edited by* Shannon, P. M. and Haughton, P.D.W. Geological Society, London, Special Publications. **188**: 1-8.

Shannon, P.M., Stoker, M.S., Praeg, D., can Weering, T.C.E, de Haas, H., Nielsen, T., Dahlgren, K.I.T., and Hjelstuen, B.O. 2005. Sequence stratigraphic analysis in deep-water, underfilled NW European passive margin basins. Marine and Petroleum Geology. **22**: 1185-1200.

Shannon, P. M., McDonnell, A., and Bailey, W.R. 2007. The evolution of the Porcupine and Rockall Basins, offshore Ireland: the geological template for carbonate mound development. International Journal of Earth Sciences. **96**: 21-35.

Shen, J., Algeo, T.J., Zhou, L., Feng, Q., Yu, J., and Ellwood, B. 2012. Volcanic perturbations of the marine environment in South China preceding the latest Permian mass extinction and their biotic effects. Geobiology. **10:** 82-103.

Shen, S., Cao, C., Zhang, H., Bowring, S.A., Henderson, C.M., Payne, J.L., Davydov, V.I., Chen, B., Yuan, D., Zhang, Y., Wang, W., and Zheng, Q. 2013. High-Resolution $\delta^{13}C_{carb}$ Chemostratigraphy from Latest Guadalupian through Earliest Triassic in South China and Iran. Earth and Planetary Science Letters. Earth and Planetary Science Letters. **375**: 156-165.

Silva, R. L., Duarte, L. V., Comas-Rengifo, M. J., Mendonça Filho, J. G., and Azerêdo, A. C. 2011. Update of the carbon and oxygen isotopic records of the Early-Late Pliensbachian (Early Jurassic, ~187 Ma): Insights from the organic-rich hemipelagic series of the Lusitanian Basin (Portugal). Chemical Geology. **283**: 177-184.

Silva, R.L., Duarte, L.V., and Mendonca-Filho, J.G. 2013. Optical and geochemical characterization of Upper Sinemurian (Lower Jurassic) fossil wood from the Lusitanian Basin (Portugal). Geochemical Journal. **47**: 489-498.

Silva, R.L., Duarte, L.V., and Comas-Rengifo, M.J. 2015a. Facies and carbon isotope chemostratigraphy of Lower Jurassic carbonate deposits, Lusitanian Basin (Portugal): Implications and limitations to the application in sequence stratigraphic studies. *In* Chemostratigraphy: concepts, techniques, and applications. Chapter 13. *Edited by* Ramkumar, M. Elsevier, pp. 341-371.

Silva, R.L., and Duarte, L.V. 2015b. Organic matter production and preservation in the Lusitanian Basin (Portugal) and Pliensbachian climatic hot snaps. Global and Planetary Change. **131**: 24-34.

Silva, R.L., Wong, C., and Wach, G. 2015c. Source Rocks and Petroleum Systems of the Scotian Basin. Canadian Society of Exploration Geophysicists Recorder **40:** 22–27.

Sinclair, I. 1995. Sequence stratigraphic response to Aptian-Albian rifting in conjugate margin basins: a comparison of the Jeanne d'Arc Basin, offshore Newfoundland, and the Porcupine Basin, offshore Ireland. In the Tectonics, Sedimentation and Palaeoceanography of the North Atlantic Region. Edited by Scrutton, R.A., Stoker, M.S., Shimmield, G.B., and Tudhope, A.W. Geological Society Special Publication. **90**: 29-49.

SLR Environmental Consulting (Ireland) Ltd. 2013. Deep Kinsale Farmin Option Sub-Area Technical Evaluation Report for Fastnet Oil and Gas plc.

Smith, J., and Higgs, K.T. 1995. Provenance implications of reworked palynomorphs in Mesozoic successions of the Porcupine and the North Porcupine basins, offshore Ireland. *In* the Petroleum Exploration of Ireland's Offshore Basins. *Edited by* Shannon, P., Haughton, D. Geological Society of London Special Volume. **93**: 291-300.

Spencer, A.M., and MacTiernan, B. 2001. Petroleum systems offshore western Ireland in an Atlantic margin context. *In* the Petroleum Exploration of Ireland's Offshore Basins. *Edited by* Shannon, P., Haughton, D., and Corcoran, D.V. Geological Society, London, Special Publications. **188**: 9-29.

Suan, G., Pittet, B., Bour, I., Mattioli, E., Duarte, L.V., and Mailliot. 2008a. Duration of the Early Toarcian carbon isotope excursion deduced from spectral analysis: Consequence for its possible causes. Earth and Planetary Science Letters. **267**: 666-679.

Suan, G., Mattioli, E., Pittet, B., Mailliot, S., and Lécuyer, C. 2008b. Evidence for major environmental perturbation prior to and during the Toarcian (Early Jurassic) oceanic anoxic event from the Lusitanian Basin, Portugal. Paleoceanography. **23**: PA1202.

Suan, G., Mattioli, E., Pittet, B., Lecuyer, C., Sucheras-Marx, B., Duarte, L.V., Philippe, M., Reggiani, L., and Martineau, F. 2010. Secular environmental precursors to Early Toarcian (Jurassic) extreme climate changes. Earth and Planetary Science Letters, **290**: 448-458.

Suan, G., Nikitenko, B.L., Rogov, M.A., Baudin, F., Spangenberg, J.E., Knyazev, V.G., Gllinskikh, L.A., Goryacheva, A.A., Adatte, T., Riding, J.B., Follmi, K.B., Pittet, B., Mattioli, E., and Lécuyer, C. 2011. Polar record of Early Jurassic massive carbon injection. Earth and Planetary Science Letters. **312**: 102-113.

Suan, G., van de Schootbrugge, B., Adatte, T., Fiebig, J., W., and Oschmann, W. 2015. Calibrating the magnitude of the Toarcian carbon cycle perturbation. Paleoceanography. **30**: 495–509.

Suarez-Ruiz, I., Flores, D., Mendonca-Filho, J.-G., and Hackley, P.C. 2012. Review and update of the applications of organic petrology: Part 1, Geological Applications. International Journal of Coal Geology.

Swart, P.K., and Merlim, L.A. 2000. The origin of dolomites in Tertiary sediments from the margin of Great Bahama Bank. Journal of Sedimentary Research. **70:** 738–748.

Swart, P.K. 2015. The geochemistry of carbonate diagenesis: The past, present and future. Sedimentology. **62:** 1233–1304.

Tissot, B.P., and Welte, D.H. 1984. Petroleum Formation and Occurrence, 2nd Edition. Springer-Verlag Berlin Heidelberg.

Trueblood, S.P., and Morton, N. 1991. Comparative sequence stratigraphy and structural styles of the Slyne Trough and Hebrides Basin. Journal of the Geological Society, London. **148**: 197-201.

Trueblood, S. 1992. Petroleum geology of the Slyne Trough and adjacent basins. *In* Basins on the Atlantic Seaboard: Petroleum Geology, Sedimentology and Basin Evolution. *Edited by* Parnell, J. Geological Society, London, Special Publications. **62**: 315-326.

Tyson, R.V. 1995. Sedimentary Organic Matter – Organic facies and palynofacies. Chapman and Hall.

Tyson, R.V., and Pearson, T.H., 1991. Modern and ancient continental shelf anoxia: an overview. *In* Modern and Ancient Continental Shelf Anoxia. *Edited by* Tyson, R.V., and Pearson, T.H. **58**: 1-24.

van Breugel, Y., Baas, M., Schouten, S., Mattioli, E., and Sinninghe Damste, J.S. 2006. Isorenieratane record in black shales from the Paris Basin, France: Constraints on recycling of respired CO_2 as a mechanism for negative carbon isotope shifts during the Toarcian oceanic anoxic event. Paleoceanography. **21:** PA4220.

van Buchem, F.S.P., de Boer, P.L., McCave, I.N., and Herbin, J.-P. 1995. The Organic Carbon Distribution in Mesozoic Marine Sediments and the Influence of Orbital Climatic Cycles (England and the Western North Atlantic). *In* Paleogeography, Paleoclimate, and Source Rocks. *Edited by* Huc, A.-Y. AAPG Studies in Geology. **40**: 303-335.

van de Schootbrugge, B., McArthur, J.M., Bailey, T.R., Rosenthal, Y., Wright, J.D., and Miller, K.G. 2005. Toarcian oceanic anoxic event: An assessment of global causes using belemnite C isotope records. Paleoceanography. **20**: PA3008.

van de Schootbrugge, B., Bailey, T.R., Rosenthal, Y., Katz, M.E., Wright, J.D., Miller, K.G., Feist-Burkhardt, S., and Falkowski, P.G. 2005. Early Jurassic climate change and the radiation of organic-walled phytoplankton in the Tethys Ocean. Paleobiology. **31**: 73-97.

van de Schootbrugge, B., Bachan, A., Suan, G., Richoz, S., and Payne, J.L. 2013. Microbes, mud, and methane: cause and consequence of recurrent Early Jurassic anoxia following the end-Triassic mass-extinction. Palaeontology. **56:** 685–709.

Van Krevelen, D.W. 1993. Coal: typology–physics–chemistry–constitution, 3rd edition. Elsevier Science Publishers.

West Virginia University – Utica Shale Appalachian Basin Exploration Consortium. 2015. Source Rock Geochemistry. *In* A geologic play book for Utica Shale Appalachian Basin Exploration.

Wignall, P.B., Bond, D.P.G., Kuwahara, K., Kakuwa, Y., Newton, R.J., and Poulton, S.W. 2010. An 80-million-year oceanic redox history from Permian to Jurassic pelagic sediments of the Mino-Tamba terrane, SW Japan, and the origin of four mass extinctions. Global and Planetary Change. **71**: 109-123.

Wrigley, R., Intawong, A., and Rodriguez, K. 2014. Ireland Atlantic Margin: a new era in a frontier basin. First Break. **32:** 95-100.

APPENDICES

BULK GEOCHEMISTRY ANALYSIS TABLES

Table A10: Bulk XRF Geochemistry Results for well 18/25-1.

Sample Depth (m)	SiO2	Al2O3	K2O	Fe2O3	MgO	TiO2
2613.0	42.12	16.58	2.04	4.56	1.09	0.79
2625.0	41.94	17.17	2.09	4.29	0.00	0.76
2637.0	44.30	18.38	2.23	4.59	2.10	0.80
2637.0	44.29	18.60	2.24	4.63	1.29	0.81
2649.0	45.25	19.91	2.18	4.91	0.00	0.89
2661.0	50.97	24.43	2.33	5.63	1.69	1.01
2673.0	39.58	17.15	1.86	4.34	1.36	0.81
2685.0	35.78	15.00	1.66	4.28	0.00	0.73
2697.0	34.30	14.72	1.65	4.50	0.00	0.75
2709.0	35.45	13.21	1.65	4.76	0.00	0.66
2721.0	32.96	10.11	1.70	3.89	1.88	0.54
2733.0	37.96	10.55	1.69	3.49	0.00	0.52
2733.0	37.70	10.46	1.70	3.51	0.00	0.50
2745.0	47.61	13.16	2.35	3.78	1.52	0.73
2786.5	40.11	12.09	2.46	4.86	1.10	0.68
2792.5	31.02	8.90	1.84	3.59	0.00	0.59
2798.5	36.04	11.75	2.23	4.48	2.96	0.64
2810.5	20.93	5.89	1.34	2.93	0.00	0.58
2822.5	26.86	8.52	1.76	4.12	2.66	0.62

Table A11: Bulk XRF Geochemistry results for well 27/13-1 (sample measurements averaged for figures).

Sample Depth (m)	SiO2	Al2O3	K2O	Fe2O3	MgO	TiO2
2095.0	43.90	16.98	2.46	5.62	0.87	0.72
2127.0	32.05	13.86	1.69	5.74	1.53	0.60
2127.0	52.66	19.23	2.87	6.67	0.00	0.88
2127.0	56.26	20.96	3.04	6.61	0.81	0.93
2157.0	45.03	17.83	2.44	6.63	0.81	0.75
2217.0	37.06	11.64	2.05	3.82	0.83	0.57
2217.0	42.32	14.73	2.44	5.32	0.00	0.72
2217.0	52.14	19.90	2.82	5.67	1.02	0.87
2333.0	39.53	14.07	2.39	4.60	0.98	0.62
2345.0	28.01	9.50	1.82	3.54	0.99	0.37
2494.1	39.11	12.04	2.76	3.64	1.82	0.56
2494.1	40.97	12.45	2.74	3.31	0.00	0.54
2494.1	37.52	11.23	2.83	4.02	0.00	0.56
2494.7	26.62	10.94	1.88	21.94	0.00	0.46
2494.7	36.65	15.73	3.24	14.35	0.00	0.67
2494.7	39.88	18.87	3.42	17.08	2.05	0.70
2496.7	41.69	12.81	2.81	3.34	1.51	0.56
2496.7	42.75	14.03	3.02	3.84	1.28	0.60
2496.7	42.92	12.96	2.96	3.75	0.74	0.60
2497.2	36.42	11.67	2.65	4.16	0.98	0.55
2497.2	41.34	13.15	2.87	3.59	0.76	0.59
2497.2	39.30	12.25	2.92	3.60	0.68	0.58
2585.0	47.75	14.57	2.92	4.55	0.00	0.67
2585.0	46.72	16.66	3.12	5.29	1.18	0.72
2585.0	48.63	18.70	3.39	5.27	1.47	0.78
2587.0	40.99	12.95	2.51	4.85	1.28	0.60
2587.0	42.56	14.89	3.25	4.50	1.80	0.68
2587.0	47.76	17.77	3.17	4.72	0.69	0.79
2665.0	46.36	15.52	3.65	6.10	1.29	0.68
2677.0	39.40	13.67	2.52	5.99	0.00	0.66
2677.0	43.66	15.20	3.07	4.95	1.42	0.66
2677.0	48.37	17.66	3.86	5.31	1.86	0.79
2685.0	37.39	10.82	2.26	5.81	0.97	0.50

STABLE ISOTOPE AND ROCK-EVAL II PYROLYSIS RESULTS

Table A12: Sample ID, age, lithostratigraphy, carbonate and kerogen $\delta^{13}C$(V-PDB), Total Organic Carbon, S1, S2, S3, Tmax, HI, and OI of the studied samples from the well 18/25-1, Slyne Basin, offshore Ireland

Sample ID	Chronostratigraphy	Formation	average MDBRT (m)	carbonate $\delta^{13}C_{V\text{-}PDB}$ (‰)	kerogen $\delta^{13}C_{V\text{-}PDB}$ (‰)	TOC (wt%)	S_1 (mg HC/g)	S_2 (mg HC/g)	S_3 (mg CO_2/g)	T_{max} (°C)	Hydrogen Index (mg HC/g TOC)	Oxygen Index (mg CO_2/g TOC)
2610 - 2616	Aalenian	inf. Middle Jurassic B	2613	-1.69	-27.01	2.3	3.98	8.4*	0.57	438	364	25
2622 - 2628	Aalenian?-Toar?	inf. Middle Jurassic B	2625	-2.12	-26.92	3.1	4.64	11.86*	0.63	442	389	21
2634 - 2640	Toarcian?	Pabba/Portree Shales	2637	-3.08	-27.25	3.1	4.71	12.56*	1.05	440	410	34
2646 - 2652	Toarcian?	Pabba/Portree Shales	2649	-2.15	-27.53	3.1	4.96	11.63*	0.62	442	372	20
2658 - 2664	Lower Toarcian	Pabba/Portree Shales	2661	-5.16	-27.89	3.2	5.23	10.69*	0.69	443	335	22
2670 - 2676	Lower Toarcian	Pabba/Portree Shales	2673	-4.39	-28.02	3.4	6.24	14.33*	0.67	442	418	20
2682 - 2688	Lower Toarcian	Pabba/Portree Shales	2685	-4.96	-28.23	4.8	8.1	19.83*	0.73	443	414	15
2694 - 2700	Lower Toarcian	Pabba/Portree Shales	2697	-4.22	-28.21	5.2	8.28	20.36	0.63	438	392	12
2706 - 2712	Lower Toar?-Pliens?	Pabba/Portree Shales	2709	-3.23	-27.70	4.8	7.7	18.34	0.61	442	385	13
2718 - 2724	Lower Toar?-Pliens?	Pabba/Portree Shales	2721	-1.68	-26.80	1.8	3.57	4.22*	0.64	439	240	36
2730 - 2736	Lower Pliensbachian	Pabba/Portree Shales - Broadford Beds	2733	-1.24	-26.24	1.2	3.29	3.12*	0.84	441	267	72
2742 - 2748	Lower Pliensbachian	Broadford Beds	2745	-0.92	-26.25	0.8	2.11	1.44*	0.75	446	179	93
2785 - 2788	Upper Sinemurian	Broadford Beds	2786.5	-2.02	-26.05	1.4	4.09	3.85*	0.94	434	273	67
2791 - 2794	Upper Sinemurian	Broadford Beds	2792.5	-2.40	-26.36	1.0	2.86	2.15*	0.79	441	224	82
2797 - 2800	Upper Sinemurian	Broadford Beds	2798.5	-0.69	-26.05	1.2	3.12	2.98*	0.91	439	242	74
2809 - 2812	Upper Sinemurian	Broadford Beds	2810.5	1.85	-26.60	0.8	1.36	1.78*	0.72	443	236	95
2821 - 2824	Upper Sinemurian	Broadford Beds	2822.5	2.22	-25.52	1.0	2	2.92*	0.84	443	289	83

Toar - Toarcian; Pliens - Pliensbachian; inf. – informal; MDBRT - Measured Depth Below Rotary Table; TOC- Total Organic Carbon; * - low temperature S_2 shoulder

Table A13: Sample ID, age, lithostratigraphy, carbonate and kerogen $\delta^{13}C$(V-PDB), Total Organic Carbon, S1, S2, S3, Tmax, HI, and OI of the studied samples from the well 27/13-1, Slyne Basin, offshore Ireland

sample ID and depth (mdBRT)	Sample Type	Chrono-stratigraphy	Formation / Group	carbonate $\delta^{13}C_{V\text{-}PDB}$ (‰)	kerogen $\delta^{13}C_{V\text{-}PDB}$ (‰)	LECO TOC (wt%)	S_1 (mg HC/g)	S_2 (mg HC/g)	S_3 (mg CO_2/g)	T_{max} (°C)	HI (mg HC/g TOC)	OI (mg CO_2/g TOC)
2095	Cuttings	(Early Bajocian) - Toarcian	Dogger	-3.98	-28.65	3.71	2.6	15.91	0.78	433*	428.84	21.02
2127	Cuttings	(Early Bajocian) - Toarcian	Dogger	-3.01	-26.46	2.97	1	11.03	0.65	428*	371.38	21.89
2157	Cuttings	(Early Bajocian) - Toarcian	Dogger	-3.16	-29.54	2.85	1.41	10.32	0.72	435*	362.11	25.26
2217	Cuttings	Pliens.	Lias	-0.14	-25.41	1.12	0.23	1.29	0.4	438*	115.18	35.71
2333	Cuttings	Pliens.	Lias	-1.07	-26.84	3.47	1.74	12.87	0.84	436*	370.89	24.21
2345	Cuttings	Pliens.	Lias	-1.01	-27.38	5.14	2.77	22.17	1.02	435*	431.32	19.84
2494.1	Core	Sinemurian	Lias	-0.50	-24.67	0.97	0.31	0.12	0.34	0	12.33	34.94
2494.7	Core	Sinemurian	Lias	-1.46	-24.52	0.99	0.26	0.07	0.2	0	7.07	20.20
2496.65	Core	Sinemurian	Lias	-0.47	-24.66	0.77	0.17	0.06	0.17	0	7.77	22.02
2497.2	Core	Sinemurian	Lias	-0.48	-24.18	0.81	0.21	0.08	0.17	0	9.91	21.07
2585	Cuttings	Sinemurian	Lias	-1.10	-25.95	0.86	0.12	0.43	0.42	438	50	48.84
2587	Cuttings	Sinemurian	Lias	-0.65	-25.92	0.61	0.07	0.22	0.42	438	36.30	69.31
2665	Cuttings	Hettangian - Rhaetian	Lias	-1.75	-25.81	1.29	0.53	1.74	0.41	438*	134.88	31.78
2677	Cuttings	Hettangian - Rhaetian	Lias	-1.44	-26.17	0.859	0.15	0.7	0.43	436	81.49	50.06
2685	Cuttings	Hettangian - Rhaetian	Lias	-1.07	-25.77	0.866	0.52	0.82	0.38	436	94.69	43.88

MDBRT - Measured Depth Below Rotary Table; TOC- Total Organic Carbon; Pliens. – Pliensbachian; * - Low Temp S2 Shoulder